SENTINEL LYMPH NODE BIOPSY FOR BREAST CANCER USING INDOCYANINE GREEN FLUORESCENCE VISUALIZATION

Zikiryakhodzhaev A.D., Saribekyan E.K., Bagdasarova D.V., Malishava L.E., Usov F.N., Starkova M.V.
P.A. Herzen Moscow Oncology Research Center – branch of FSBI NMRRC of the Ministry of Health of the Russian Federation, Moscow, Russia

Abstract

We presented the preliminary results of sentinel lymph node biopsy (SLN) using the method of fluorescent visualization with the indocyanine green. The study included 40 breast cancer patients with the prevalence of the cTis-2N0M0 process. 1 ml of Indocyanine Green (ICG) aqueous solution was administered periareolarly and subcutaneously from the tumor side with total drug dose of 5 mg. In the following few minutes the ICG trail along the lymphatic vessels was observed by its fluorescence in the infrared spectral range using a special camera with image transmitted to a computer screen. After the trail reached the axillary region and broke off, skin and subcutaneous tissue incision in axillary area was made, and the superficial fascia was dissected. The first contrasted lymph nodes were extracted. The incidence of SLN was 92.5%. Metastases were detected in 20% of cases. On average, it took 17.6 minutes to identify and remove the SLN. In 7 patients the use of the fluorescent SLN detection method was combined with radioisotope (Technefite ^{99m}Tc colloid) – in all cases the same SLN was identified. The use of the ICG lymphotropic dye with the subsequent detection of SLN by the fluorescence method makes it possible to diagnose the status of SLN with a high degree of accuracy and can be comparable in effectiveness with the isotopic method. The specificities of lymphatic drainage were found out with the use of fluorescence lymphography: inverse dependence of the lymphatic drainage rate on the body mass index and breast size, and absence of dependence on degree of ptosis of breast.

Keywords: breast cancer, sentinel lymph node biopsy, fluorescence lymphography, indocyanine green.

For citations: Zikiryakhodzhaev A.D., Saribekyan E.K., Bagdasarova D.V., Malishava L.E., Usov F.N., Starkova M.V. Sentinel lymph node biopsy for breast cancer using indocyanine green fluorescence visualization, *Biomedical Photonics*, 2019, vol. 8, no. 4, pp. 4–10. (in Russian) doi: 10.24931/2413–9432–2019–8–4–4–10

Contacts: Bagdasarova D.V., e-mail: dasha.bagdasarova@gmail.com

БИОПСИЯ СТОРОЖЕВОГО ЛИМФАТИЧЕСКОГО УЗЛА ПРИ РАКЕ МОЛОЧНОЙ ЖЕЛЕЗЫ С ПРИМЕНЕНИЕМ МЕТОДА ФЛУОРЕСЦЕНТНОЙ ВИЗУАЛИЗАЦИИ КРАСИТЕЛЯ ИНДОЦИАНИН ЗЕЛЕНЫЙ

А.Д. Зикиряходжаев, Э.К. Сарибекян, Д.В. Багдасарова, Л.Е. Малишава, Ф.Н. Усов, М.В. Старкова
МНИОИ им. П.А. Герцена – филиал ФГБУ «НМИЦ радиологии» Минздрава России, Москва, Россия

Резюме

В работе представлены результаты исследования биопсии сторожевого лимфатического узла (СЛУ) с помощью метода флуоресцентной визуализации красителя индоцианин зеленый. В исследование были включены 40 пациенток с раком молочной железы с распространенностью процесса cTis-2N0M0. 1 мл водного раствора красителя индоцианина зеленый вводили периареолярно внутрикожно и подкожно со стороны опухоли в дозе активного вещества 5 мг. В ближайшие минуты наблюдали движение красителя по лимфатическим путям в виде «дорожки» способом флуоресценции в инфракрасном спектре с помощью специальной камеры с передачей изображения на экран компьютера. После того, как дорожка подходила к подмышечной области и обрывалась,

производили разрез кожи и подкожной клетчатки в подмышечной области, рассекали поверхностную фасцию. Выделяли первые контрастированные лимфатические узлы. Частота выявления СЛУ составила 92,5%, из них метастазы выявлены в 20% случаях. В среднем на этап идентификации и удаления СЛУ уходило 17,6 мин. У 7 больных комбинировали применение метода флуоресцентного (краситель ICG) определения СЛУ с радиоизотопным (коллоид Технефит ^{99m}Tc) – во всех случаях идентифицировали одни и те же СЛУ. Применение лимфотропного красителя индоцианина зеленого с последующим выявлением СЛУ методом флуоресценции позволяет с высокой степенью точности диагностировать состояние СЛУ, а также сопоставимо по эффективности с изотопным методом. Выявлены особенности лимфооттока в молочной железе с помощью флуоресцентной лимфографии: обратная зависимость скорости лимфооттока от индекса массы тела и размера молочной железы, отсутствие зависимости от степени птоза железы.

Ключевые слова: рак молочной железы, биопсия сторожевого лимфатического узла, флуоресцентная лимфография, индоцианин зеленый.

Для цитирования: Зикиряходжаев А.Д., Сарибекян Э.К., Багдасарова Д.В., Малишава Л.Е., Усов Ф.Н., Старкова М.В. Биопсия сторожевого лимфатического узла при раке молочной железы с применением метода флуоресцентной визуализации красителя индоцианин зеленый // Biomedical Photonics. – 2019. – Т. 8, № 4. – С. 4–10. doi: 10.24931/2413–9432–2019–8–4–4–10

Контакты: Багдасарова Д.В., e-mail: dasha.bagdasarova@gmail.com

Introduction

Sentinel lymph node biopsy is an objective diagnostic criterion that allows for assessing the extent of the malignant process and plays a key role in the treatment of patients with early breast cancer [1]. The "sentinel" lymph node (SLN) is the node that is the first on the path of lymph outflow from the organ under investigation; the term was introduced by L. R. Braithwaite, a British scientist, in 1923 [2]. The presence or absence of metastases in it determines the required scope of lymphodissection. The absence of metastasis in the SLN makes it possible to predict the absence of metastases in the remaining lymph nodes of the axillary and subclavian tissue in more than 90% of cases, and not to perform a full regional lymphadenectomy, a surgery that often results in complications such as long-term lymphorrhea, secondary infection, lymphedema of the arm, impaired limb function and the development of post-mastectomy syndrome [3, 4].

Currently, there are two main methods for detecting and identifying SLN, which use different lymphography techniques: the use of a radiopharmaceutical agent or fluorescent dye. These methods can be used in combination [5, 6]. The isotope method for determining SLN in breast cancer has been used since the late 1990s [7, 8]. This method is well studied and was presented in many publications, both foreign and Russian [9-13]. The method is based on the selective ability of unchanged reticular-endothelial cells of the lymph nodes to capture radionuclide-labeled colloidal particles coming with lymph from the tissue depot after their introduction. As a rule, a solution of sodium pertechnetate, ^{99m}Ts from the technetium-99m generator and lyophilizate is used, 1 ml of which is injected peritumorally or periareolarly into the tumor projection zone. To assess the state of regional lymphatic collectors and search for "sentinel" lymph nodes, scintigraphy is performed with the use of a standard tomographic gamma camera. During an intraoperative search for SLN, a portable gamma scanner (GammaFinder II, etc.) is used, with the possibility of contact detection of the radioactivity level in the lymph nodes in question. When an SLN is identified, it is removed and undergoes urgent diagnostics with the ise of histological or cytological methods [14]. The method of using a radioisotope colloid has a fairly high SLN detection rate, which varies from 91% to 97% [15]. The indicators of sensitivity, specificity, and accuracy are 83.3%, 100%, and 94%, respectively [16]. According to one of the main meta-analyses published in 2006, which included data from 8,059 patients who underwent SLN biopsy with the use of only the radioisotope method, the average SLN detection rate was 97%, and the average false-negative result was 7.4% [15]. The use of a combination of radioisotope colloid and blue dye methods led to an improvement in detection indicators (OR = 2.03, 95% CI 1.53–2.69, $P < 0.05$). And the false negative result indicator for a combination of two methods does not change significantly and is 7.5% (95% CI 4.8–11.5%) [16].

The method of determining SLN with fluorescent lymphography is relatively new: the first publication on its application appeared in 1999 [17]. SLN biopsy with the use of a fluorescent dye is a convenient and safe intraoperative method for assessing the condition of the lymph nodes, the main disadvantage of which is the rapid passage of the dye, which places great demands on the experience of the surgeon. The dye currently used is a fluorescent agent indocyanine green (ICG), the distribution of which along the lymphatic pathways is determined by fluorescence in the infrared spectrum of radiation. In a meta-analysis published by T. Sugie et al. in 2016, it was confirmed that the accuracy indicators for determining SLN with the use of the ICG method and the method with a radioisotope colloid do not differ [18].

In Russia, a minor-scale experience of the use of ICG is represented by the work of S. M. Portnoy et al. The study included 81 patients with stage 0–III breast cancer. SLNs were detected in 75 patients (93%) and not found in 6 observations. In the first group, which included 8 patients with breast cancer cTisN0M0, SLN was found in 7, all of them without metastatic lesions. In the second group, which included 56 patients with cT1–4N0M0 breast cancer, SLN was detected in 54 (96%) patients, among which metastases in the SLN were detected in 15 (28%) cases. A false negative result was obtained in 2 (4%) out of 54 cases. In the third group, consisting of 17 patients with cT1–4N1–3M0 breast cancer after effective systemic therapy with undetectable regional metastases, SLN was detected in 14 (82%) patients, while in 5 (36%) cases metastases were detected in the SLN. False-negative results were found in 2 (14%) of 14 patients. The fluorescence was performed with the Photo dynamic eye camera (Hamamatsu, Japan) [19].

In this study, we have explored the possibility of determining SLN with the technique of fluorescent lymphography based on the indocyanin green dye and SPY 2000 device. The difference between the method used and other systems of fluorescent intraoperative navigation is the use of a laser radiation source operating in a narrow-band range of 805 nm at the peak of absorption of fluorescent contrast.

Research and biopsy of the sentinel lymph node is currently a necessary procedure in the treatment and diagnostic process, which corresponds to international clinical recommendations (NCCN, ESSMO, etc.), as well as the recommendations of the Association of Oncologists of Russia. The use of fluorescent lymphography with dye has a significant advantage over the isotope method as it does not involve the risks of radiation, and there is also no need to comply with the numerous standards and conditions or to bear the costs related to the materials and technology as it is required when working with radio sources.

Materials and methods

The study involved 40 patients, including 7 people with cTisN0M0 process prevalence, 20 people with cT1N0M0, 13 people with cT2N0M0. The patients' age ranged from 34 to 80 years, averaging 52.8. The body mass index (BMI) was calculated by the formula: BMI = m/h^2, where m is the patient's body weight (kg), h is the patient's(m). BMI values were determined according to the generally accepted scale: the normal BMI range is 18.5-25 kg/m^2, 25-29.9 kg/m^2 means the person is overweight, 30-34.9 kg/m^2 is I degree of obesity; 35-39.9 kg/m^2 is II degree of obesity; more than 40 kg/m^2 is III degree of obesity. The body mass index of the patients included in the study ranged from 18.0 to 38.9, with the body mass deficit registered in 2 people, the normal weight in 21, 10 of the women were overweight, and obesity of I-III degree was observed in 7 women in the sample. In terms of the size of the mammary glands (by bra number), the distribution of the women was as follows: 12 women with small breast size (No. 1, 2), 22 women with medium size (No. 3, 4), and 6 women with large size (No. 5, 6). As the first stage of treatment, all patients underwent organ-preserving surgery or subcutaneous mastectomy with endoprosthesis reconstruction, with SLN biopsy. Indocyanine green (ICG) was used as a staining agent. The agent emits fluorescent radiation when exposed to light in the near-infrared range of about 820 nm. The dye is supplied in a 25 mg bottle.

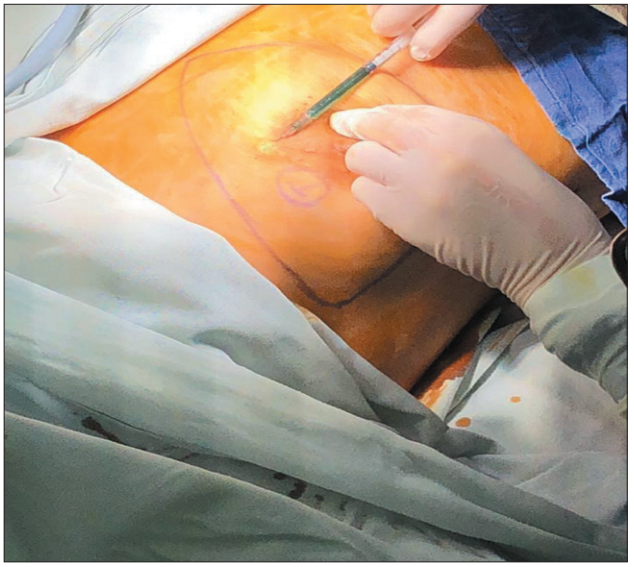

Рис. 1. Периареолярное введение раствора индоцианина зеленого
Fig. 1. Periareolar injection of Indocyanine green

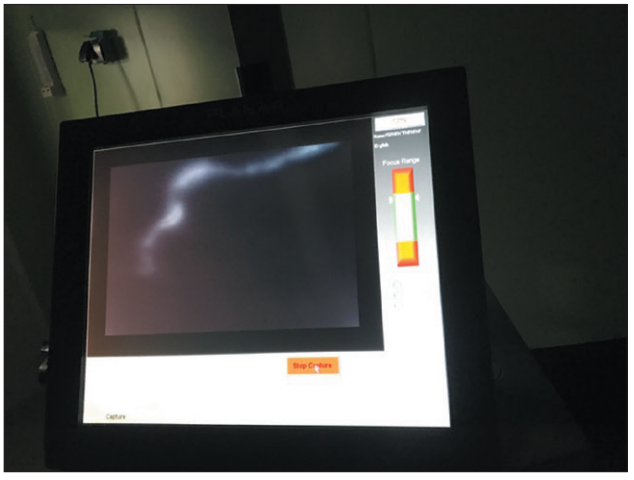

Рис. 2. Флуоресцентная «дорожка» на экране аппарата SP-2000
Fig. 2. Fluorescent "trace" on the screen of SP-2000

Before the procedure, the contents of the vial were dissolved in 5 ml of water for injection. Next, a G30 thickness needle was used to draw 1 ml of the resulting solution into a U100 insulin syringe. After the patient was put under general anaesthetic, 1 ml of ICG solution (5 mg/ml) was administered periareolarly, subcutaneously (Fig. 1). Then, for 10 seconds, manual massage of the breast was performed (5-7 circular movements) at the injection site, which provided an increase in pressure in the tissues and contributed to faster penetration of the drug into the lymphatic vessels. A few minutes later, with the operating room light turned off, the dye movement along the lymphatic pathways was detected by fluorescence in the infrared spectrum, which was achieved with a laser radiation source with a wavelength of 805 nm, SPY 2000 device (Novadaq Technologies Inc., Canada) with a special camera, which made it possible to see the image of the fluorescent "track" on a computer screen (Fig. 2). After the "path" approached the axillary area and broke off, an incision of the skin and subcutaneous tissue was made in the projection of the "break" in the axillary area, the superficial fascia was dissected, and contrasted lymph nodes were isolated with surgical instruments (Fig. 3, 4). The isolated lymph nodes were removed and cut along the length in 2-3 parallel planes, depending on their size (Fig. 5). Scrapings were taken from the surfaces of lymph nodes and placed on the slides, stained with hematoxylin-eosin, followed by an urgent cytological study, the results of which resolved the question of whether to perform lymphodissection. Upon detection of metastases, regional (axillary) lymph node dissection was performed . A revision of cellular tissue of the subclavian zone was performed. In the absence of suspicious areas, the subclavian tissue with lymph nodes was preserved. Statistical processing of the obtained results was performed by STATISTICA supplied by StatSoft, Inc. (2014).

Results

The method of determining the SLN with ICG agent was used on 40 patients. The rate of SLN detection was 92.5% of the cases (37 patients) ($p<0.0047$). Metastases were detected in 20% of cases (8 patients) ($p<0.0016$), of which in 6 cases, as a result of urgent intraoperative cytological examination, in 2 cases, by planned histological examination (false negative result). All patients identified with metastasis underwent level I or II lymph node dissection. The metastatic focus looked like a whitish area on the green plane of the stained lymph node. In 4 observations (10%), the dye fluorescence was present not only in the SLN, but also in the usual area of axillary cellular tissue. Skin pigmentation at the site of dye administration remained from several hours to 2 days. No local or general reactions were observed. On average, it took 17.6 minutes to identify and remove the SLN, and the time was further reduced due to sufficient practice

Рис. 3. Разрез кожи и подкожно-жировой клетчатки в аксиллярной области
Fig. 3. Skin and subcutaneous tissue incision in axillary area

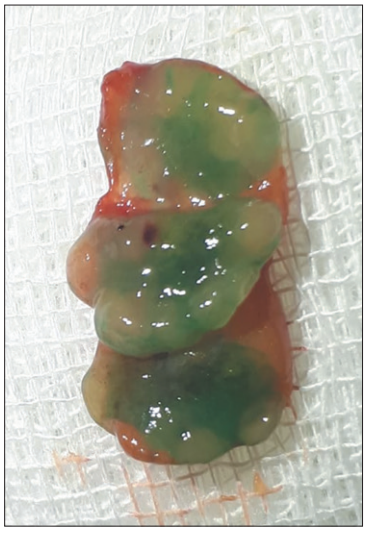

Рис. 4. Сторожевой лимфатический узел с накопленным индоцианином зеленым
Fig. 4. Sentinel lymph node with accumulated Indocyanine green

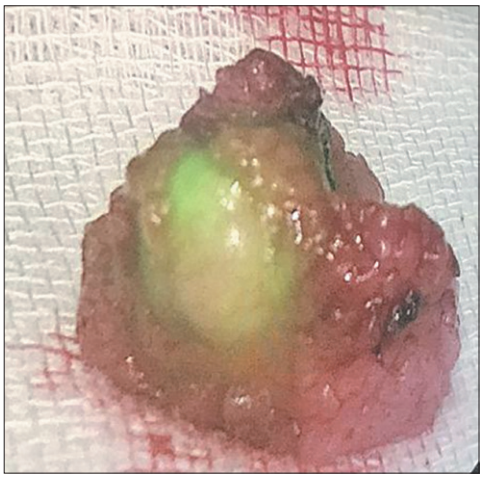

Рис. 5. Сторожевой лимфатический узел на разрезе
Fig. 5. Dissected sentinel lymph node

with the technique. The waiting period for an urgent cytological response was 15-20 minutes. Special attention was paid to the time of the appearance and development of the "track" of the dye movement. In the vast majority of cases (92%), the dye was distributed along a single radial main path running in the direction from the areola to the area of the axillary collector. A rare finding was a reticular type of lymph outflow (4%) with a dominant direction to the axillary area.

In 3 (7.5%) observations, it was not possible to trace the path of the lymph flow due to the absence of a dominant pathway. Of these, in 1 case, a marked SLN was detected, despite the absence of a dye path leading to it. In one more observation, the fluorescent focus in the axillary region was found to be a section of axillary fiber without a lymph node. The distance from the ICG injection site to the axillary area varied from 9 to 24 cm, with an average of 15.2 cm. In 65% of the observations, the track developed and reached the axillary area within 2 to 6 minutes. The maximum time was 21 minutes. The rate of ICG spread had an inverse correlation with the body mass index (6.1 minutes for the normal BMI versus 8.3 minutes for overweight persons) and the size of the breast ($p<0.005$), and demonstrated almost no dependence of the path length, i. e., the distance from the areola to the axillary area and the degree of breast ptosis. In other words, ICG was slower to reach and accumulate in women with excessive fat development, i.e. in cases where a less developed lymphatic drainage system can be expected. In 8 randomly selected patients, for the purpose of double simultaneous control, the use of the fluorescent (ICG dye) method for determining SLN was combined with the use of a radioisotope (Technefit ^{99m}Tc colloid). The same SLNs were identified in all the observations. In one case, it was not possible to identify the SLN, since no accumulation of either radiopharmaceutical or dye was detected. This case is of particular interest, as it further confirms the objectivity and comparability of both methods for determining SLN.

Discussion

The high accuracy of SLN determination with a fluorescent dye makes the technique the method of choice. A significant advantage of ICG in comparison with the more common alternative radioisotope method is the absence of radioactivity and a simpler procedure, as it is not necessary to comply with many standards established by the sanitary and epidemiological authorities, such as the use of a special room, protective aprons for personnel, etc. A disadvantage is the need to strictly follow the sequence of stages of the operation: a separate incision has to be made in the projection of the suspected SLN, since damage to the lymphatic pathways before they flow into the SLN will cause rapid diffuse staining of tissues making it impossible to identify the SLN. Moreover, for the detection of an isotope preparation by the sensor, the depth of the SLN occurrence is practically unimportant. When ICG is used, the overdeveloped subcutaneous fat layer in the axillary area requires the surgeon to work in the required speed mode, as slowing down results in the risk of staining the remaining non-sentinel lymph nodes, which seriously hinders identification of the true SLN. Taking into account the high accuracy of both fluorescent lymphography (92.5%) and radioisotope methods of SLN identification (91-97% according to the literature), we do not believe it is practical to combine them, due to the complexity and lengthening of the procedure, not to mention a significant increase in the cost of the use of a combination of the two methods.

Conclusion

The use of the lymphotropic dye indocyanin green for the detection of SLN by fluorescence in the infrared range allows for a high degree of accuracy in the diagnosis of the condition of SLN, and is comparable in efficiency to the isotope method in the group of patients without excess weight. A limitation is the superficial visualization of the lymph flow pathways, which makes it difficult or impossible to apply the technique in a methodically accurate way in overweight patients.

It is also worth noting that the use of the fluorescent lymphography method allowed us to study the specifics of lymph outflow in the mammary glands depending on some clinical and constitutional parameters, this data being absent in the world literature.

REFERENCES

1. Lyman G.H., Somerfield M.R., Bosserman L.D., Perkins C.L., Weaver D.L., Giuliano A.E. Sentinel Lymph Node Biopsy for Patients With Early-Stage Breast Cancer: American Society of Clinical Oncology Clinical Practice Guideline Update, *J Clin Oncol*, 2017, vol. 35(5), pp. 561–564.
2. Braithwaite L.R. The flow of lymph from the ileocaecal angle, and its possible bearing on the cause of duodenal and gastric ulcer, *Br J Surg*, 1923, vol. 11, pp. 7–26.

ЛИТЕРАТУРА

1. Lyman G.H., Somerfield M.R., Bosserman L.D., et al. Sentinel Lymph Node Biopsy for Patients With Early-Stage Breast Cancer: American Society of Clinical Oncology Clinical Practice Guideline Update // J Clin Oncol. – 2017. – Vol. 35(5). – P. 561–564.
2. Braithwaite L.R. The flow of lymph from the ileocaecal angle, and its possible bearing on the cause of duodenal and gastric ulcer // Br J Surg. – 1923. – Vol. 11. – P. 7–26.

3. Shaw J.H., Rumball E.M. Complications and local recurrence following lymphadenectomy, *Br J Surg*, 1990, vol. 77, pp. 760–764.
4. Kissin M.W., Querci della Rovere G., Easton D., Westbury G. Risk of lymphedema following the treatment of breast cancer, *Br J Surg*, 1986, vol. 73, pp. 580–584.
5. Schaafsma B.E., Verbeek F.P., Rietbergen D.D., van der Hiel B., van der Vorst J.R., Liefers G.J., Frangioni J.V., van de Velde C.J., van Leeuwen F.W., Vahrmeijer A.L. Clinical trial of combined radio- and fluorescence-guided sentinel lymph node biopsy in breast cancer, *Br J Surg*, 2013, vol. 100(8), pp. 1037–1044.
6. Ballardini B., Lissidini G., Veronesi P. The indocyanine green method is equivalent to the (99m) Tc-labeled radiotracer method for identifying the sentinel node in breast cancer: A concordance and validation study, *Fluorescence Imaging for Surgeons: Concepts and Applications*, 2015, vol. 39(12), pp. 255–266.
7. Giuliano A.E., Kirgan D.M., Guenther J.M., Morton D.L. Lymphatic mapping and sentinel lymphadenectomy for breast cancer, *Ann Surg*, 1994, Vol. 220(3), pp. 391–8.
8. Krag D.N., Weaver D.L., Alex J.C., Fairbank J.T. Surgical resection and radiolocalization of the sentinel lymph node in breast cancer using a gamma probe, *Surg Oncol*, 1993, vol. 2(6), pp. 335–9.
9. Dashyan G.A., Krivorot'ko P.V., Novikov S.N. *Biopsiya signal'nyh limfaticheskih uzlov pri rake molochnoy zhelezy: uchebno-metodicheskoe posobie dlya obuchayushchihsya v sisteme vysshego i dopolnitel'nogo professional'nogo obrazovaniya* [Signal lymph node biopsy for breast cancer: teaching aid for students in higher and continuing professional education]. Sankt-Peterburg, NII onkologii im. N.N. Petrova Publ., 2015. 44 p.
10. Starkova M.V., Zikiryahodzhaev A.D., Grushina T.I., Surkova V.S., Slavnova E.N., Leont'ev A.V. Diagnostic significance of sentinel lymph node biopsy in patients with early breast cancer, *Onkologiya. Zhurnal im. P.A. Gertsena*, 2019, vol. 8, no. 6, pp. 422–427. (in Russian)
11. Ashikaga T., Krag D.N., Land S.R., Julian T.B., Anderson S.J., Brown A.M., Skelly J.M., Harlow S.P., Weaver D.L., Mamounas E.P., Costantino J.P., Wolmark N. Morbidity results from the NSABP-B32 trial comparing sentinel lymph node dissection versus axillary dissection, *J Surg Oncol*, 2010, vol. 102(2), pp. 111–18.
12. Bergkvist L., Frisell J., Liljegren G., Celebioglu F., Damm S., Thörn M. Multicentre study of detection and false-negative rates in sentinel node biopsy for breast cancer, *Br J Surg*, 2001, vol. 88(12), pp. 1644–1648.
13. Edge J., Lloyd N., van der Velde C., Whittaker J. Sentinel lymph node biopsy: An audit of intraoperative assessment after introduction of a cytotechnology service, *South African Journal of Surgery*, 2015, vol. 53(2), p. 47.
14. Ermakov A.V., Zikiryahodzhaev A.D., Saribekyan E.K., Ablitsova N.V., Usov F.N. Biological conceptualization of the sentinel lymph node (Literature review), *Zlokachestvennye opuholi*, 2016, vol. 4, pp. 5–13. (in Russian)
15. Kim T., Giuliano A.E., Lyman G.H. Lymphatic mapping and sentinel lymph node biopsy in early-stage breast carcinoma: a meta-analysis, *Cancer*, 2006, vol. 106(1), pp. 4–16.
16. He P.S., Li F., Li G.H., Guo C., Chen T.J. The combination of blue dye and radioisotope versus radioisotope alone during sentinel lymph node biopsy for breast cancer: A systematic review, *BMC Cancer*, 2016, vol. 16, pp. 107.
17. Motomura K., Inaji H., Komoike Y., Kasugai T., Noguchi S., Koyama H. Sentinel node biopsy guided by indocyanine green dye in breast cancer patients, *Jpn J Clin Oncol*, 1999, vol. 29(12), pp. 604–607.

3. Shaw J.H., Rumball E.M. Complications and local recurrence following lymphadenectomy // Br J Surg. – 1990. – Vol. 77. – P. 760–764.
4. Kissin M.W., Querci della Rovere G., Easton D., Westbury G. Risk of lymphedema following the treatment of breast cancer // Br J Surg. – 1986. – Vol. 73. – P. 580–584.
5. Schaafsma B.E., Verbeek F.P., Rietbergen D.D., et al. Clinical trial of combined radio- and fluorescence-guided sentinel lymph node biopsy in breast cancer // Br J Surg. – 2013. – Vol. 100(8). – P. 1037–1044.
6. Ballardini B., Lissidini G., Veronesi P. The indocyanine green method is equivalent to the (99m) Tc-labeled radiotracer method for identifying the sentinel node in breast cancer: A concordance and validation study // Fluorescence Imaging for Surgeons: Concepts and Applications. – 2015. – Vol. 39(12). – P. 255–266.
7. Giuliano A.E., Kirgan D.M., Guenther J.M., Morton D.L. Lymphatic mapping and sentinel lymphadenectomy for breast cancer // Ann Surg. – 1994. – Vol. 220(3). – P. 391–8.
8. Krag D.N., Weaver D.L., Alex J.C., Fairbank J.T. Surgical resection and radiolocalization of the sentinel lymph node in breast cancer using a gamma probe // Surg Oncol. –1993. – Vol. 2(6). – P. 335–9.
9. Дашян Г.А., Криворотько П.В., Новиков С.Н. Биопсия сигнальных лимфатических узлов при раке молочной железы: учебно-методическое пособие для обучающихся в системе высшего и дополнительного профессионального образования. – СПб.: НИИ онкологии им. Н.Н. Петрова, 2015. – 44 с.
10. Старкова М.В., Зикиряходжаев А.Д., Грушина Т.И., Суркова В.С., Славнова Е.Н., Леонтьев А.В. Диагностическая значимость биопсии сторожевого лимфатического узла у больных ранним раком молочной железы // Онкология. Журнал им. П.А. Герцена. – 2019. – Т. 8, № 6. – С. 422–427.
11. Ashikaga T., Krag D.N., Land S.R., et al. Morbidity results from the NSABP-B32 trial comparing sentinel lymph node dissection versus axillary dissection // J Surg Oncol. – 2010. – Vol. 102(2). – P. 111–18.
12. Bergkvist L., Frisell J., Liljegren G., et al. Multicentre study of detection and false-negative rates in sentinel node biopsy for breast cancer // Br J Surg. – 2001. – Vol. 88(12). – P. 1644–1648.
13. Edge J., Lloyd N., van der Velde C., Whittaker J. Sentinel lymph node biopsy: An audit of intraoperative assessment after introduction of a cytotechnology service // South African Journal of Surgery. – 2015. – Vol. 53(2). – P. 47.
14. Ермаков А.В., Зикиряходжаев А.Д., Сарибекян Э.К., Аблицова Н.В., Усов Ф.Н. Биологическая концептуализация сторожевого лимфатического узла (Литературный обзор) // Злокачественные опухоли. – 2016. – Т. 4. – С. 5–13
15. Kim T., Giuliano A.E., Lyman G.H. Lymphatic mapping and sentinel lymph node biopsy in early-stage breast carcinoma: a meta-analysis // Cancer. – 2006. – Vol. 106(1). – P. 4–16.
16. He P.S., Li F., Li G.H., et al. The combination of blue dye and radioisotope versus radioisotope alone during sentinel lymph node biopsy for breast cancer: A systematic review // BMC Cancer. – 2016. – Vol. 16. – P. 107.
17. Motomura K., Inaji H., Komoike Y., et al. Sentinel node biopsy guided by indocyanine green dye in breast cancer patients // Jpn J Clin Oncol. – 1999. – Vol. 29(12). – P. 604–607.
18. Sugie T, Ikeda T, Kawaguchi A, et al. Sentinel lymph node biopsy using indocyanine green fluorescence in early-stage breast cancer: a meta-analysis // Int J Clin Oncol. – 2017. – Vol. 22. – P. 11.
19. Портной С.М., Кузнецов А.В., Шакирова Н.М. и др. Биопсия сигнального лимфатического узла с использованием флуорес-

18. Sugie T, Ikeda T, Kawaguchi A, Shimizu A., Toi M. Sentinel lymph node biopsy using indocyanine green fluorescence in early-stage breast cancer: a meta-analysis, *Int J Clin Oncol*, 2017, vol. 22, p. 11.
19. Portnoy S.M., Kuznetsov A.V., Shakirova N.M., Kozlov N.A., Maslyaev A.V., Karpov A.V., Kampova-Polevaya E.B., Mistakopulo M.G., Egorov Yu.S., Anurova O.A., Shendrikova T.A., Gornostaeva A.S. Signal lymph node biopsy using fluorescence lymphography in patients with breast cancer. Methodological features, *Onkoginekologiya,* 2017, no. 1(21), pp. 11–18. (in Russian)

центной лимфографии у больных раком молочной железы. Методические особенности // Онкогинекология. – 2017. – № 1(21). – С. 11–18.

MICROBIOLOGICAL STUDY OF THE EFFICIENCY OF ROOT CANAL TREATMENT WITH ER:YAG LASER

Razumova S.N., Brago A.S., Barakat H.B., Kozlova Yu.S., Velichko E.V., Vasiliev Yu.L.
Peoples Friendship University of Russia (RUDN university), Moscow, Russia

Abstract

Mechanical and drug treatment of the root canal are the most important components of the success of endodontic treatment. This work presents the results on the effectiveness of the root canal disinfection using an erbium laser in combination with a 17% solution of ethylenediaminetetraacetic acid (EDTA) in vitro and in clinical studies. An in vitro study was carried out on removed intact teeth infected with strains of Enterococcus faecalis, Streptococcus sanguinis, and Candida albicans. An experimental group of teeth was treated medically according to a standard protocol using 3% solution of sodium hypochlorite and 17% solution of EDTA followed by irradiation with erbium laser. The control group was treated similarly but without laser irradiation. The treatment effectiveness was evaluated by the reduction of CFU. After the treatment, in the control group after the mechanical and drug treatment, the CFU amount lowered by 4 times, while the complete sterilization was observed in the experimental group. The clinical studies included two groups of 35 patients each diagnosed with chronic periodontitis. In the experimental group of patients, at the final stage, treatment with erbium laser for 1 min using endodontic piece (40 mJ power, 2940 nm wavelength, 10 Hz pulse rate) and a 17% EDTA solution was performed before filling. Periodontitis treatment in the control group was carried out without the laser treatment. The control group of patients saw the reduction on CFU after the mechanical and drug treatment by 3–6 times, while the experimental group achieved the complete sterilization of the root canals. The obtained results prove that the modification of the root canal treatment by the inclusion of erbium laser irradiation is a promising direction in endodontics.

Keywords: erbium laser (Er:YAG), laser-activated irrigation, endodontic treatment, microbiological study, root canal.

For citations: Razumova S.N., Brago A.S., Barakat H.B., Kozlova Yu.S., Velichko E.V., Vasil'ev Yu.L. Microbiological study of the efficiency of root canal treatment with Er:YAG laser, *Biomedical Photonics*, 2019, vol. 8, no. 4 , pp. 11–16 (in Russian). doi: 10.24931/2413– 9432–2019–8–4–11–16

Contacts: Razumova S.N., e-mail: razumova_sv@mail.ru

МИКРОБИОЛОГИЧЕСКОЕ ИССЛЕДОВАНИЕ ЭФФЕКТИВНОСТИ ОБРАБОТКИ КОРНЕВОГО КАНАЛА ЭРБИЕВЫМ ЛАЗЕРОМ

С.Н. Разумова, А.С. Браго, Х.Б. Баракат, Ю.С. Козлова, Э.В. Величко, Ю.Л. Васильев
Российский университет дружбы народов, Москва, Россия

Резюме

Механическая и медикаментозная обработка корневого канала – важнейшие составляющие успеха эндодонтического лечения. В статье представлены результаты исследования эффективности дезинфекционной обработки корневого канала 17%-ым раствором этилендиаминтетрауксусной кислоты (ЭДТА) в сочетании с эрбиевым лазером (Er:YAG) *in vitro* и в клинических исследованиях. Исследование *in vitro* выполнено на интактных удаленных зубах, инфицированных штаммами *Enterococcus faecalis*, *Streptococcus sanguinis* и *Candida albicans*. Опытную группу зубов обрабатывали медикаментозно по стандартному протоколу с использованием 3%-го раствора гипохлорита натрия и 17%-го раствора ЭДТА с последующим облучением эрбиевым лазером. Обработку контрольной группы зубов проводили аналогичным образом, но без облучения лазером. Эффективность обработки оценивали по уменьшению титра КОЕ. В контрольной группе титр КОЕ после механической и медикаментозной обработки снизился в 4 раза, а в опытной группе была достигнута полная стерилизация корневых каналов. В клинические исследования были включены две группы пациентов по 35 человек с диагнозом хронический пародонтит. В опытной группе пациентов на последнем этапе лечения проводили обработку корневых каналов эрбиевым лазером в течение одной минуты эндодонтической насадкой с энергией 40 мДж с длиной волны 2940 нм, при частоте импульса 10 Гц с 17%-ым раствором ЭДТА и обтурировали. В контрольной группе проводили лечение периодонтита без обработки лазером. В контрольной группе пациентов титр КОЕ после механической и медикаментозной обработки снизился в 3–6 раз, а в опытной группе была достигнута полная стерилизация корневых каналов. Полученные результаты доказывают, что модификация протокола обработки корневого канала излучением эрбиевого лазера является перспективным направлением в эндодонтии.

Ключевые слова: эрбиевый лазер (Er:YAG), лазерная обработка, эндодонтическое лечение, микробиологическое исследование, корневой канал.

Для цитирования: Разумова С.Н., Браго А.С., Баракат Х.Б., Козлова Ю.С., Величко Э.В., Васильев Ю.Л. Микробиологическое исследование эффективности обработки корневого канала эрбиевым лазером // Biomedical Photonics. – 2019. – Т. 8, № 4. – С. 11–16. doi: 10.24931/2413– 9432–2019–8–4–11–16

Контакты: Разумова С.Н., e-mail: razumova_sv@mail.ru

Introduction

The main tasks of mechanical, medical treatment and shaping of the root canal which is convenient for the chosen technique of obturation are the removal of infected dentin and disinfection of the root canal.

The existing variety of root canal treatment techniques demonstrated the lack of a universal approach to these tasks.

The main antiseptic and lubricant is a 3-5% of sodium hypochlorite. Its disadvantage is the rapid inactivation during processing and heating, which requires constant irrigation of the treated area with a new portion of the solution. In addition, hypochlorite is not active against certain forms of microorganisms, for example, *Enterococcus faecalis*. To expand the antibacterial spectrum in modern protocols, it is often recommended to use chlorhexidine 2% or calcium hydroxide in the form of pastes for temporary filling for 10-14 days. After using of calcium hydroxide, repeated treatment of the root canal with a 3% sodium hypochlorite solution is recommended, followed by washing. In addition to that, before obturation, the root canal must be treated with a 17% solution of ethylenediaminetetraacetic acid (EDTA) to remove the smear layer. Then it is needed to disinfect the canal, dry and obturate. According to various authors, the antibacterial effectiveness of this technique is 50-70% [1-3]. An increase in the effectiveness of drug treatment can be achieved by activating solutions to penetrate deeper into the infected areas of the root canal system. For this, physical methods of solution activation are used: sound, ultrasonic, hydrodynamic and laser techniques.

Experimental and clinical developments on the use of laser technologies in dentistry and in particular in endodontics have been conducted since 1988 and to date, extensive clinical experience has been gained on the use of diode lasers in the protocol for endodontic root canal treatment [4-6]. Erbium laser radiation has been used in clinical dentistry as an alternative to the mechanical method of preparing hard tooth tissues since 1997 [7, 8]. The possibilities of using Er:YAG laser radiation (2.94 μm) including the treatment of caries and its complications, sealing fissures, resection of the apex of the roots in chronic periodontitis, as well as patchwork operations in surgical periodontics [8].

The effects of traditional using of laser in endodontics are ablation of tissue remains, destruction of bacteria, and removal of the smear layer [7, 8].

For that, the aim of this research was to study the effectiveness of disinfection of the root canal with an erbium laser (Er:YAG) after standard mechanical and drug treatment of the canal.

Materials and methods

To study the effectiveness of mechanical and drug treatment of the root canal with an erbium laser, 20 intact single-rooted extracted teeth due to periodontal disease were selected for the study.

The teeth were disinfected and processed by the standard mechanical protocol (hand tools K-files, K-Reamer, H-files, machine tools profiles, M2) and drug treatment, using 3% sodium hypochlorite and 17% EDTA solution with passive ultrasonic for solutions activation. Then the teeth were sanitized in a 75% alcohol solution, washed with sterile distilled water and infected with strains of *Enterococcus faecalis, Streptococcus sanguinis* and *Candida albicans*. After incubation for 7 days, dentin scrapings were taken from the walls of the root canal. then, the teeth were prepared mechanically using hand and machine tools and medically using 3% sodium hypochlorite solution and 17% EDTA solution with passive ultrasonic activation of irrigants. After EDTA treatment, all teeth were randomly divided into two groups. In the first group, the root canals were treated with a 17% EDTA solution in combination with an erbium laser for 1 minute with an energy of 40 mJ, a wavelength of 2940 nm, and a pulse frequency of 10 Hz. The teeth of the second group were not treated with laser. Before medical treatment of the root canal and immediately after its completion, dentin scrapings were taken for microbiological examination. Dentin was taken from the walls of the root canal with a sterile H-file. Dentin samples from the root canal were placed in a transport medium. Sowing the contents of the root canal was carried out on solid nutrient media. Cultivated in an aerobic incubator (Binder, Germany) and a CO_2 incubator (Lamsystems, Russia) in accordance with the requirements for incubation conditions for various microorganisms. Quantitative assessment of the results of sowing was carried out according to the Gould method. Identification results were taken into account by MASS spectrometry (MALDI-TOF), Mylа-MC (BioMerieux, France).

To study the antibacterial properties of an erbium laser *in vivo*, 70 patients with a diagnosis of chronic peri-

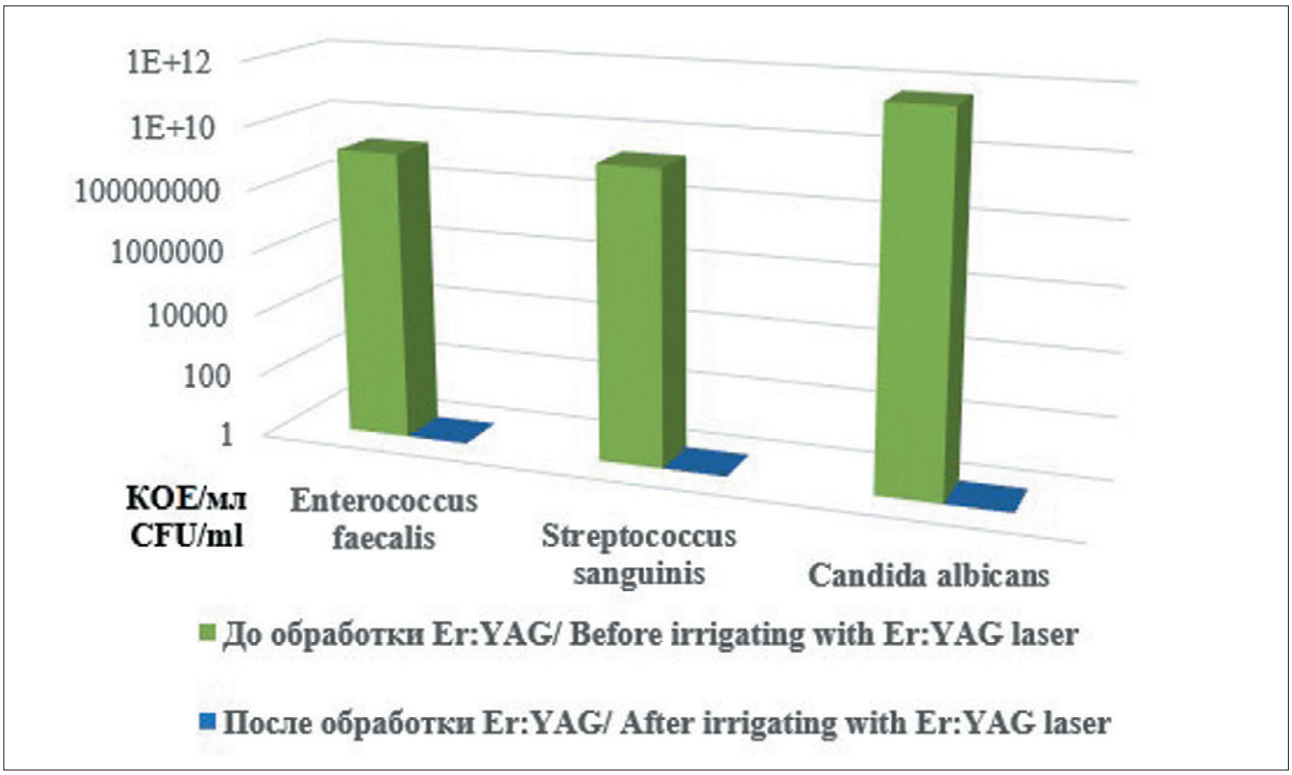

Рис. 1. Микробиологическое исследование в опытной группе на удаленных зубах с применением эрбиевого лазера в сочетании с 17%-ым раствором ЭДТА
Fig. 1. Microbiological study on group 1 extracted teeth using Er:YAG laser

odontitis (K04.5 chronic apical periodontitis. Apical granuloma) aged 35-60 years were selected. The test group consisted of 35 patients (19 women and 16 men). Endodontic treatment was performed according to standard methods. The operation field was cleaned with brushes with paste and 2% chlorhexidine solution and isolated with cofferdam. The old restoration was removed with sterile boron. Then the boron was replaced, the tooth cavity was opened, the root canals were mechanically and medically treated with manual and machine tools. Root canal irrigation was performed with 3% sodium hypochlorite with passive ultrasonic activation of the solutions. At the final stage, the canal was treated with a 17% solution of EDTA with an erbium laser for one minute using an endodontic tip, with an energy of 40 mJ, a wavelength of 2940 nm, and a pulse frequency of 10 Hz. A laser fiber was inserted into the orifice of the root canal without touching its walls. Root canal filling was performed at the same visit. The comparison group consisted of 35 (20 women and 15 men) patients who received the same root canal treatment without using an erbium laser.

Results

In the test group of extracted teeth (the group treated with erbium laser), high titers of *Enterococcus faecalis, Streptococcus sanguinis* and *Candida albicans* strains were shown before drug treatment of the root canal. After mechanical and drug treatment of the root canals with 17% EDTA in combination with erbium laser, no colonies were recorded in all tested samples. This indicates the sterilization of the root canal (Fig. 1).

In the control group of extracted teeth (treated without erbium laser), a significant decrease in the titer of *Enterococcus faecalis, Streptococcus sanguinis and Candida albicans* strains was established. After mechanical and drug treatment of the root canals on the extracted teeth, a significant decrease by 4 times in the titer of colonies of the above microorganisms was recorded ($p < 0.05$) (Fig. 2)

According to that, this *in vitro* study showed that mechanical and drug treatment of the root canal reduced the number of microorganisms to titers 10^2 and 10^3 CFU/ml and high efficiency of root canal treatment was observed when applied erbium laser for one minute, with a power of 40 mJ, and a pulse frequency of 10 Hz.

To determine the efficacy of root canal treatment with an erbium laser in clinical trial, two groups of patients with a diagnosis of chronic periodontitis (K04.5 chronic apical periodontitis. Apical granuloma) aged 35 to 60 years were included in the study. At the stages of endodontic treatment, materials were collected for microbiological examination: before and after mechanical, drug treatment of the root canal, as well as after using erbium laser.

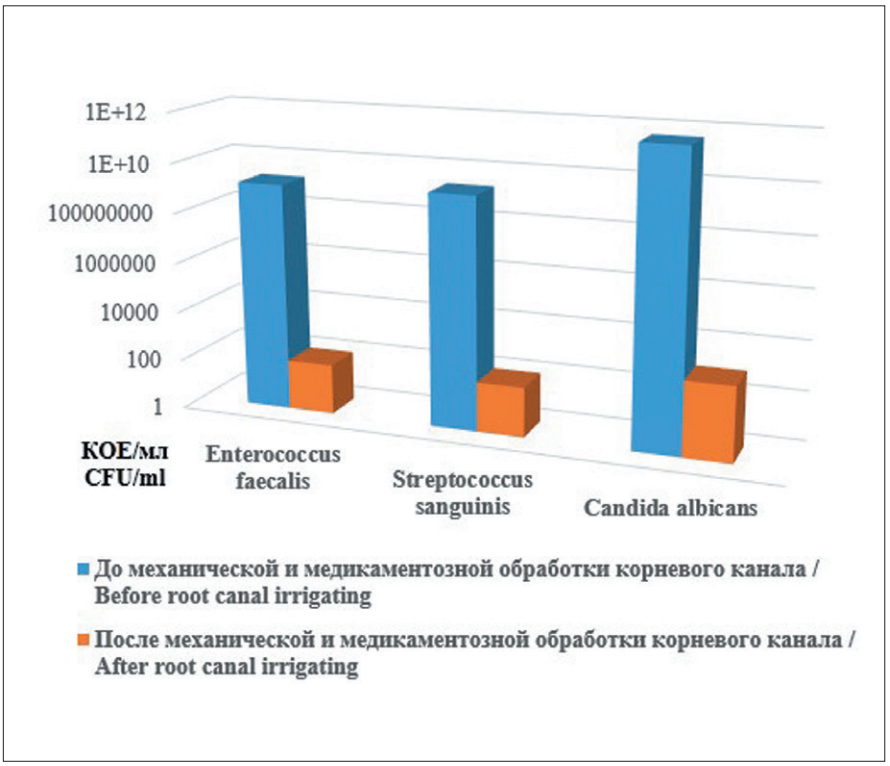

Рис. 2. Микробиологическое исследование в контрольной группе на удаленных зубах без применения эрбиевого лазера
Fig. 2. Microbiological examination in control group on extracted teeth without using ER:YAG laser

In the test group, high titers of *Enterococcus Haemolyticus, Staphylococcus epidermalis, Streptococcus mitis* and *Streptococcus mutans* from 10^5 to 10^8 cells/ml medium were observed immediately after mechanical treatment of the root canals (without drug treatment). After drug treatment of root canals, a significant decrease in the titer of microorganisms by four times to 10^2 CFU/ml was recorded ($p < 0.05$). The data was presented in Table 1. In root canals, treated with erbium laser in combination with 17% EDTA in all tested samples, colonies growth was not recorded. This indicates sterilization of the root canal.

In the control group, patients received a similar protocol for endodontic treatment and materials were collected before and after drug treatment of the root canal. The data was presented in Table 2. Before root canal treatment, as in the main group, high titers of *Enterococcus Haemolyticus, Staphylococcus epidermalis, Streptococcus mitis* and *Streptococcus mutans* from 10^5 to 10^8 CFU / ml of medium were observed. After drug treatment, a significant decrease in the titer of microorganisms to 10^2-10^3 CFU / ml ($p < 0.05$) was detected and only *Streptococcus mitis* growth was not recorded.

Discussion

The quality of drug treatment of the root canal, carried out according to the endodontic treatment protocols adopted in the Russian Federation, is not sufficient to achieve a long-term clinical effect. The modification of the protocol for treating the root canal by radiation of an erbium laser with a wavelength of 2940 nm, a power of 40 mJ, and a pulse frequency of 10 Hz showed a high quality of sterilization of the root canal. Similar results on the effect of Er, Cr: YSGG laser with a wavelength of 2780 nm were obtained in studies of T.V. Furtseva and others. [9]. Authors, L.U. Orekhova et al. [10], I.I. Malov et al. [11], S.L. Blashkova et al. [12] in their studies, it was demonstrated the high efficiency of using lasers in endodontics. Similar data to our results were published by E. Henninger et al. [13]: the authors studied the radiation efficiency of an erbium laser on strains of *Streptococcus gordonii* in combination with *Actinomyces oris* or *Fusobacterium nucleatum* and showed the effectiveness of this treatment in endodontic infections. Researchers from different countries show high efficiency of root canal treatment with both diode and erbium lasers [14-16].

Conclusion

Within the limits of this study, the efficiency of root canal treatment with an erbium laser with a wavelength of 2940 nm, energy of 40 mJ, pulse frequency of 10 Hz, and a power of 0.5–8.4 W is quite high. Modification of the irrigation protocol for endodontic treatment, in particular, chronic periodontitis K04.5, by the action of radiation from an erbium laser is an effective method and more further studies are needed in this field.

Таблица 1
Результаты микробиологического исследования основной группы пациентов на этапах эндодонтического лечения
Table 1
Results of a microbiological study of the main group of patients at various stages of endodontic treatment

Опытная группа Main group	Enterococcus Faecalis КОЕ/мл CFU/ml	Staphylococcus Haemolyticus КОЕ/мл CFU/ml	Staphylococcus epidermalis КОЕ/мл CFU/ml	Streptococcus mitis КОЕ/мл CFU/ml	Streptococcus mutans КОЕ/мл CFU/ml
До обработки канала Before irrigation	10^8	10^8	$10^5 – 10^8$	10^7-10^8	10^7
После медикамен тозной обработки канала After root canal irrigation	10^3	10^2	10^2	10^2	10^2
После медикамен тозной обработки канала и обработки лазером After root canal irrigation and Er:YAG laser	Нет роста No growth	Нет роста No growth	Нет роста No growth	Нет роста No growth	Нет роста No growth

Таблица 2
Результаты микробиологического исследования пациентов группы сравнения на этапах эндодонтического лечения
Table 2
The results of a microbiological study of the control group of patients at the stages of endodontic treatment

Контрольная группа Control group	Enterococcus Faecalis КОЕ/мл CFU, cell/ml	Staphylococcus Haemolyticus КОЕ/мл CFU, cell/ml	Staphylococcus epidermalis КОЕ/мл CFU, cell/ml	Streptococcus mitis КОЕ/мл CFU, cell/ml	Streptococcus mutans КОЕ/мл CFU, cell/ml
До обработки канала Before root canal irrigation	10^8	10^8	10^5 -10^8	10^7- 10^8	10^7
После медикаментоз ной обработки канала After root canal irrigation	10^3	10^2	10^2	Нет роста No growth	10^2
Значение критерия p P-value	0.009	0.009	0.04	0.000	0.009

REFERENCES

1. Risovannaya O.N. Study of the effect of bacteriotoxic light therapy on pathogens of inflammatory diseases of the oral cavity, *Kubanskiy nauchnyy meditsinskiy vestnik*, 2005, no. 4, pp. 25–30. (in Russian)
2. Risovannyy S.I., Risovannaya O.N. Photoactivated disinfection in endodontics, *Dental Yug*, 2006, no. 6/41, pp. 22–25. (in Russian)
3. Mitronin A.V., CHunihin A.A., Mitronin V.A., Basova A.A., Abaev Z.M. Actual technologies in endodontic treatment, *Meditsinskiy alfavit*, 2014, vol. 3., no. 13, pp. 40–43. (in Russian)
4. Manak T.N., Isapur P.N., Paliy L.I. Laser application in endodontics, *Voennaya meditsina*, 2015, no. 3 (36), pp. 127–136. (in Russian)
5. Mitronin A.V., Belyaeva T.S., Zhekova A.A. Laser technologies in the endodontic treatment of chronic apical periodontitis: a comparative assessment of antibacterial effectiveness, *Endodontiya Today*, 2016, no. 2, pp. 27–29. (in Russian)
6. Spiridonova O.I., Kupriyanova L.Yu., Nikitina M.V. Laser application in endodontics Comparative characteristic with traditional root canal treatment methods, *News of Science and Education*, 2018, vol. 6, no. 4, pp. 003–006. (in Russian)
7. Gutknecht N., Hassan N.A., Martins M.R., et al. Bactericidal effect of 445-nm blue diode laser in the root canal dentin on Enterococcus faecalis of human teeth, *Laser Dent Sci*, 2018, vol. 2, pp. 247–254.
8. Asnaashari M., Safavi N. Disinfection of Contaminated Canals by Different Laser Wavelengths, while Performing Root Canal Therapy, *Journal of Lasers in Medical Sciences*, 2013, vol. 4, no. 1, pp. 8–16.
9. Furtsev T.V., Kazanovskaya A.A., Prudnikova S.V. Comparative results of antibacterial treatment of root canals according to the standard protocol using sodium hypochlorite (NAOCL) and laser ER, CR: YSGG wavelength of 2780 nm, *Rossiyskiy stomatologicheskiy zhurnal*, 2018, vol. 22, no. 4, pp. 184–187. (in Russian)
10. Orekhova L.Yu., Porhun T.V., Vashneva V.Yu., Rubezhova E.A. Comparative analysis of the degree of mechanical cleaning of the root canal wall using various laser systems and photosensitizers, *Endodontiya Today*, 2018, no. 4, pp. 67–69. (in Russian)
11. Malov I.I., Karpunina A.V., Semenova N.V, Matveeva A.S., Yastrebova O.Yu. Comparative characteristics of modern and traditional root canal disinfection methods, *Problemy nauchnoy mysli*, 2019, vol. 5., no. 3, pp. 31–34. (in Russian)
12. Blashkova S.L., Krikun E.V., Garaev M.M. Comparative characteristics of the dentin surface of the root canal during decontamination with a diode laser depending on the irrigation solution, *Endodontiya Today*, 2018, no. 2, pp. 11–14. (in Russian)
13. Henninger E., Berto L.A., Eick S., Lussi A., Neuhaus K.W. In Vitro Effect of Er:YAG Laser on Different Single and Mixed Microorganisms Being Associated with Endodontic Infections, *Photobiomodul, Photomed Laser Surg*, 2019, vol. 37, pp. 369–375.
14. Todea D.C.M., Luca R.E., Bălăbuc C.A., Miron M.I., Locovei C., Mocuţa D.E. Scanning electron microscopy evaluation of the root canal morphology after Er:YAG laser irradiation, *Rom J Morphol Embryol*, 2018, vol. 59(1), pp. 269–275.
15. Tokuc M., Ozalp S., Topcuoglu N., Kulekci G. Bactericidal Effect of 2780 nm Er,Cr:YSGG Laser Combined with 940 nm Diode Laser in Enterococcus faecalis Elimination: A Comparative Study, *Photobiomodul Photomed Laser Surg*, 2019, vol. 37(8), pp. 489–494.
16. Dragidella A. et al. Antimicrobial efficacy of erbium laser in the endodontic treatment of infected root canals, *Romanian archives of microbiology and immunology*, 2018, vol. 77, is. 1, pp. 41–49.

ЛИТЕРАТУРА

1. Рисованная О.Н. Изучение влияния бактериотоксической светотерапии на патогенные возбудители воспалительных заболеваний полости рта // Кубанский научный медицинский вестник. – 2005. – № 4. – С. 25–30.
2. Рисованный С.И., Рисованная О.Н. Фотоактивируемая дезинфекция в эндодонтии // Дентал Юг. – 2006. – № 6/41. – С. 22–25.
3. Митронин А.В., Чунихин А.А., Митронин В.А. и соавт. Современные технологии в эндодонтическом лечении // Медицинский алфавит. – 2014. – Т. 3., № 13. – С. 40–43.
4. Манак Т.Н., Исапур П.Н., Палий Л.И. Применение лазера в эндодонтии // Военная медицина. – 2015. – № 3 (36). – С. 127–136.
5. Митронин А.В., Беляева Т.С., Жекова А.А. Лазерные технологии в эндодонтическом лечении хронического апикального периодонтита: сравнительная оценка антибактериальной эффективности // Эндодонтия Today. – 2016. – № 2. – С. 27–29.
6. Спиридонова О.И., Куприянова Л.Ю., Никитина М.В. Применение лазера в эндодонтии Сравнительная характеристика с традиционными методами лечения корневых каналов // News of Science and Education. – 2018. – Т. 6, № 4. – С. 003–006.
7. Gutknecht N., Hassan N.A., Martins M.R., et al. Bactericidal effect of 445-nm blue diode laser in the root canal dentin on Enterococcus faecalis of human teeth // Laser Dent Sci. – 2018. – Vol. 2. – P. 247–254.
8. Asnaashari M., Safavi N. Disinfection of Contaminated Canals by Different Laser Wavelengths, while Performing Root Canal Therapy // Journal of Lasers in Medical Sciences. – 2013. – Vol. 4, No. 1. – P. 8–16.
9. Фурцев Т.В., Казановская А.А., Прудникова С.В. Сравнительные результаты антибактериальной обработки корневых каналов по стандартному протоколу с применением гипохлорита натрия (NAOCL) Ии лазера ER, CR: YSGG длиной волны 2780 НМ // Российский стоматологический журнал. – 2018. – Т. 22, № 4. – С. 184–187.
10. Орехова Л.Ю., Порхун Т.В., Вашнева В.Ю. и соавт. Сравнительный анализ степени механической очистки стенки корневого канала при использовании различных лазерных систем и фотосенсибилизаторов // Эндодонтия Today. – 2018. – № 4. – С. 67–69.
11. Малов И.И., Карпунина А.В., Семенова Н.В. и соавт. Сравнительная характеристика современных и традиционных методов дезинфекции корневого канала // Проблемы научной мысли. – 2019. – Т. 5., № 3. – С. 31–34.
12. Блашкова С.Л., Крикун Е.В., Гараев М.М. Сравнительные характеристики поверхности дентина корневого канала при деконтаминации диодным лазером в зависимости от ирригационного раствора // Эндодонтия Today. – 2018. – № 2. – С. 11–14.
13. Henninger E., Berto L.A., Eick S., et al. In Vitro Effect of Er:YAG Laser on Different Single and Mixed Microorganisms Being Associated with Endodontic Infections // Photobiomodul, Photomed Laser Surg. – 2019. – Vol. 37. – P. 369–375.
14. Todea D.C.M., Luca R.E., Bălăbuc C.A., et al. Scanning electron microscopy evaluation of the root canal morphology after Er:YAG laser irradiation // Rom J Morphol Embryol. – 2018. – Vol. 59(1). – P. 269–275.
15. Tokuc M., Ozalp S., Topcuoglu N., Kulekci G. Bactericidal Effect of 2780nm Er,Cr:YSGG Laser Combined with 940nm Diode Laser in Enterococcus faecalis Elimination: A Comparative Study // Photobiomodul, Photomed Laser Surg. – 2019. – Vol. 37(8). – P. 489–494.
16. Dragidella A. et al. Antimicrobial efficacy of erbium laser in the endodontic treatment of infected root canals // Romanian archives of microbiology and immunology. –2018. – Vol. 77, Is. 1. – P. 41–49.

A DIFFUSION EQUATION BASED ALGORITHM FOR DETERMINATION OF THE OPTIMAL NUMBER OF FIBERS USED FOR BREAST CANCER TREATMENT PLANNING IN PHOTODYNAMIC THERAPY

Ismael F.S.[1], **Amasha H.M.**[1, 2], **Bachir W.H.**[1, 3]
[1]Damascus University, Damascus, Syria
[2]Syrian Private University, Damascus, Syria
[3]Al-Sham Private University, Damascus, Syria

Abstract

It is essential in interstitial Photodynamic therapy (iPDT) treatment planning to ensure a homogeneous distribution within a tumor volume using cylindrical diffusing fibers while keeping the surrounding tissue intact. Light distribution is simulated through two algorithms based on the diffusion equation assuming diffusers as light sources. The first algorithm analyzes the diffusion equation and studies the effects of different variables (optical properties, delivered power, diffuser length, and position). Next, optical properties of breast were applied to estimate the volume that receives accepted light dose from one diffuser. In the second algorithm, multiple diffusers were simulated in order to find the relation between the volume and the number of required diffusers which are needed to cover cubical or cylindrical volume with sufficient light dose. Throughout this study, real values of optical properties, clinical laser power, and treatment time were considered to evaluate sufficient light doses. This study is in agreement with previous works in that optical properties are the major factors influencing light distribution in iPDT. It is shown that for a homogeneous phantom mimicking breast cancer and cubical or cylindrical shape, the number of required fibers N equal W×L or D^2 respectively.

Keywords: iPDT, diffusion equation, cylindrical diffuser fiber, sufficient light dose, breast cancer.

For citations: Ismael F.S., Amasha H.M., Bachir W.H. A diffusion equation based algorithm for determination of the optimal number of fibers used for breast cancer treatment planning in photodynamic therapy, *Biomedical Photonics*, 2019, vol. 8, no. 4, pp. 17–27. doi: 10.24931/2413–9432–2019–8–4–17–27

Contacts: Ismael F.S., e-mail: fatimah.esm@gmail.com

АЛГОРИТМ ОПРЕДЕЛЕНИЯ ОПТИМАЛЬНОГО ЧИСЛА ВОЛОКОН ИСПОЛЬЗУЕМЫХ ПРИ ВНУТРИТКАНЕВОЙ ФОТОДИНАМИЧЕСКОЙ ТЕРАПИИ РАКА МОЛОЧНОЙ ЖЕЛЕЗЫ НА ОСНОВАНИИ ДИФФУЗИОННОГО УРАВНЕНИЯ

Ismael F.S.[1], **Amasha H.M.**[1, 2], **Bachir W.H.**[1, 3]
[1]Университет Дамаска, Дамаск, Сирия
[2]Частный университет Сирии, Дамаск, Сирия
[3]Частный университет Аль-Шам, Дамаск, Сирия

Резюме

При планировании внутритканевой фотодинамической терапии (iPDT) с использованием цилиндрических диффузных волокон важно обеспечить однородное распределение света по всему объему опухоли, сохранив при этом целостность окружающей ткани. Авторы данной статьи смоделировали распределение света с помощью двух алгоритмов, основанных на уравнении диффузии, в которых в качестве источников света используются цилиндрические диффузоры. Первый алгоритм анализирует уравнение диффузии и изучает влияние различных переменных (оптических свойств источника, применяемой мощности, длины диффузора и его положения). Затем были использованы параметры оптических свойств молочной железы для оценки объема, который рассчитывает световую дозу от одного диффузора. Во втором алгоритме было смоделировано несколько рассеивателей для нахождения соотношения между объемом и количеством рассеивателей, необходимых для покрытия кубического или цилиндрического объема достаточной световой дозой. На протяжении всего этого исследования рассматривались реальные значения оптических свойств, клинической мощности лазера и времени лечения для оценки достаточных световых доз. Это исследование согласуется

с предыдущими работами в том, что оптические свойства являются основными факторами, влияющими на распределение света при iPDT. Показано, что, для однородного фантома, имитирующего рак молочной железы, кубической или цилиндрической формы, количество требуемых волокон N равно W×L или D^2, соответственно.

Ключевые слова: внутритканевая фотодинамическая терапия, уравнение диффузии, волокно с цилиндрическим диффузором, достаточная световая доза, рак молочной железы.

Для цитирования: Ismael F.S., Amasha H.M., Bachir W.H. A diffusion equation based algorithm for determination of the optimal number of fibers used for breast cancer treatment planning in photodynamic therapy // Biomedical Photonics. – 2019. – Т. 8, № 4. – С. 17–27. doi: 10.24931/2413–9432– 2019–8–4–17–27

Контакты: Ismael F.S., e-mail: fatimah.esm@gmail.com

Introduction

Photodynamic therapy (PDT) combines a light sensitive compound (photosensitizer) with light to generate reactive oxygen species, which, in sufficient quantities, lead to tissue destruction [1]. The development of photoactive compounds that absorb light at longer wavelengths, with greater penetration in tissue, has led to the development of treatments for larger, deep-seated tumors [2].

The diffusion approximation to modeling light transport works well for biological tissues at near-infrared PDT treatment wavelengths, where light scattering dominates over absorption. In addition, numerical solution of the diffusion equation, as used here, allow for the modeling of light transport in systems with time frames that are feasible for clinical application. Also, diffusion theory enables quick estimation of the fluence rate distribution in a homogeneous medium [3].

Recently, computer simulations suggested that cylindrical diffusing fibers (CDFs) are more effective than flat-cut fibers in delivering the therapeutic light in iPDT especially for bulky tumors [4, 5]. B. Farina et al. [6] simulated cylindrical diffuser as linear array of ideal point sources to extract fluence rate distribution in hollow organ. Baran and Foster [7] used GPU for simulation. They modeled the diffuser based on TiO_2 particles. This model predicts a fluence distribution similar to that modeled by B Farina et al. They compared the radial degradation of fluence from the diffuser for both models and demonstrated that a model based on a linear of point sources is sufficient for determining fluence distribution. Baran and Foster in Ref [5], used the same diffuser modeled by them to make comparison between numbers of cylindrical diffusing fibers and flat cleaved ones.

A number of research groups have focused their efforts on optimizing the fiber placements. T.M. Baran et al. [5] demonstrated optimization of six CDFs positions in order to create treatment plans for iPDT of (6.1×7.5×7 cm) in brain. M.D. Altschuler et al. [8] used twelve CDFs in (2.5×3×5 cm). E. Oakley et al. [9] also demonstrated a treatment plan using finite element method and eleven CDFs to deliver an accepted light dose to (5×4×4 cm) in head and neck cancer. Those studies did not indicate to the ability of single CDF to deliver accepted light doses around it. In the current study, benefits from analyzing the diffusion equation were taken to determine the whole volume with optical properties of breast cancer that has accepted light dose of all its points. This simulation study contains two codes which are regarded as important prior steps for practical procedure that we are planning to do in the laboratory. First code provides programming description of single CDF using diffusion equation. Four available CDFs in the laboratory were simulated in the second code. Results of this study clarifies interaction between external laser power, CDF length and medium optical properties and how it could be useful to determine the required number and full length of fiber tip to cover full volume with suitable fluence rate.

Materials and Methods

Tissue model and software algorithm

Following diagrammatic analysis of equation 2 assumes a cube (5^3 cm^3), divided into fractional (0.5^3 cm^3) cubes, fractional cubes could be smaller if requested. CDF position is the central cube (x, y, z) = (2.5, 2.5, 5). While assuming that the decrement of CDF length starts from the top surface of the cube, the coordinate (z) must be equal to the full length of the corresponding cube. Figure 1 represents the tissue model. The core of the PDT treatment planning simulation is the calculation of the light intensity (fluence rate) distribution in tissue generated by a CDF. Therefore, first code is made as flexible as to calculate the fluence rate $\varphi(r)$ as a function of each variable (h, l, s, μ_{eff}, μ_a) independently in every point (pixel) in the cube. The second code allows choosing CDFs number (maximum is four). In addition to changing l, s, μ_{eff}, μ_a, t, *volume* and *distance between pixels*. Figure 2 displays the schematic of the codes. The light distribution, diffusion equation and tissue model were modeled in Matlab (2016a).

Throughout the paper, each observing point receives N rays. N represents the number of source points along the CDF. The points located at equal distances away from

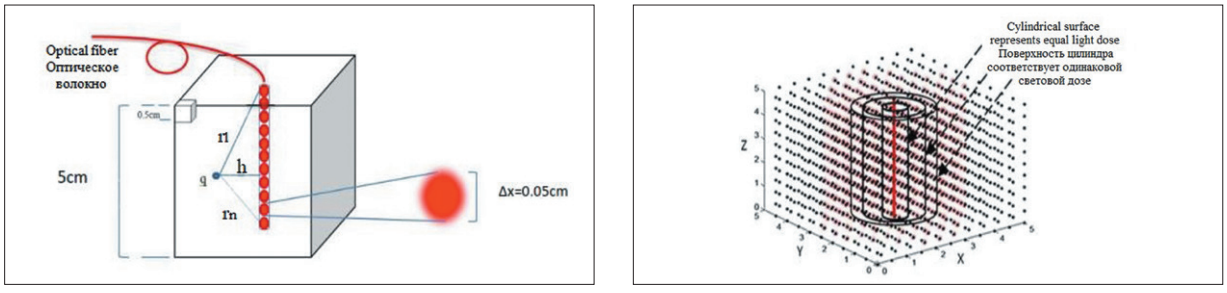

a b

Fig. 1.
a – Cube, fractional cubes, CDF, point source and observing points are the components of the tissue model. Each point receives N rays. N is the number of total source points along the CDF (Dimensions are for clarification and they are not no scale);
b – Cylindrical surfaces represent points that have equal fluence rate

Рис. 1.
a – Куб, дробные кубы, оптическое волокно с цилиндрическим диффузором (CDF), точечный источник и точки наблюдения являются компонентами модели ткани. Каждая точка получает N лучей. N – это общее количество точек-источников вдоль CDF (размеры даны для пояснения, и они не в масштабе);
b – Цилиндрические поверхности представляют точки с одинаковой скоростью потока

CDF receive equal light dose and form a cylindrical surface around CDF (fig. 1b).

Laser treatment fiber

This study provides profiling of optical fiber which is made from RD-ML50 (Medlight S.A, Switzerland). Treatment fiber specifications are as follows: transmission of 630–760 nm, overall diameter 1 mm, illumination length of 50 mm, maximum (CW) power density (in air) of 0.5 W/cm, absolute maximum input power of 2.0 W (CW). Treatment regions: breast, prostate, brain, heart, lung and diaphragm. The diffuser length is 5 cm or less (in increments of 0.5 cm); density power, W/cm and energy, J/cm were specified for each fiber) [10].

Diffusion theory

Cylindrical diffusor fiber was modeled in two geometries. Two equations can be found in the literature that estimate the fluence rate emitted from a light source of a length l in heterogeneous/homogeneous media (equations 1 and 2). Equation 1 discretizes the diffusing part of the optical fiber as a sum of several point light sources [11–13]. Equation 2 considers the whole fiber as a finite line light source with 2D cylindrical light emission characteristics [14]. The first equation 1 is considered as complex equation to estimate the fluence rate, on the basis that the calculation of the fluence rate at a distance r from the fiber is the sum of each light source contribution. Whereas equation 2 computes the fluence rate values using the minimal distance r from the fiber.

$$\varphi(r) = \frac{3\, s\, l\, \mu_s'}{4\pi} \cdot \frac{1}{N-1} \cdot \sum_{i=1}^{N} \frac{e^{-\mu_{eff}\, r_i}}{r_i} \quad (1)$$

$$\varphi(r) = P \sqrt{\frac{2\delta}{\pi r}} \cdot \frac{e^{-r/\delta}}{2\pi \cdot \mu_a \cdot \delta^2} \quad (2)$$

Where P is power of one point, $D = \frac{1}{3\,(\mu_a + \mu_s')}$, δ is the optical penetration depth in m and is equal to $\sqrt{D/\mu_a}$, s is the power of the point source in mW/cm; $\varphi(r)$ is the fluence rate in mW/cm; the quantity $\mu_{eff} = \sqrt{(3 \cdot \mu_a \cdot (\mu_a + \mu_s'))}$ is the effective attenuation coefficient in tissues. The differential $\Delta x = l/(N-1)$ is the length of the elemental (discretized) source segment. The odd integer N is the number of points used in the summation over the source, with one point always placed in the middle of the CDF. The distance between the i_{th} point of the linear light source and the observing point is $r_i = \sqrt{x_i^2 + h^2}$, where $x_i = [(i-1-(N-1)/2) \cdot \Delta x]$ is the cylindrical coordinate along the fiber from the center of the linear source. h is the distance between the observing point and the fiber axis as it is shown in fig. 1a. The numerical value of the summation should be independent of N (or Δx) if N is large enough. Accurate results of the summation can be obtained if $\Delta x = 0.05$ cm. In this study, summing $N = 101$ is available [8, 15]. Obviously, equation 2 is simpler than 1. Depending on geometrical optics equation 1 could be regarded as more accurate method than the equation 2. That is why fluence rate is estimated using the equation 1 throughout this study. For simplicity, we use the light fluence (fluence rate × exposure time) for the PDT dose throughout the paper. The illumination time, through this study, was not fixed (300 sec in the first algorithm and 150 sec in the second algorithm). Final light dose at each point is the summing of light doses that were received from all diffusers. Specifically, tissue necrosis occurs above a threshold light dose [16]. The higher threshold of target dose is determined by minimizing damage to surrounding tissue. To make this study closer to reality, thresholds light dose are assumed to be 20–50 J/cm^2 and 90–300 J/cm^2 with optical properties of breast and prostate cancer, respectively [8, 17].

Optical properties of the studied tissues and patient's prostate

Optical properties at 732 nm in human prostate before and after PDT are taken from Altschuler et al. [8] and listed in table 1. While Optical properties of heart, breast,

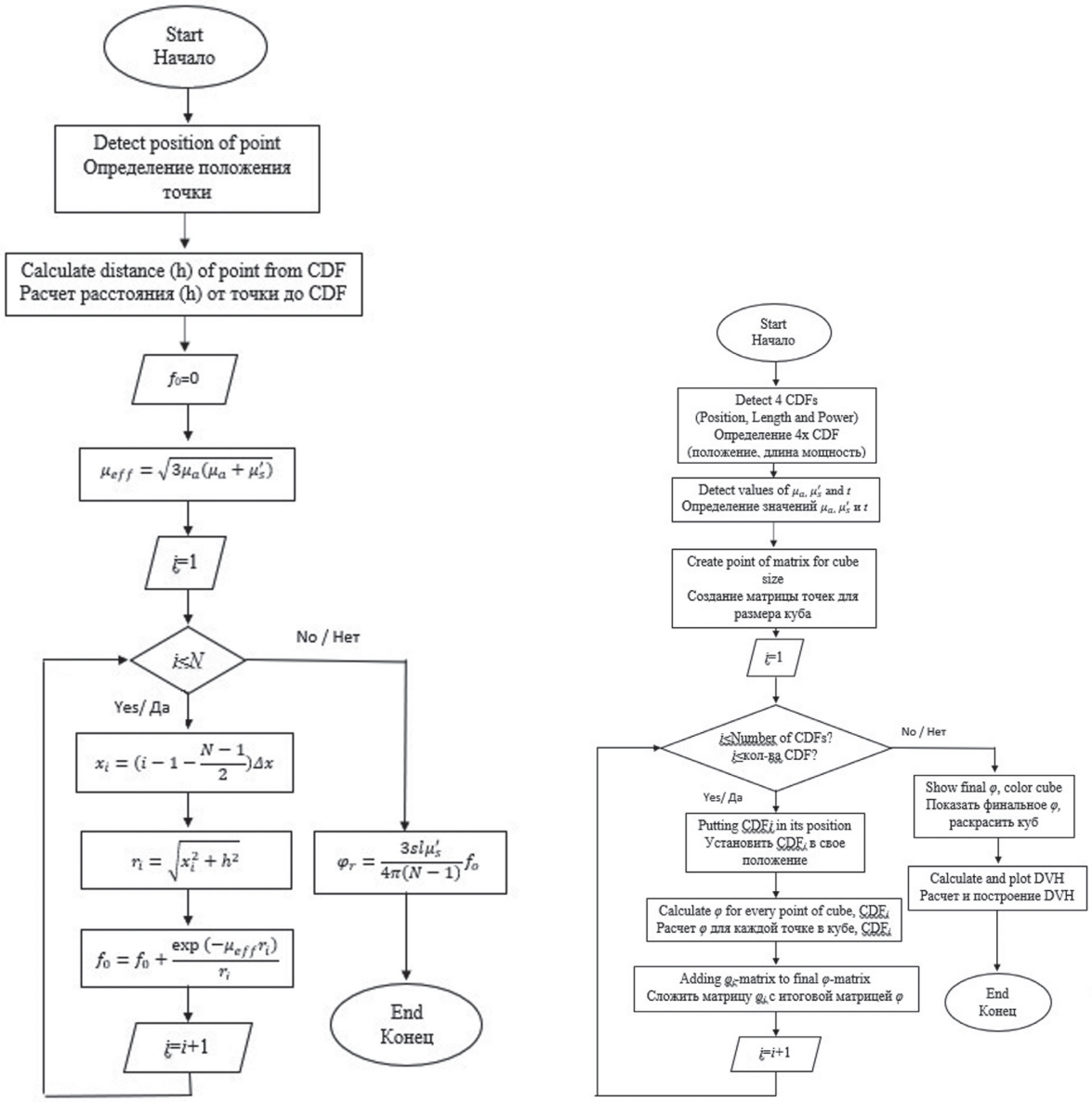

Fig. 2. The block diagram illustrating two software planning algorithms:
a – Algorithm code for analyzing diffusion theory and CDF specification;
b – Algorithm code to calculate total fluence light and plotting color cube and Dose Volume Histogram (DVH)

Рис. 2. Блок-схема, иллюстрирующая два алгоритма программы:
a – Алгоритм кода для анализа теории диффузии и спецификации цилиндрических диффузоров (CDF);
b – Алгоритм кода для расчета общей плотности света и построения цветового куба и гистограммы доза-объем (DVH)

Table 1
Optical properties at 732 nm in human prostate gland (before and after PDT) for patient number 3 and 5 [8]
Таблица 1
Оптические свойства предстательной железы (до и после ФДТ) для 732 нм пациентов 3 и 5 [8]

Patient Number Номер пациента	Before PDT До ФДТ		After PDT После ФДТ	
	μ_a, cm^{-1}	μ_s', cm^{-1}	μ_a,	μ_s', cm^{-1}
3	0.15	22.0	0.07	33.4
5	0.21	11.8	0.13	7.18

Table 2
Optical properties of human heart, breast, lung, diaphragm tissues [11]
Таблица 2
Оптические свойства тканей сердца, молочной железы, легких, диафрагмы человека [11]

Tissue Ткань	λ,nm	μ_a, cm^{-1}	Average Усредненное	μ_s', cm^{-1}	Average Усредненное
Heart Сердце	661	[0.18–0.12]	0.15	[5.22–90.80]	48
Breast (normal) Молочная железа (норма)	660	[0.037–0.11]	0.074	[11.4–13.5]	12.45
Breast (tumor) Молочная железа (опухоль)	690	[0.07–0.1]	0.085	[14.7–17.3]	16
Lung Легкое	661	[0.49–0.88]	0.68	[21.14–22.52]	21.83
Diaphragm Диафрагма	661	[0.15–1.08]	0.62	[9.65–21.7]	15.7

lung, diaphragm tissues are taken from Julia J.L. Sandell and T.C. Zhu review [11] and given in table 2.

Results and discussion

The present study was independent of allowed illumination/dark time or oxygen consumption. Each factor in equation 1 has a different effect. Throughout this part increment in distance is 0.125 cm. Illumination treatment time is 5 min. Source power is 0.5 mW/cm. The following disscution presents four effects.

Distance perpendicular to the fiber axis (h)

Figure 3*a* shows the variation of calculated light fluence distribution for different distances in the same prostate gland (optical properties are taken from table 1). The average optical properties were very different between the upper and lower line. The light fluence rate at 0.5 cm far away from the CDF varied from 64.59 J/cm^2 (before PDT) to 30.5 J/cm^2 (after PDT). Significant change of optical properties was observed before and after PDT treatment in the same patient number 3. Figure 3*b* shows the variation of calculated light fluence distribution for different distances in heart, breast, lung and diaphragm (optical properties are mentioned in the table 2). As a result, closed values of fluence rate were observed when optical properties approximately the same (of lung and diaphragm). Absorption coefficient of breast is the smallest, so it allows higher distribution light (φ=50 J/cm^2 at 0.5 cm away from CDF). From figure 3*b*; the values of φ are 50 J/cm^2 at 0.375 cm for heart, and 50 J/cm^2 at 0.5 cm for breast. Thus, practically two CDFs are required to deliver 100 J/cm^2 for points at those distances. In contrast, for lung or diaphragm two CDFs deliver accepted fluence rate 90 J/cm^2 at 0.125 cm only. More explanation is provided in following absorption and scattering coefficients effects.

Absorption and scattering coefficients effects

Remarkable advances were made in the last two decades to determine the *in vivo* optical properties in humans in a variety of organs. The absorption coefficient varies largely over the visible spectrum, while the scattering coefficient of tissue decreases monotonically as the wavelength increases [18]. The presence of chromophores affects the absorption coefficient. Although the actual range of the *in vivo* optical properties is tissue type dependent, generally varied in the ranges μ_a =0.03–1.6 cm^{-1} and μ_s'=1.2–40 cm^{-1} [11]. Since equation 1 is a nonlinear equation of two parameters μ_a and μ_s', it was very difficult to separate effects of μ_s' and μ_a from

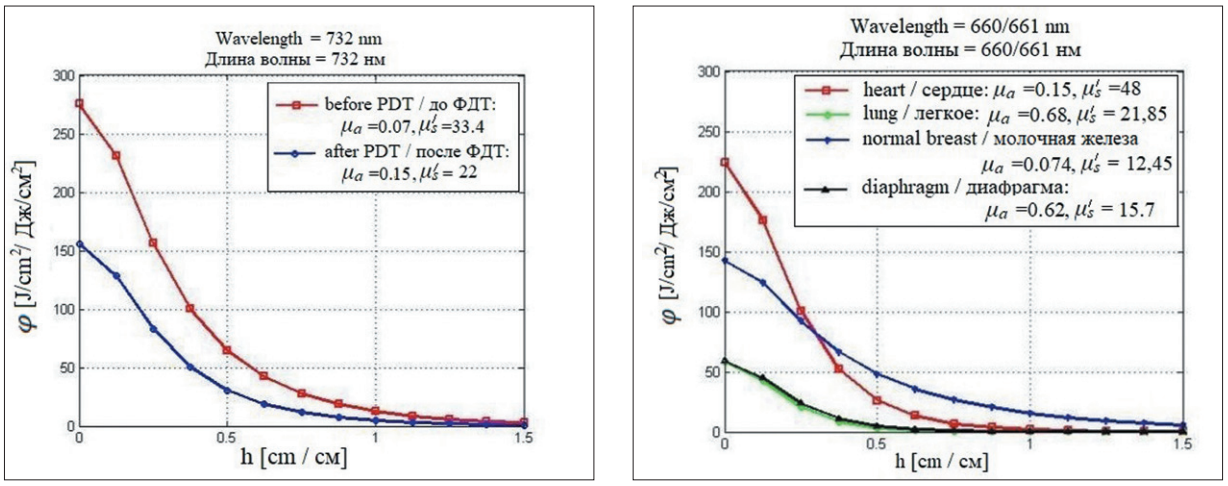

a b

Fig. 3. Fluence rate curve plotted at different distances:
a – in prostate gland;
b – for other organs
Рис. 3. Кривая светового потока на разных расстояниях:
a – в предстательной железе;
b – для других органов

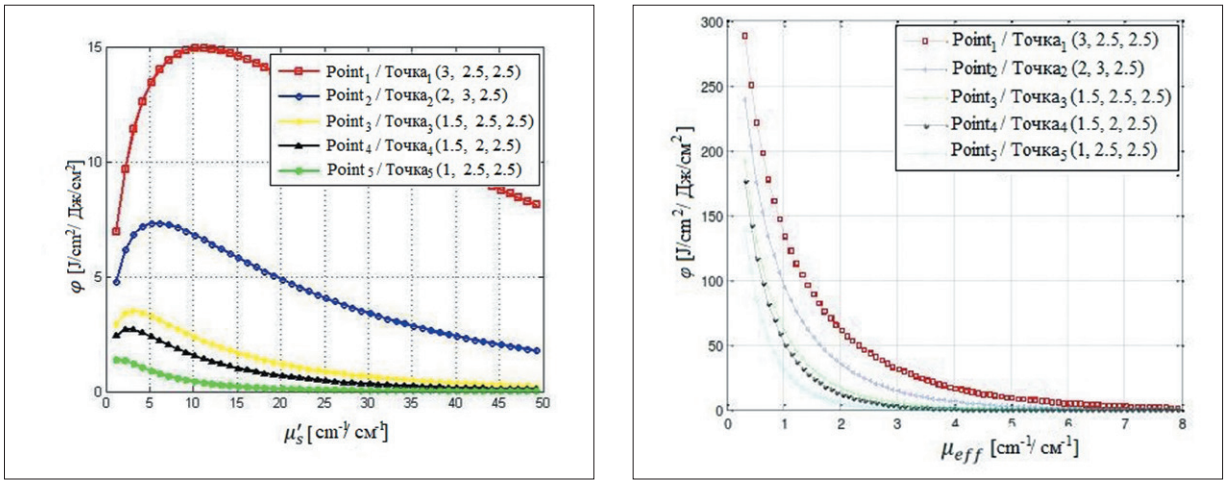

a b

Fig. 4. The dependence of light fluence rate at different points from:
a – μ_s' ;
b – μ_{eff}
Рис. 4. Зависимость интенсивности светового потока в разных точках от:
a – μ_s' ;
b – μ_{eff}

each other. Now, the studied medium is supposed to be heterogeneous, and five observing points are considered. Therefore, to understand the effective attenuation coefficient effect, it is required to fix μ_s' at 20.6 cm^{-1} (is the average of its range) and μ_{eff} is changing along 0.33–14.13 cm^{-1}. We used these values to understand the expected standard behavior of optical properties, and to anticipate the variation in tissue constitution that yields the tissue optical properties at any desired wavelength [19].

In the opposite case, μ_s' is changed along its range and μ_{eff} is fixed at value (7.23 cm^{-1}); the average of its range. To explain μ_{eff} and μ_s' effects, five observing points were taken at the distances (h1=0.5, h2=0.7, h3=1, h4=1.12, h5=1.5) cm away from CDF. These five points represent

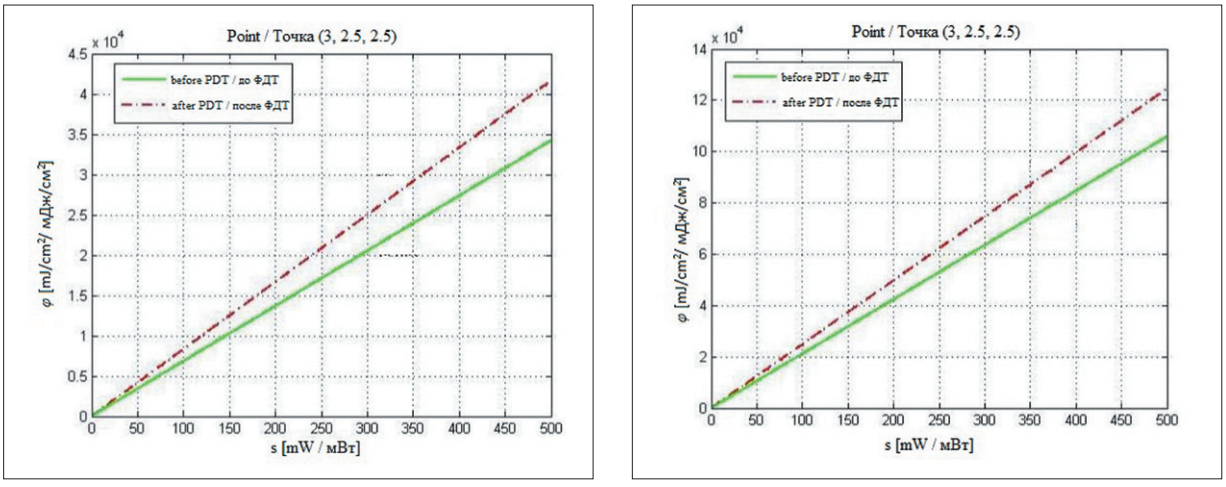

Fig. 5. Fluence rate as a function of power density s:
a – Before PDT: μ_s'=11.8 cm^{-1}, μ_a=0.21 cm^{-1}; after PDT: μ_s'=7.18 cm^{-1}, μ_a=0.13 cm^{-1}
b – Before PDT: μ_s' =22 cm^{-1}, μ_a=0.15 cm^{-1}; after PDT: μ_s'=33.4 cm^{-1}, μ_a=0.07 cm^{-1}

Рис. 5. Интенсивность оптического потока как функция плотности мощности s:
a – До ФДТ: μ_s' =11.8 см$^{-1}$, μ_a=0.21 см$^{-1}$; после ФДТ: μ_s'=7.18 см$^{-1}$, μ_a=0.13 см$^{-1}$
b – До ФДТ μ_s'=22 см$^{-1}$, μ_a=0.15 см$^{-1}$; после ФДТ: μ_s'=33.4 см$^{-1}$, μ_a=0.07 см$^{-1}$

the nearest five cylindrical surfaces. Figure 4 shows the relationship between the light fluence rate and the optical properties.

Figure 4*a* shows that the fluence rate (for point 1) rapidly increases between 1.2 and 10 cm^{-1}, then approximately fixed between 10 and 15 cm^{-1}. As a result, reduced scattering coefficient does not cause increase in fluence rate after value 10 cm^{-1}. For point 2, decline in fluence rate occurs after 7 cm^{-1}. Although the difference in distance is only 2 mm between point 1 and 2, there is a large difference in fluence rate between them. For other points higher values of fluence rate are along 1.2–5 cm^{-1}. As a result, in experimental phantom, for higher distances, it is good to make μ_s'≤ ~10 cm^{-1}. For larger distances (0.7, 1, 1.12, 1.5 cm), it is better to make μ_s' ~ 5, 3.2, 3.2, 1.2 cm^{-1}, respectively. Figure 4b shows the relationship between the light fluence rate and the effective attenuation coefficient as exponential decay curves. As shown in figure, it is clear that values corresponding to point 1 (0.5 cm) have higher fluence rate values, while lower lines represent other points respectively. For $\varphi(r)$ that was lower than 90 J/cm^2; μ_{eff} is 1.53 cm^{-1} for h_1. For other points μ_{eff} was 1, 0.73, 0.6, 0.5 cm^{-1}, respectively. Two algorithms allow to change ranges and values of μ_s' and μ_{eff} to get accepted light dose and could be useful in preparing phantoms at laboratories. As a result, knowledge of optical properties of tissues is of great importance for interpretation and quantification of the diagnostic data. Fluence rate at virtual diffuser points depends on optical properties of studied medium. It was ~87.7 J/cm^2 with prostate optical properties μ_s' =14.3, μ_a =0.3 cm^{-1}. While it became 199.5 J/cm^2 when μ_a decreases by ten times. It is well known that absorption coefficient is included in μ_{eff} expression. From our findings and for the optical properties of all biological tissues studied in ref. [11], it was found that the absorption coefficient μ_a has a more significant influence on light fluence rate distribution than reduced scattering coefficient μ_s'. It is noteworthy to say that our results are valid for wavelength range 600–800 nm at certain wavelengths of human tissues that was also mentioned in ref. [11].

Power density effects (s)

Source catheters are used for both light delivery and measurement of optical properties. Usually, the light dose is given in terms of external power density delivered by the light system. As it is noted in fiber specifications, *s* is 0.5 mW/cm at maximum allowed input power 2W. The power is considered to be 0.5 mW/cm through all previous study. Consequently, power of full diffuser length is 2.5 W. Maximum power density (in air) is 500 mW/cm (CW) as mentioned in the technical specifications of Medlight CDFs [10], so the power is varied between 0 and 500 mW/cm through the two codes. Optical properties of patients were taken from ref. [8]. As can be seen in figure 5*a*, optical properties of patient number 5 were μ_s' =11.8 cm^{-1}, μ_a =0.21 cm^{-1} (before PDT). After PDT, the values changed to μ_s'=7.18 cm^{-1}, μ_a =0.13 cm^{-1}. Fluence rate became larger after PDT [8].

Figure 5*b* shows linear relationship between *s* and $\varphi(r)$ that to deliver accepted fluence rate 90 J/cm^2, applied power should equal at least ~432 mW/cm, while after PDT it decreased to 369 mW/cm. If *s* is limited at 250, flu-

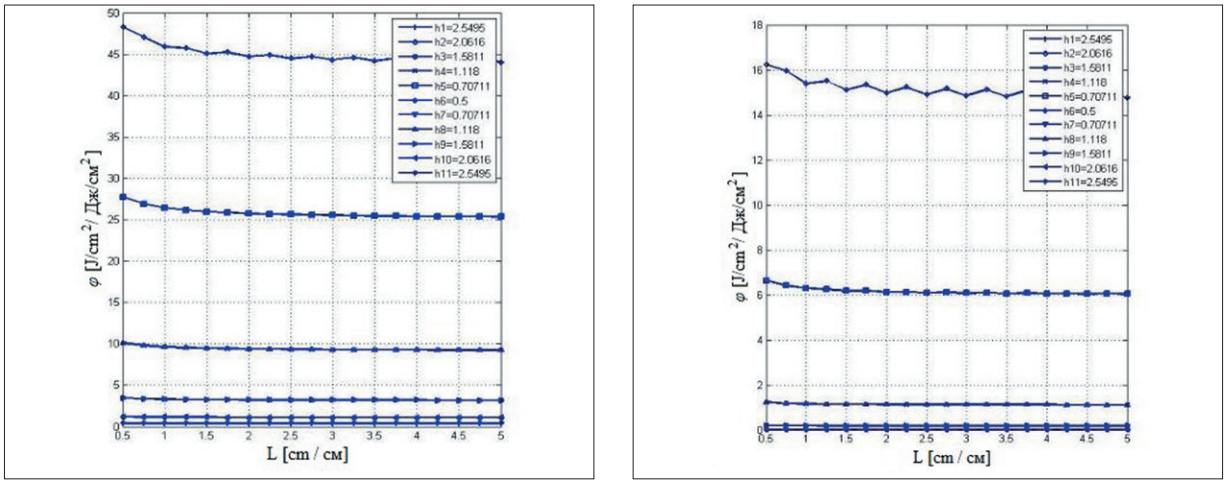

Fig. 6. Fluence rate as function of diffuser length *L*. s = 0.5 mW/cm, μ_s' = 14 cm^{-1}, *t* = 5 min:
a – μ_a=0.09 cm^{-1}
b – μ_a=0.3 cm^{-1}
Рис. 6. Интенсивность оптического потока как функция длины диффузора *L*. s=0.5 мВт/см, μ_s' = 14 см$^{-1}$, *t* = 5 мин.
a – μ_a=0.09 см$^{-1}$
b – μ_a=0.3 см$^{-1}$

ence rate is 50 J/cm^2 (before) and 61.5 (after). It was clear that fluence rate became higher after the PDT. Results for patients 2, 4, 12 and 9 [8] confirm that μ_a has a significant effect on light fluence rate distribution.

Cylindrical diffuser length effect

Returning to equation 1; the fluence rate clearly appears proportional to the tip length. Increasing the fluence rate is related to the density of number of source points over the diffuser (N). As a result, the fluence rate at certain point is not affected by varying tip length. This result is illustrated by figure 6.

Figure 6 shows the relationship between φ and *L*. The CDF was positioned at cube center, each line represented two opposite distances. Distances furthest from CDF were shown in small rectangle. As it was expected, light fluence rate was not affected by increasing length, for similar inputs and distances, but if μ_a is changed to 0.3 cm^{-1}, then fluence rate will decrease to about 15 J/cm^2 at h6=0.5 cm while it is about 45 J/cm^2 with μ_a=0.09 cm^{-1}.

Clearly there is a big difference between $\varphi(h6)$ and $\varphi(h5)$. As a result, there is major attenuation in fluence rate as distance increases.

Fluence rate calculations were done using basic diffusion equation (eq. 1). As it is well known, the generating of matrixes in order to calculate fluence rate at each point is a cumbersome procedure. Conditions were determined to accept fluence rate. This condition could be changed as required for a given tissue, photosensitizer or wavelength. Our results agreed with prior works where optical properties have considerable effect on light distribution in any given medium [11]. However, in real clinical producers, CDF length cannot be changed and practically, due to fixed distances between slots used for guiding PDT fibers inside the tissue which equal 0.5 cm on average [8], distance between tow CDFs could not be less than 0.5 cm.

Volume versus number of CDFs

Actual input parameters had been taken into following consideration. Optical properties of breast cancer are μ_a = 0.085 cm^{-1}, μ_s' = 16 cm^{-1} [11]. First algorithm is used to

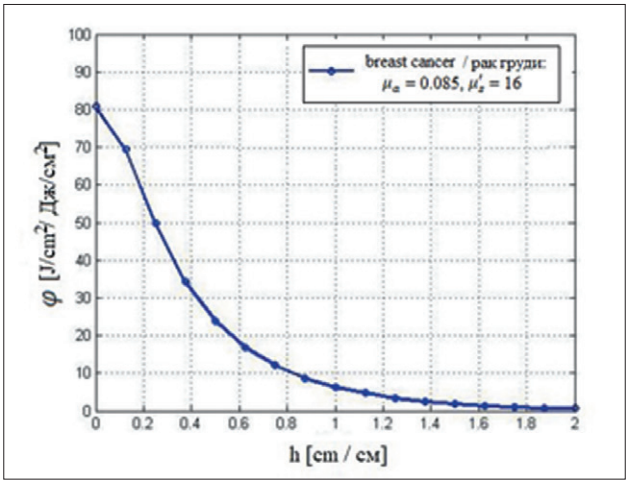

Fig. 7. Fluence rate is as a function of distance for breast cancer tissue. Input parameters are: s=50 mW/cm, t=150 sec. Light dose at h=0.5 cm is 24 J/cm^2 for breast
Fig. 7. Интенсивность светового потока как функция расстояния для ткани рака молочной железы. Входные параметры: *s*=50 мВт/см, *t*=150 сек. Световая доза при *h*=0.5 cm равна 24 Дж/см^2 для молочной железы

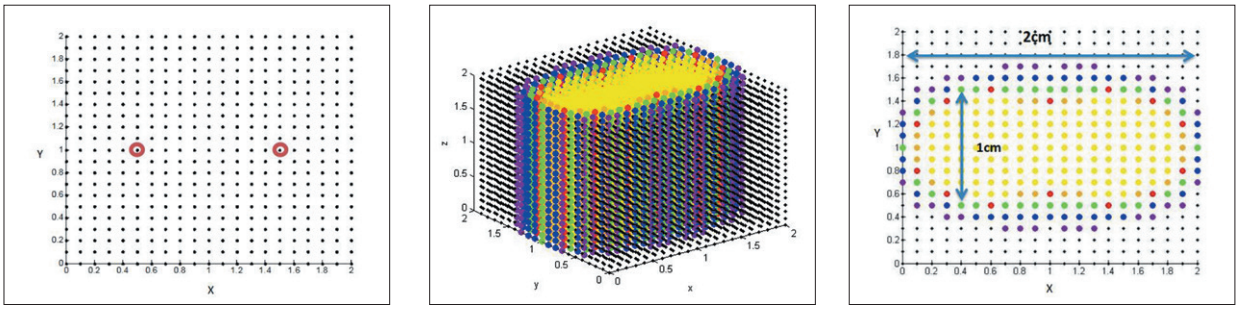

Рис. 8. Light distribution resulted from two CDFs with s = 50 mW/cm, *t* = 150 sec, μ_a = 0.085 cm^{-1}, μ_s' = 16 cm^{-1}:
a – Top-down view shows positions of CDFs placed at (0.5, 1, 2), (1.5, 1, 2);
b – Yellow points have accepted dose and form volume 1x2x2 cm;
c – Top-down view of cube after light distribution: light dose in red points is less than 20 J/cm^2 and more than 15 J/cm^2, green points represent pixels which have dose that is less than 15 J/cm^2 and more than 10 J/cm^2, blue/ violet points have the dose that is less than 10 J/cm^2

Рис. 8. Распределение света, полученное при использовании двух CDF при s = 50 мВт/см, t = 150 с, μ_a = 0,085 см$^{-1}$, μ_s' = 16 см$^{-1}$:
a – Положение CDF, размещенных в точках (0.5, 1, 2), (1.5, 1, 2) (вид сверху);
b – Желтым цветом выделены точки, получившие необходимую световую дозу. Их объем составляет 1x2x2 см.
c – Распределение света (вид сверху): доза света в красных точках составляет менее 20 Дж/см^2 и более 15 Дж/см^2, зеленые точки представляют пиксели с дозой менее 15 Дж/см^2 и более 10 Дж/см^2, синие/фиолетовые точки имеют дозу менее 10 Дж/см^2

estimate fluence rate along 2.5 cm far away from single CDF (full length of tip is 5 cm) is placed at center of cube (5×5×5 cm). Initial position of CDF is (x=2.5 cm, y=2.5 cm, z=5 cm); since x, y can be changed along X and Y axes from 0.5 cm to 5 cm, while z must be set at the full length of CDF.

Figure 7 shows that sufficient light dose is reached for approximately 0.25–0.5 cm around CDF. Higher threshold of 50 J/cm^2 is exceeded at h $\leq$ 0.25 cm. As a result, for optical properties of breast cancer, accepted light dose reaches to volume of one cylinder with full diameter of D = 1 cm. Figure 8 is the result of second algorithm. Figure 8*a* shows two CDFs in a line. As can be seen from figure 8*a*, two CDFs can cover two centimeters in one direction of volume. While approximately only one centimeter in the vertical orientation could be covered with light dose of 20–50 J/cm^2.

Length of CDFs must be near the height of the volume. For the breast cancer tissue, the covered volume equals approximately 1×N×L (cm) as represented in figure 8c. N is the number of CDFs, L is the length of diffusers. The volume (with accepted light dose) is 1×2×2=4 cm^3. To cover full cube size which is 2×2×2 (cm), four CDFs must be placed at (0.5, 0.5, 2), (0.5, 1.5, 2), (1.5, 1.5, 2), (1.5, 0.5, 2) (fig. 9*a*). The maximum covered volume with accepted light dose equals four times of cylinder c1 (cylinder c1 is indicated in figure 9*b*).

It can be concluded that for delivering sufficient light dose (20–50 J/cm^2) to any phantom which has cuboid or cylindrical shape and has optical properties of breast cancer, it is needed to place (W×L) or (D^2) CDFs respectively with distance (1 cm) between each two CDFs. Where, W, L are the rectangular sides and D is the cylinder diameter. Practically, optimization theories are applied to optimize places of a lower number of CDFs [5, 8]. Finding an algorithm to choose suitable powers represents another practical solution to reduce required fibers.

Dose-volume histogram

A DVH, more properly called a cumulative dose volume histogram, expresses the percentage of an organ that has received more than a given dose [20]. It is useful to summarize the volumetric distribution of light doses. Second code allows plotting DVH (fig. 9*c*) that corresponds to figure 9*b*. For higher accuracy; distance between pixels has been reduced to 0.05 cm. Consequently, number of slices is 40 slices (2/0.05 cm); total considered points are 40×40×number of slices. Plotting the prism with finer voxels causes much longer time to get φ_{total} matrix (final fluence rates resulting from four CDFs), while the time needed to calculate the DVH is only a second or so because no feasibility procedures are involved. Using DVH, it is possible to estimate percentage of points which accumulated sufficient light doses. With optical properties of breast cancer, sufficient light doses are attained in more than 95% of all cube points. Figure 9*c* shows DVH. Another case is studied with optical properties of brain cancer (μ_a = 0.2 cm^{-1}, μ_s' = 5 cm^{-1}) [5] (all other inputs are fixed). Results indicate that percentage of the covered volume with accepted light dose is reduced to 10% of the number of pixels with brain cancer (μ_a = 0.2 cm^{-1}, μ_s' = 5 cm^{-1}). Low level of percent coverage imposes using much more CDFs. T.M. Baran and

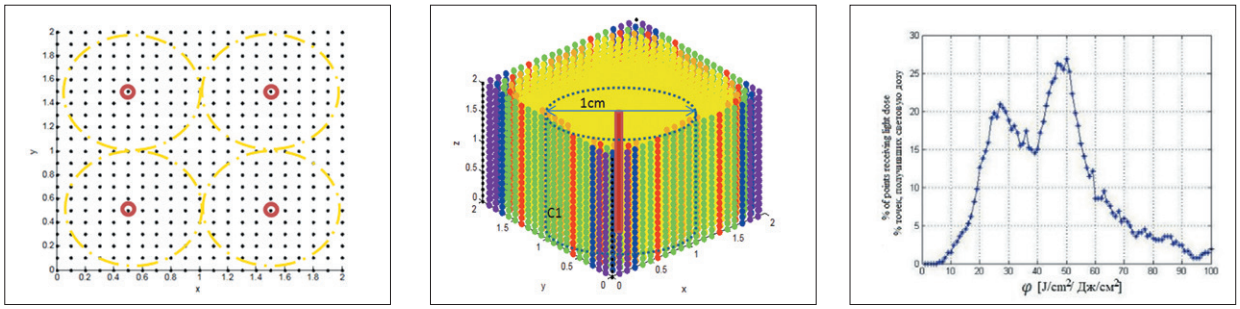

a b c

Рис. 9. Light distribution from four CDFs with *s* = 50 mW/cm, *t* = 150 sec, μ_a = 0.085 cm^{-1}, μ_s' = 16 cm^{-1}:
a – Four CDFs placed at (0.5, 0.5, 2), (0.5, 1.5, 2), (1.5, 1.5, 2), (1.5, 0.5, 2);
b – The distributed light forms a volume that is approximately 2x2x2 cm. Colors are the same as in figure 8;
c – The Dose-volume histogram for the results of four CDFs with 40x40x40 pixels. The vertical axis is the percent of total pixels that receive light doses. Summing the number of points showed that more than 63000 pixels out of 64000 received sufficient light dose

Рис. 9. Распределение света, полученное при использовании четырех CDF при *s* = 50 мВт/см, *t* = 150 с, μ_a = 0,085 см$^{-1}$, μ_s' = 16 см$^{-1}$:
a – Положение четырех CDF, размещенных в точках (0,5, 0,5, 2), (0,5, 1,5, 2), (1,5, 1,5, 2), (1,5, 0,5, 2);
b – Распределение света образует объем, который составляет примерно 2x2x2 см. Цвета такие же, как на рисунке 8.
c – Гистограмма «Объем-доза» для результатов четырех CDF с 40x40x40 пикселей. Вертикальная ось – процент от общего количества пикселей, которые получают световые дозы. Суммирование общего количества пикселей показало, что более 63000 пикселей из 64000 получили достаточную световую дозу

T.H. Foster et al. [7] used eight CDFs to deliver 2270–2350 J (333–1178 J/cm^2) to accumulate 90 J/cm^2 in 90% of tumor volume that was 5 cm^3 approximately. By raising the delivered power (*s*) or time treatment the percentage of coverage rises as well. In this regard, consumption of oxygen and the kind of photosensitizer must be considered in *in vivo* studies according to the treated organ.

Conclusion

This study is considered as the first inclusive description of cylindrical diffuser fibers using basic equation of diffusion theory (eq. 1). It was found that optical properties and distance away from CDF had the major effects on light distribution. For light absorbing media (i.e. prostate) which is virtually made of blood, high power is required in order to attain adequate light distribution in the tissue. On the other hand, for highly scattering media such as breast tissue, increasing the number of CDF fibers with lower power is highly recommended to avoid thermal collateral damage. Moreover, the study provides a guideline for proper localization of optical detectors inside tissue for investigating fluorescence during PDT. In addition, this simulation was very accurate in calculating the light doses at each point because of small size of voxels. Using specific colors for each range of light dose allowed estimating the whole volume covered by the sufficient light dose without referring to the matrixes. This simulation would be flexible regarding changes in variables in equation 1 including time, distance between points and the size of volume structure.

REFERENCES

1. Dougherty T.J., Gomer C.J., Henderson B.W., Jori G., Kessel D., Korbelik M., Moan J., Peng Q. Photodynamic therapy, *J Natl Cancer Inst*, 1998, vol. 90(12), pp. 889–905.
2. Wilson B.C., Patterson M.S., Lilge L. Implicit and explicit dosimetry in photodynamic therapy: a New paradigm, *Lasers Med Sci*, 1997, vol. 12(3), pp. 182–99.
3. Haskell, R.C., Svaasand L.O., Tsay T.T., Feng T.C., McAdams M.S., Tromberg B.J. Boundary conditions for the diffusion equation in radiative transfer, *Journal of the Optical Society of America A*, 1994, vol. 11(10), pp. 2727–2741.
4. Shafirstein G., Bellnier D., Oakley E., Hamilton S., Beeson K., Parilov E., Potasek M. Interstitial Photodynamic Therapy—A Focused Review, *Cancers*, 2017. – vol. 9(2), e12. doi:10.3390/can-

ЛИТЕРАТУРА

1. Dougherty T.J., Gomer C.J., Henderson B.W., Jori G., Kessel D., Korbelik M., Moan J., Peng Q. Photodynamic therapy // J Natl Cancer Inst. – 1998. – Vol. 90(12). – P. 889–905.
2. Wilson B.C., Patterson M.S., Lilge L. Implicit and explicit dosimetry in photodynamic therapy: a New paradigm // Lasers Med Sci. – 1997. – Vol. 12(3). – P. 182–99.
3. Haskell R.C., Svaasand L.O., Tsay T.T. et al., Boundary conditions for the diffusion equation in radiative transfer // Journal of the Optical Society of America A. – 1994. – Vol. 11(10). – P. 2727–2741.
4. Shafirstein G., Bellnier D., Oakley E., et al. Interstitial Photodynamic Therapy—A Focused Review // Cancers. – 2017. – Vol. 9(2). – E12. doi:10.3390/cancers9020012.

cers9020012.
5. Baran T.M., Foster T.H. Comparison of flat cleaved and cylindrical diffusing fibers as treatment sources for interstitial photodynamic therapy, *Med. Phys*, 2014, vol. 41(2), 022701. doi: 10.1118/1.4862078.
6. Farina B., Saponaro S., Pignoli E., Tomatis S., Marchesini R. Monte Carlo simulation of light fluence in tissue in a cylindrical diffusing fiber geometry, *Phys Med Biol*, 1999, vol. 44(1), pp. 1–11.
7. Baran T.M., Foster T.H. New Monte Carlo model of cylindrical diffusing fibers illustrates axially heterogeneous fluorescence detection: simulation and experimental validation, *J Biomed Opt*, 2011, vol. 16(8),085003. doi: 10.1117/1.3613920.
8. Altschuler M.D., Zhu T.C., Li J., Hahn S.M. Optimized interstitial PDT prostate treatment planning with the Cimmino feasibility algorithm, *Med. Phys.*, 2005, vol. 32, pp. 3524–3536.
9. Oakley E., Bellnier D.A., Hutson A., Wrazen B., Arshad H., Quon H., Shafirstein G. Surface Markers for Guiding Cylindrical Diffuser Fiber Insertion in Interstitial Photodynamic Therapy of Head and Neck Cancer, *Lasers Surg Med*, 2017, vol. 49(6), pp. 599–608.
10. *Cylindrical light diffuser Model RD.* Available at: http://www.medlight.com/pdf/Doc_RD_0801E.pdf. (accessed 28.11.2019)
11. Sandell J.L., Zhu T.C. A review of in-vivo optical properties of human tissues and its impact on PDT, *Journal of Biophotonics*, 2011, vol. 4(11–12), pp. 773–87.
12. Dimofte A., Finlay J.C., Liang X., Zhu T.C. Determination of optical properties in heterogeneous turbid media using a cylindrical diffusing fiber, *Physics in Medicine and Biology*, 2012, vol. 57(19), pp. 6025–46.
13. Dimofte A., Finlay J.C., Zhu T.C. A method for determination of the absorption and scattering properties interstitially in turbid media, *Physics in Medicine and Biology*, 2005, vol. 50(10), pp. 2291–311.
14. Jacques S.L., Pogue B.W. Tutorial on diffuse light transport, *Journal of Biomedical Optics*, 2008, vol. 13(4), pp. 041302.
15. Liang X., Wang K.K., Zhu T.C. Feasibility of interstitial diffuse optical tomography using cylindrical diffusing fibers for prostate PDT, *Physics in Medicine and Biology*, 2013, vol. 58(10), pp. 3461–80.
16. Patterson M.S., Madsen S.J., Wilson B.C. Experimental tests of the feasibility of singlet oxygen luminescence monitoring in vivo during photodynamic therapy, *J Photochem Photobiol B*, 1990, vol. 5(1), pp. 69–84.
17. Filonenko E.V., Saribekyan E.K., Ivanova-Radkevich V.I. Capabilities of Intraoperative Photodynamic Therapy For Treatment Of Locally Advanced Breast Cancer, *Biomedical Photonics*, 2016, vol. 5, no. 1, pp. 9–14. doi: 10.24931/2413–9432–2016–5–1–9–14.
18. Nakai T., Nishimura G., Yamamoto K., Tamura M. Expression of optical diffusion coefficient in high-absorption turbid media, *Phys. Med. Biol.*, 1997, vol. 42, pp. 2541–2549.
19. Jacques S.L. Optical properties of biological tissues: a review, *Phys. Med. Biol.*, vol. 58(11), pp. 37–61.
20. Rendon A., Beck J.C., Lilge L. Treatment planning using tailored and standard cylindrical light diffusers for Photodynamic therapy of the prostate, *Phys Med Biol*, 2008, vol. 53(4), pp. 1131–1149.

5. Baran T.M., Foster T.H. Comparison of flat cleaved and cylindrical diffusing fibers as treatment sources for interstitial photodynamic therapy // Med. Phys. – 2014. – Vol. 41(2). – 022701. doi: 10.1118/1.4862078.
6. Farina B., Saponaro S., Pignoli E., Tomatis S., Marchesini R. Monte Carlo simulation of light fluence in tissue in a cylindrical diffusing fiber geometry // Phys Med Biol. – 1999. – Vol. 44(1). – P. 1–11.
7. Baran T.M., Foster T.H. New Monte Carlo model of cylindrical diffusing fibers illustrates axially heterogeneous fluorescence detection: simulation and experimental validation // J Biomed Opt. – 2011. – Vol. 16(8). – 085003. doi: 10.1117/1.3613920.
8. Altschuler M.D., Zhu T.C., Li J., Hahn S.M. Optimized interstitial PDT prostate treatment planning with the Cimmino feasibility algorithm // Med. Phys. – 2005. – Vol. 32. – P. 3524–3536.
9. Oakley E., Bellnier D.A., Hutson A., et al. Surface Markers for Guiding Cylindrical Diffuser Fiber Insertion in Interstitial Photodynamic Therapy of Head and Neck Cancer // Lasers Surg Med. – 2017. – Vol. 49(6). – P. 599–608.
10. Cylindrical light diffuser Model RD. Available at: http://www.medlight.com/pdf/Doc_RD_0801E.pdf. (accessed 28.11.2019)
11. Sandell J.L., Zhu T.C. A review of in-vivo optical properties of human tissues and its impact on PDT //Journal of Biophotonics. – 2011. – Vol. 4(11–12). – P. 773–87.
12. Dimofte A., Finlay J.C., Liang X., Zhu T.C. Determination of optical properties in heterogeneous turbid media using a cylindrical diffusing fiber //Physics in Medicine and Biology. – 2012. – Vol. 57(19). – P. 6025–46.
13. Dimofte A., Finlay J.C., Zhu T.C. A method for determination of the absorption and scattering properties interstitially in turbid media // Physics in Medicine and Biology. – 2005. – Vol. 50(10). – P. 2291–311.
14. Jacques S.L., Pogue B.W. Tutorial on diffuse light transport // Journal of Biomedical Optics. – 2008. – Vol. 13(4). – P. 041302.
15. Liang X., Wang K.K., Zhu T.C. Feasibility of interstitial diffuse optical tomography using cylindrical diffusing fibers for prostate PDT // Physics in Medicine and Biology. – 2013. – Vol. 58(10). – P. 3461–80.
16. Patterson M.S., Madsen S.J., Wilson B.C. Experimental tests of the feasibility of singlet oxygen luminescence monitoring in vivo during photodynamic therapy // J Photochem Photobiol B. – 1990. – Vol. 5(1). – P. 69–84.
17. Filonenko E.V., Saribekyan E.K., Ivanova-Radkevich V.I. Capabilities of Intraoperative Photodynamic Therapy For Treatment Of Locally Advanced Breast Cancer // Biomedical Photonics. – 2016. – Vol. 5, No. 1. – P. 9–14. doi: 10.24931/2413–9432–2016–5–1–9–14.
18. Nakai T., Nishimura G., Yamamoto K., Tamura M. Expression of optical diffusion coefficient in high-absorption turbid media // Phys. Med. Biol. – 1997. – Vol. 42. – P. 2541–2549.
19. Jacques S.L. Optical properties of biological tissues: a review // Phys. Med. Biol. – Vol. 58(11). – P. 37–61.
20. Rendon A., Beck J.C., Lilge L. Treatment planning using tailored and standard cylindrical light diffusers for Photodynamic therapy of the prostate // Phys Med Biol. – 2008. – Vol. 53(4). – P. 1131–1149.

REVIEWS

CURRENT STATE OF METHODS OF CORRECTION OF INVOLUTIONAL CHANGES OF SKIN AND THE PLACE OF PHOTODYNAMIC THERAPY AMONG THEM

Beimanova M.A.[1], **Potekaev N.N.**[1,2], **Petunina V.V.**[2]
[1]Moscow Research and Practical Center for Dermatovenereology and Cosmetology, Moscow, Russia
[2]The Russian National Research Medical University named after N.I. Pirogov, Moscow, Russia

Abstract

This work is a review of modern scientific data on the process of aging, as well as the prospect of using photodynamic therapy for correction of involutional skin changes in the age cohorts, cohorts with a burdened medical history, including cancerous and precancerous skin neoplasms. The data on the predicted increase in life expectancy and, as a consequence, the potential risk of pathologies, including those with skin localization, progression of malignancy processes, as well as the formation of *de novo* elements, is presented. The increase in life expectancy also demonstrates the socialization of the elderly population, along with the increasing need for correction of involutional skin changes. However, considering the risks associated with the chronic diseases and increased malignancy in this cohort, methods have to be carefully selected. One such technique is photodynamic therapy (PDT). PDT is actively used in oncology, and recently has been increasingly showing its aesthetic effectiveness. It can be predictably used not only on cancer patients, but also in an age cohort.

Keywords: photodynamic therapy, correction of involutional changes, actinic keratosis.

For citations: Beimanova M.A., Potekaev N.N., Petunina V.V. Current state of methods of correction of involutional changes of skin and the place of photodynamic therapy among them, *Biomedical Photonics*, 2019, vol. 8, no. 4, pp. 28–35. (in Russian) doi: 10.24931/2413–9432– 2019–8–4–28–35

Contacts: Beimanova M.A., e-mail: beimanova@mail.ru

СОВРЕМЕННОЕ СОСТОЯНИЕ МЕТОДОВ КОРРЕКЦИИ ИНВОЛЮЦИОННЫХ ИЗМЕНЕНИЙ КОЖИ И МЕСТО ФОТОДИНАМИЧЕСКОЙ ТЕРАПИИ СРЕДИ НИХ

М.А. Бейманова[1], **Н.Н. Потекаев**[1,2], **В.В. Петунина**[2]
[1]Московский научно-практический центр дерматовенерологии и косметологии, Москва, Россия
[2]Российский национальный исследовательский медицинский университет имени Н.И. Пирогова, Москва, Россия

Резюме

Данная работа представляет собой обзор современных научных данных о процессах старения кожи, а также о перспективе использования метода фотодинамической терапии для коррекции инволюционных изменений кожи у возрастного населения. Приводятся данные прогнозируемого увеличения продолжительности жизни и, как следствие, потенциального риска возникновения патологий, в том числе кожной локализации. Увеличение продолжительности жизни также демонстрирует и социализацию пожилого населения, вместе с тем возрастающую потребность в преображении и коррекции инволюционных изменений кожи, но, учитывая риски в связи с наличием хронических заболеваний и возрастающей малигнизации данной когорты, следует тщательно подбирать методики, учитывая вышеперечисленные особенности. Одним из таких методов является фотодинамическая терапия. Фотодинамическая терапия активно применяется в онкологии, а в последнее время все чаще показывает свою эффективность в эстетическом направлении, соответственно прогнозируемо может использоваться не только у онкологических больных, но и возрастной когорты.

Ключевые слова: фотодинамическая терапия, коррекция инволюционных изменений, актинический кератоз.

Для цитирования: Бейманова М.А., Потекаев Н.Н., Петунина В.В. Современное состояние методов коррекции инволюционных изменений кожи и место фотодинамической терапии среди них // Biomedical Photonics. – 2019. – Т. 8, № 4. – С. 28–35. doi: 10.24931/2413–9432– 2019–8–4–28–35

Контакты: Бейманова М.А., e-mail: beimanova@mail.ru

Medicine has been developing rapidly in many areas recently, and cutaneous science is no exception. Thanks to the OMICS revolution, researchers have come to understand that the skin is one of the main links of the key neuro-immune-endocrine axes of the body. Stratification of skin diseases and individual skin conditions allows for the implementation of targeted and effective treatment methods. Close attention to skin conditions is due to a significant increase in the average life expectancy of a person, as well as an alarming increase in the number of patients with such diagnoses as diabetes, skin cancer and other chronic diseases. At the same time, demographic trends observed all over the world make it more important to find clinical solutions for numerous age-related (involution-type) skin disorders caused by external and internal factors. In the context of a deep study of human skin aging, it is emphasized that maintaining functional activity in this complex multicellular organ is key to maintaining the quality of life in old age [1].

The recent advances in the study of age-related skin changes have led to the development of classifications of types of aging. In particular, one of them was proposed in 2014 by Zh. Yu. Yusova and is presented below:

1. *Aging of the wrinkled type* is more often observed in people with dry, dehydrated skin, and the signs of aging are observed before the age of 40, with the spread of wrinkles throughout the face. In this type, the skin has gray color, and the dominant involution signs are wrinkles. Characteristic features: pronounced "crow's feet" in the periorbital area, wrinkling of the upper and lower eyelids, "corrugation" in the upper lip and chin area. Some atrophic changes are observed, as well as blood circulation disorders in the dermis. Ultrasound examination reveals a set of linear structures in the epidermis, many areas with a high degree of the dermis fraying, thinning and the reduction of its acoustic density.

2. *Deformational type aging* is more often observed in people with oily skin prone to greasiness, which is characterized by a decrease in elasticity, turgor and the formation of a tired-looking face. The external signs of this type of aging are pitting edema, a pronounced nasolabial fold, and later the corners of the mouth become drooping. Other characteristics observed are couperosis and rosacea, smoothing of the face oval, sagging cheeks, double chin, folds on the neck. Wrinkles for this type of aging are less pronounced and are not the leading sign of the process. In this type of aging, poor microcirculation is also observed, but due to a decrease in venous blood flow and the formation of edema in the tissues. The ultrasound picture is characterized by an inhomogeneous hypoechoic structure, a dense epidermis, and the inclusion of intercellular fluid.

3. *Mixed-type aging* refers to aging which is a combination of the two types described above. It is possible to distinguish a special type, which features a combination of both wrinkles and pastiness, but in people with a mixed type of skin aging, hyperkeratosis and pigmentation are observed, and skin thinning and complex microcirculation disorders are present: both blood flow to the dermis and venous outflow are abnormal. In some areas, ultrasound reveals the acoustic characteristics of the first and second types of skin aging: before the cosmetic correction, the chin and cheeks feature heterogeneous, hypoechogenic structure with a dense epidermis and areas of fraying, a subepidermal hypoechogenic band in the periorbital area, dermis thinning, with the decrease in its the density [2].

The classification of the skin aging mechanisms, combined with the understanding of the process, helps to make a correction plan for the improvement of the appearance of mature and senior individuals. Most studies focus on the influence of solar radiation as the main inducer of aging, but in older people, many additional factors that go beyond environmental conditions should be considered. Lifestyle factors such as diet, sleep, and smoking are currently undergoing thorough analysis, as are the general age-related conditions (menopause, diabetes, and heart and lung diseases). All these factors can accelerate the natural deterioration of skin structure and function, which can affect the effectiveness of involution changes treatment. The search for new approaches to managing skin aging is becoming more and more relevant [3].

New scientific evidence has been obtained recently to support the long-debated assumption that air pollution is also one of the causes of premature skin aging. This conclusion is based on epidemiological and mechanistic data. In particular, exposure to the corresponding particulate matter and nitrogen dioxide (NO_2) is associated with an increased risk of developing facial pigmentation. In addition, genetic studies indicate modification of gene penetration under environmental

influence: women carrying certain genetic variants of the aryl-carbohydrate receptor signaling pathway have a higher risk of developing facial pigmentation spots in response to exposure to fine particulate matter of a certain size. Mechanistic studies prove a causal relationship, since local exposure of human skin *ex vivo* or *in vivo* to non-toxic concentrations of standardized diesel exhaust mixture increases skin pigmentation, causing *de novo* synthesis of melanin through an oxidative stress reaction. Therefore, the use of anti-pollution cosmetics containing antioxidants, as well as aryl hydrocarbon receptor antagonists, is effective for preventing or reducing the development of skin pigmentation. In a real-life situation, human skin is affected by both environmental factors simultaneously, i. e., solar radiation and mechanical irritation. Relevant epidemiological studies show that solid particles present in the troposphere and solar ultraviolet radiation interact with each other. This makes it possible to discuss environmentally caused skin aging [4].

Taking into account the speed of adverse changes in the environmental situation, it is necessary to recognize the fact that facial aging is one of the most popular topics of modern "cutaneous science". Changes in the human face inevitably progress over time; however, there are many methods, both surgical and non-surgical, that can reduce the stigma of aging and provide patients with a desired appearance [5].

The shifting attitude to age-related changes in the skin within the healthy lifestyle trend has been reflected in the establishment of public health programs in a number of countries. Since facial wrinkles can be seen as a marker of internal aging, there is an incentive to motivate people to adopt a number of healthy behaviors in senior age [6].

The mechanisms of skin aging include the action of reactive oxygen intermediates (ROI), mitochondrial DNA mutations and telomere shortening, as well as hormonal changes [1]. The variable that determines the rate of aging of the skin or tissue as a whole is the predominance of tissue degeneration over tissue regeneration. One distinguishes between the mechanisms of internal and external aging (photoaging). Special emphasis is placed on the influence of ultraviolet (UV) exposure on the visual signs of skin aging and the variability of UV effect depending on the geographic location of a particular person and their skin type. UV radiation has a direct photochemical impact on the DNA, RNA, proteins and vitamin D. At the same time, it is shown that skin aging processes are initiated and often spread not only under the influence of UV, but also as a result of oxidative phenomena, despite the recently recognized adaptive responses to oxidative stress [7].

The increase in the average age of men and women initiated the formation of the foundations of the so-called "successful aging", the founders of which are considered to be P. B. Baltes and M. M. Baltes, who proposed a model of selective optimization with compensation [8]. It included the maintenance of health and the achievement of apparent well-being. E. Kahana and B. Kahana focused on social and psychological resources of a human being, preventive and corrective adaptations, psychological, existential and social well-being [9, 10]. The theory of "successful aging" was further advanced by C. A. Depp and D. V. Jeste, who showed that even in the presence of disability, it is possible to maintain physical and cognitive functioning and life satisfaction in general [11, 12].

Active longevity is currently promoted by Russian researchers, but it is foreign scientists who first produced an evidence-based prediction of increased life expectancy. It is expected that in the near future life expectancy will increase in 35 developed countries, with a probability of at least 65% for women and 85% for men. There is a 90% probability that life expectancy at birth among South Korean women in 2030 will exceed 86.7 years, which corresponds to the world's highest life expectancy in 2012, and 57% probability for this indicator to reach 90 years. The projected life expectancy of women in South Korea follows that of France, Spain and Japan. There is a more than 95% probability that life expectancy at birth among men in South Korea, Australia, and Switzerland will exceed 80 years in 2030, and a more than 27% probability that it will exceed 85 years. More than half of the projected increase in life expectancy at birth for women will be due to an increase in life expectancy over the age of 65. Thus, researchers point to a constant increase in life expectancy, as well as the need for careful planning of health care, social services and pensions [13-15].

The improvement of the quality of life due to the growth of therapeutic possibilities for the treatment of chronic diseases is one of the factors that promote the development of correction treatments against involutional skin changes. The prospects for further expansion of the range of health, i. e., a period free from age-related disability and diseases, are evaluated critically. Understanding human aging is a major challenge for the physiological sciences. This is becoming an increasingly urgent issue because of the increasing proportion of people who live to old age, and because of changes in the main reasons for the continued increase in life expectancy. The previous increase was almost entirely due to the prevention of mortality in childhood and middle age. This process has been so successful that there is little room for significant further increases from the achieved level in the developed countries. The recent increase in life expectancy is due to a new reason. As a rule, we reach old age with better health, and now the mortality rate in old age is lower. At the same time, biologic science has established that there is almost certainly no fixed program of aging that is caused

by the accumulation of damage throughout life. It becomes obvious that the aging process is much more malleable than we used to think. This leads researchers to look for factors that regulate this malleability, and to identify relationships between, on the one hand, the internal biological processes that cause many chronic diseases and disorders, among which age is by far the largest risk factor, and, on the other hand, social factors and lifestyle that affect our individual health pathways in old age [16].

Most researchers believe that one of the key directions in the development of anti-aging technologies should be the enhancement of socialization among people of senior age. In this aspect, non-invasive methods of correction of involution-type skin changes are the most promising field of dermatology and cosmetology, as evidenced by the variety of methods proposed for correcting age-related skin changes.

The main noninvasive methods of correction of involution changes in the skin of the face

1. *CO_2 laser (λ10.6 μm)*

A CO_2 laser is a laser that operates on gas mixtures. The radiation of this laser is absorbed by water molecules of tissues and cells, which leads to vaporization (evaporation), and, as a result, the emission of tissue structures with the formation of a damage zone (ablation crater). The disadvantage of the CO_2 laser is the release of thermal energy in the tissue around the ablation site. If the power increases, tissue removal accelerates, while the depth of thermal exposure is reduced. The wavelength (λ) of 10.6 microns pertains to long-wave radiation, and its use allows to penetrate to a considerable depth, unlike with other lasers [17].

There are 2 modes:

1. Fractional: a) rejuvenation, b) correction of scarring or stretch marks of the skin
2. Continuous: a) removal of skin neoplasms, b) surgery.

2. *Er:YAG laser (λ 2.94 μm)*

Er:YAG refers to solid-state lasers, and their working medium is erbium and yttrium aluminium garnet. It is characterized by high absorption of water molecules. Its wavelength is 2940 nm. It has a smaller area and depth of penetration, in contrast to the CO_2 laser, which results in a faster healing of the surface which was treated. [18]

A more superficial effect in contrast to a CO_2 laser:

- rejuvenation (laser peeling)
- correction of scarring and stretch marks of the skin.

3. *Er:glass laser (λ 1.54 μm)*

Er:glass laser on erbium glass. Chromophores are water-containing components of the dermis, which allows the thermal effect to act directly without damaging the epidermis, with the activation of neocollagenesis and reparative processes. The wavelength of 1540 (1550 nm), which affects the infrared range of radiation, is used for ablative fractional photothermolysis [19].

Applications:

- correction of involution changes of the skin
- correction of scarring and stretch marks of the skin
- dentistry
- ophthalmology

4. *Intense pulsed light (IPL)*

Intense pulsed light (IPL) is produced by a source of electromagnetic radiation with a wide range of wavelengths, i. e., polychromatic light (from 420 nm to the mid-infrared spectrum) and is delivered in the form of flashes (pulses) rather than as constant light. As a rule, IPL technology involves the use of filters in order to work with certain chromophores. The main chromophores are melanin and oxyhemoglobin. Blue and green light produce an effect on the surface layers, while orange and yellow spectra act on the middle layers of the skin, and infrared light influences the deep ones. Green light reaches the level of the papillary dermis and has an effect on the vessels in this layer [20, 21].

The red spectrum is used for epilation of dark hair, while the green spectrum is for vascular malformations and correction of hyperpigmentation.

5. *Exposure to high frequency radio waves*

Morphological changes caused by exposition to high-frequency radio waves occur in the deep layers of the dermis and the adjacent fat tissue. At the same time, remodeling of the extracellular matrix of the dermis causes the expansion of its deep layers with the accumulation of collagens of the 1st and 3rd types and maintaining the ratio between them in favor of type 1 collagen. Activation of neoangiogenesis in the dermis can be considered a key anti-aging factor of radio wave exposure, which occurs gradually, reaching its maximum 12 months after a single exposure [22]. The correction of involution changes of the skin includes RF-microneedling and RF-lifting.

6. *Photodynamic therapy (PDT)*

PDT is a two-component treatment method: one of the components is a photosensitizer (PS), the other is the light of a low-energy laser, the wavelength of which corresponds to the peak of the PS absorption. PDT is essentially selective destruction of pathological tissue, which is achieved due to the difference in the concentration of PS in pathological and normal tissues, as well as due to the local application of a light source.

PDT is used in various areas of modern dermatology and cosmetology. Some see this technique as a new opportunity for the treatment of micro-

bial infections complicated by microbial resistance. Clinical experience with PDT in the field of dermatology for the treatment of infections is mainly related to the use of 5-aminolevulinic acid (5-ALA) and the use of phenothiazine modifications in dentistry. It is expected that in the coming years, PDT will be introduced for the treatment of complex infections, and will be administered with the use of modern antimicrobial PSs targeted at microbial cells [23]. Treatment of papillomatoses with a combination of surgery and PDT is recognized as effective and safe: with a relapse rate of 25%, the level of satisfaction with treatment in patients was 95% three months after treatment and 100% six months after treatment [24].

The prospects and results of PDT application receive increasing attention at various international conferences, where the issue is discussed by medical cosmetology experts. PDT can help correct pigmentation, reduce skin roughness, eliminate fine lines and improve the complexion, as well as reduce actinic elastosis. The anti-aging effect of various PDT methods used in different modes with different PSs is documented in research publications. In particular, it is proved that topical PDT "stops" some signs of skin aging: the severity of fine wrinkles, spotty hyperpigmentation, tactile irregularity and yellow color decrease. It has been confirmed by immunohistochemistry methods that PDT normalizes collagen production and increases epidermal proliferation. An indirect stimulation of neocollagenesis occurs under the influence of cytokine production [25]. Due to the effect of PDT on the skin, its texture improves, its elasticity increases, the number of small wrinkles decreases, and deeper ones become less pronounced and increase skin elasticity [26]. In support of the above, the results of a number of studies are provided in the following part.

The most commonly used PSs in cosmetology are 5-aminolevulinic acid (5-ALA) and its methyl esther (MAL). Their use significantly increases the efficiency of PDT, both in its classic version with the use of activating light sources and with daylight. Just two sessions of PDT of the facial skin with MAL using red light (37 J/cm^2) resulted in a significant increase in collagen deposition and a decrease in of solar elastosis signs. An immunohistochemical study confirmed an increase in the expression of procollagen-I and matrix metalloproteinase 9 genes [27]. The effectiveness of MAL as a PS in combination with the therapeutic effect of red color was also evaluated in a double-blind randomized placebo-controlled study of the treatment of photoaging of face skin. In this study, half of the participant's face was exposed to PDT, with a second course 2-3 weeks later, and the other half of the face was irradiated with red light without the use of PS (placebo). The primary result was the assessment of the total photo damage 1 month after the second session. Secondary control points were a comparative assessment of the skin condition in terms of the presence of fine wrinkles, pigmentation, tactile roughness, yellowness, erythema and telangiectasia 1 month after the second session. The use of MAL showed significantly higher effectiveness of facial skin photoaging treatment compared to placebo. This therapy was found to be effective for all other specific secondary indicators, except for telangiectasis [28, 29].

As for the frequency of procedures with MAL, cosmetologists usually recommend 2 or 3 procedures with an interval of 3-6 months before clinically and aesthetically visible results of the therapy are achieved. The choice of the interval between PDT courses depends, first of all, on the initial clinical indicators and the individual reparative potential of the patient, which are revealed after the first PDT procedure. However, an interval of 4 weeks, or even longer, should be observed between treatments in the case of additional intermediate effects on the skin (any of the types) [30].

It is believed that one of the ways to improve the effectiveness of PDT against actinic keratosis is to use it in combination with drug therapy. For example, researchers have examined the effectiveness of a combination of PDT amd Imiquimod and 5-Fluorouracil creams, Ingenol mebutat gels, Tazarotene and Calcipotriol ointment. Patients receiving combined treatment showed a higher clearance rate of actinic keratosis (HR 1.63; 95% CI 1.15-2.33; P = 0.007). Similarly, the clearance of actinic keratosis in PDT with topical applications was higher compared to monotherapy (HR 1.48; 95% CI 1.04-2.11; P = 0.03). A subgroup analysis was performed for PDT in combination with Imiquimod, revealing an increased total clearance rate compared to monotherapy (HR 1.57, 95% CI 1.09-2.25, P = 0.02). No PDT-induced pain or registration of local skin reactions after treatment were reported. The combination of PDT with other local medicinal effects actually improves the clearance rates of actinic keratosis compared to any monotherapy. This study highlights that the sequential use of two treatment methods provides an effective therapy in patients with multiple foci of actinic keratosis [31].

In addition to the combination with medications, the authors also report that the combination of PDT with various physical techniques, such as microdermabrasion, microneedle exposure, and laser therapy, improves the clinical effectiveness and cosmetic results of treatment of actinic keratosis [32].

Taking into account the impairment of the environment and its role in the aging process, the increasing share of elderly people in the society, as well as the accumulation of cancer and precancerous skin pathologies, it is possible to talk about the prospects of PDT methods for cosmetic correction in persons with a burdened history.

REFERENCES

1. Tobin D.J. Introduction to skin aging, *J Tissue Viability*, 2017, vol. 26(1), pp. 37–46.
2. Yusova Zh.Yu. Involutional skin changes: classification and ultrasound changes. In *Perspektivy razvitiya sovremennoj mediciny. Sbornik nauchnykh trudov po itogam mezhdunarodnoi nauchno-prakticheskoi konferentsii* [Prospects for modern medicine development. Conference proceedings]. Voronezh, 2014. 170 p.
3. Addor F.A.S. Beyond photoaging: additional factors involved in the process of skin aging, *Clin Cosmet Investig Dermatol*, 2018, vol. 11, pp. 437–443. doi: 10.2147/CCID.S177448
4. Schikowski T., Krutmann J. Air pollution (particulate matter and nitrogen dioxide) and skin aging, *Hautarzt*, 2019, vol. 70(3), pp. 158–162. (in German)
5. Shah A.R., Kennedy P.M. The Aging Face, *Med Clin North Am*, 2018, vol. 102(6), pp. 1041–1054. doi: 10.1016/j.mcna.2018.06.006
6. Bhatt N., Agrawal S., Mehta K. Risk factors and self-perception for facial aging among Nepalese population, *J Cosmet Dermatol*, 2019. doi: 10.1111/jocd.12885
7. Kammeyer A., Luiten R.M. Oxidation events and skin aging, *Ageing Res Rev*, 2015, vol. 21, pp. 16–29. doi: 10.1016/j.arr.2015.01.001
8. Baltes P.B., Baltes M.M. Psychological perspectives on successful aging: The model of selective optimization with compensation. In *Successful aging: Perspectives from the behavioral sciences*. United Kingdom, Cambridge University Press, 1990. pp. 1–34.
9. Kahana E., Kahana B. Contextualizing successful aging: New directions in age-old search. In *Invitation to the life course: A New look at old age*. Amityville, NY, Baywood Publishing Company, 2003. pp. 225–255.
10. Kahana E., Kahana B., Kercher K. Emerging lifestyles and proactive options for successful aging, *Ageing International*, 2003, vol. 28, pp. 155–180.
11. Depp C.A., Jeste D.V. Definitions and predictors of successful aging: A comprehensive review of larger quantitative studies, *American Journal of Geriatric Psychiatry*, 2006, vol. 14, pp. 6–20. doi: 10.1097/01.JGP.0000192501.03069.bc
12. Phelan E.A., Larson E.B. "Successful aging"—Where next?, *Journal of the American Geriatric Society*, 2002, vol. 50, pp. 1306–1308.
13. Kontis V., Bennett J.E., Mathers C.D., Li G., Foreman K., Ezzati M. Future life expectancy in 35 industrialised countries: projections with a Bayesian model ensemble, *Lancet*, 2017, vol. 389, pp. 1323–1335. doi: 10.1016/S0140–6736(16)32381–9
14. Vijg J., Le Bourg E. Aging and the Inevitable Limit to Human Life Span, *Gerontology*, 2017, vol. 63(5), pp. 432–434. doi: 10.1159/000477210
15. Shetty A.K., Kodali M., Upadhya R., Madhu L.N. Emerging Anti-Aging Strategies – Scientific Basis and Efficacy, *Aging Dis*, 2018, vol. 9(6), pp. 1165–1184. doi: 10.14336/AD.2018.1026
16. Kirkwood T.B.L. Why and how are we living longer?, Exp Physiol, 2017, vol. 102(9), pp. 1067–1074. doi: 10.1113/EP086205.

ЛИТЕРАТУРА

1. Tobin D.J. Introduction to skin aging // J Tissue Viability. – 2017. – Vol. 26(1). – P. 37–46.
2. Юсова Ж.Ю. Инволюционные изменения кожи: классификация и ультразвуковые изменения. В сборнике: Перспективы развития современной медицины, Сборник научных трудов по итогам международной научно-практической конференции. – Воронеж, 2014. – 170 с.
3. Addor F.A.S. Beyond photoaging: additional factors involved in the process of skin aging // Clin Cosmet Investig Dermatol. – 2018. – Vol. 11. – P. 437–443. doi: 10.2147/CCID.S177448
4. Schikowski T., Krutmann J. Air pollution (particulate matter and nitrogen dioxide) and skin aging // Hautarzt. – 2019. – Vol. 70(3). – P. 158–162. (in German)
5. Shah A.R., Kennedy P.M. The Aging Face // Med Clin North Am. – 2018. – Vol. 102(6). – P. 1041–1054. doi: 10.1016/j.mcna.2018.06.006
6. Bhatt N., Agrawal S., Mehta K. Risk factors and self-perception for facial aging among Nepalese population // J Cosmet Dermatol. – 2019. doi: 10.1111/jocd.12885
7. Kammeyer A., Luiten R.M. Oxidation events and skin aging // Ageing Res Rev. – 2015. – Vol. 21. – P. 16–29. doi: 10.1016/j.arr.2015.01.001
8. Baltes P.B., Baltes M.M. Psychological perspectives on successful aging: The model of selective optimization with compensation. In Baltes P.B., Baltes M.M, editors. (Eds.), Successful aging: Perspectives from the behavioral sciences. – United Kingdom: Cambridge University Press, 1990. – P. 1–34.
9. Kahana E., Kahana B. Contextualizing successful aging: New directions in age-old search. In Settersten R. Jr, editor. (Ed.), Invitation to the life course: A New look at old age. – Amityville, NY: Baywood Publishing Company, 2003. – P. 225–255.
10. Kahana E., Kahana B., Kercher K. Emerging lifestyles and proactive options for successful aging // Ageing International. – 2003. – Vol. 28. – P. 155–180.
11. Depp C.A., Jeste D.V. Definitions and predictors of successful aging: A comprehensive review of larger quantitative studies // American Journal of Geriatric Psychiatry. – 2006. – Vol. 14. – P. 6–20. doi: 10.1097/01.JGP.0000192501.03069.bc
12. Phelan E.A., Larson E.B. "Successful aging"—Where next? // Journal of the American Geriatric Society. – 2002. – Vol. 50. – P. 1306–1308.
13. Kontis V., Bennett J.E., Mathers C.D., Li G., Foreman K., Ezzati M. Future life expectancy in 35 industrialised countries: projections with a Bayesian model ensemble // Lancet. – 2017. – Vol. 389. – P. 1323–1335. doi: 10.1016/S0140–6736(16)32381–9
14. Vijg J., Le Bourg E. Aging and the Inevitable Limit to Human Life Span // Gerontology. – 2017. – Vol. 63(5). – P. 432–434. doi: 10.1159/000477210
15. Shetty A.K., Kodali M., Upadhya R., Madhu L.N. Emerging Anti-Aging Strategies – Scientific Basis and Efficacy // Aging Dis. – 2018. – Vol. 9(6). – P. 1165–1184. doi: 10.14336/AD.2018.1026

17. Sheptii O.V., Kruglova L.S., Zhukova O.V., Ektova T.V., Raksha D.A., Shmatova A.A. High-energy laser radiation in dermatology and cosmetology, *Rossiiskii zhurnal kozhnykh i venericheskikh bolezney*, 2012, no. 6, pp. 39–43. (in Russian)
18. Karabut M.M., Gladkova N.D., Feldshtein F.I. Fractional laser photothermolysis in the treatment of skin defects: possibilities and effectiveness (review), *Sovremennye tekhnologii v meditsine*, 2016, vol. 8, no. 2, pp. 98–108. (in Russian) doi:10.17691/stm2016.8.2.14
19. Potekaev N.N., Kruglova L.S. *Lazer v dermatologii i kosmetologii* [Laser in dermatology and cosmetology]. Alkor Pablishers, 2018. 290 p.
20. Gupta G. Diode Laser: Permanent hair "Reduction" Not "Removal", *Int J Trichology*, 2014, vol. 6(1), pp. 34. doi: 10.4103/0974–7753.136762.
21. Di Bernardo B.E., Pozner J.N. Intense Pulsed Light Therapy for Skin Rejuvenation, *Clin Plast Surg*, 2016, vol. 43(3), pp. 535–40. doi: 10.1016/j.cps.2016.03.008.
22. Trufanov V.D., Kogan E.A., Yutskovskaya Ya.A., Faizullina N.M., Ivanov S.Yu. High frequency radio waves – an innovative approach to the correction of age-related skin changes: clinical, immunohistochemical study, *STM*, 2016, vol. 8, no. 1, pp. 106–116. (in Russian) doi: http://doi.org/10.17691/stm2016.8.1.14
23. Kharkwal G.B., Sharma S.K., Huang Y.Y., Dai T., Hamblin M.R. Photodynamic therapy for infections: clinical applications, *Lasers Surg Med*, 2011, vol. 43(7), pp. 755–67. doi: 10.1002/lsm.21080
24. Gao Y., Wang H.L., Wang W.S., Liu J., Lu Y.G. Treatment of lip florid papillomatosis with topical ALA-PDT combined with curettage: Outcome and safety, *Photodiagnosis Photodyn Ther*, 2016, vol. 15, pp. 83–7. doi: 10.1016/j.pdpdt.2016.05.012
25. Kohl E., Torezan L.A.R., Landthaler M., Szeimies R.M. Aesthetic effects of topical photodynamic therapy, *J Eur Acad Dermatol Venereol*, 2010, vol. 24, pp. 1261– 9.
26. Lucena S.R., Salazar N., Gracia-Cazaña T. Combined Treatments with Photodynamic Therapy for Non-Melanoma Skin Cancer, *Int J Mol Sci*, 2015, vol. 16(10), pp. 25912–33. doi: 10.3390/ijms161025912
27. Szeimies R.M., Torezan L., Niwa A., Valente N., Unger P., Kohl E., Schreml S., Babilas P., Karrer S., Festa-Neto C. Clinical, histopathological and immunohistochemical assessment of human skin field cancerization before and after photodynamic therapy, *Br J Dermatol*, 2012, vol.167, pp. 150– 9.
28. Sanclemente G., Medina L., Villa J.F., Barrera L.M., Garcia H.I. A prospective split-face double-blind randomized placebo-controlled trial to assess the efficacy of methyl aminolevulinate + red-light in patients with facial photodamage, *J Eur Acad Dermatol Venereol*, 2011, vol. 25, pp. 49–58.
29. Philipp-Dormston W.G. Photodynamic therapy for aesthetic-cosmetic indications, *G Ital Dermatol Venereol*, 2018, vol. 153(6), pp. 817–826. doi: 10.23736/S0392–0488.18.05982–5.
30. Karrer S., Kohl E., Feise K., Hiepe-Wegener D., Lischner S., Philipp-Dormston W. Photodynamic therapy for skin rejuvenation: review and summary of the literature--results of a consensus conference of an expert group for aesthetic photodynamic

16. Kirkwood T.B.L. Why and how are we living longer? // Exp Physiol. – 2017. – Vol. 102(9). – P. 1067–1074. doi: 10.1113/EP086205.
17. Шептий О.В., Круглова Л.С., Жукова О.В., Эктова Т.В., Ракша Д.А., Шматова А.А. Высокоэнергетическое лазерное излучение в дерматологии и косметологии // Российский журнал кожных и венерических болезней. – 2012. – № 6. – С. 39–43.
18. Карабут М.М., Гладкова Н.Д., Фельдштейн Ф.И. Фракционный лазерный фототермолиз в лечении кожных дефектов: возможности и эффективность (обзор) // Современные технологии в медицине. – 2016. – Т. 8, №. 2. – С. 98–108. doi:10.17691/stm2016.8.2.14
19. Потекаев Н.Н., Круглова Л.С. Лазер в дерматологии и косметологии. – Алькор Паблишерс, 2018 г. – 290 с.
20. Gupta G. Diode Laser: Permanent hair "Reduction" Not "Removal" // Int J Trichology. – 2014. – Vol. 6(1). – P. 34. doi: 10.4103/0974–7753.136762.
21. Di Bernardo B.E., Pozner J.N. Intense Pulsed Light Therapy for Skin Rejuvenation // Clin Plast Surg. – 2016. – Vol. 43(3). – P. 535–40. doi: 10.1016/j.cps.2016.03.008.
22. Труфанов В.Д., Коган Е.А., Юцковская Я.А., Файзуллина Н.М., Иванов С.Ю. Радиоволны высокой частоты – инновационный подход к коррекции возрастных изменений кожи: клиническое, иммуногистохимическое исследование // СТМ. – 2016. – Т. 8, № 1. – С. 106–116. doi: http://doi.org/10.17691/stm2016.8.1.14
23. Kharkwal G.B., Sharma S.K., Huang Y.Y., Dai T., Hamblin M.R. Photodynamic therapy for infections: clinical applications // Lasers Surg Med. – 2011. – Vol. 43(7). – P. 755–67. doi: 10.1002/lsm.21080
24. Gao Y., Wang H.L., Wang W.S., et al. Treatment of lip florid papillomatosis with topical ALA-PDT combined with curettage: Outcome and safety // Photodiagnosis Photodyn Ther. – 2016. – Vol. 15. – P. 83–7. doi: 10.1016/j.pdpdt.2016.05.012
25. Kohl E., Torezan L.A.R., Landthaler M., Szeimies R.M. Aesthetic effects of topical photodynamic therapy // J Eur Acad Dermatol Venereol. – 2010. – Vol. 24. – P. 1261– 9.
26. Lucena S.R., Salazar N., Gracia-Cazaña T. Combined Treatments with Photodynamic Therapy for Non-Melanoma Skin Cancer // Int J Mol Sci. – 2015. – Vol. 16(10). – P. 25912–33. doi: 10.3390/ijms161025912
27. Szeimies R.M., Torezan L., Niwa A. et al. Clinical, histopathological and immunohistochemical assessment of human skin field cancerization before and after photodynamic therapy // Br J Dermatol. – 2012. – Vol. 167. – P. 150–9.
28. Sanclemente G., Medina L., Villa J.F. et al. A prospective split-face double-blind randomized placebo-controlled trial to assess the efficacy of methyl aminolevulinate + red-light in patients with facial photodamage // J Eur Acad Dermatol Venereol. – 2011. – Vol. 25. – P. 49–58.
29. Philipp-Dormston W.G. Photodynamic therapy for aesthetic-cosmetic indications // G Ital Dermatol Venereol. – 2018. – Vol. 153(6). – P. 817–826. doi: 10.23736/S0392–0488.18.05982–5.
30. Karrer S., Kohl E., Feise K., et al. Photodynamic therapy for skin rejuvenation: review and summary of the literature--results of a

therapy, *J Dtsch Dermatol Ges*, 2013, vol. 11(2), pp. 137–48. doi: 10.1111/j.1610–0387.2012.08046.x.

31. Heppt M.V., Steeb T., Leiter U., Berking C. Efficacy of photodynamic therapy combined with topical interventions for the treatment of actinic keratosis: a meta-analysis, *J Eur Acad Dermatol Venereol*, 2019. doi: 10.1111/jdv.15459
32. Nguyen K., Khachemoune A. An Update on Topical Photodynamic Therapy for Clinical Dermatologists, *J Dermatolog Treat*, 2019. doi: 10.1080/09546634.2019.1569752.

consensus conference of an expert group for aesthetic photodynamic therapy // J Dtsch Dermatol Ges. – 2013. – Vol. 11(2). – P. 137–48. doi: 10.1111/j.1610–0387.2012.08046.x.

31. Heppt M.V., Steeb T., Leiter U., Berking C. Efficacy of photodynamic therapy combined with topical interventions for the treatment of actinic keratosis: a meta-analysis // J Eur Acad Dermatol Venereol. – 2019. doi: 10.1111/jdv.15459.
32. Nguyen K., Khachemoune A. An Update on Topical Photodynamic Therapy for Clinical Dermatologists // J Dermatolog Treat. – 2019. doi: 10.1080/09546634.2019.1569752.

NEW APPROACHES TO FORMATION OF DIAGNOSIS-RELATED GROUPS FOR PAYMENT FOR RADIOTHERAPY AND CHEMOTHERAPY BASED ON CLINICAL GUIDELINES WITH THE USE OF STANDARDIZED MODULES OF HEALTHCARE

Ledovskikh Yu.A.[1], Semakova E.V.[1], Omelyanovskiy V.V.[1], Kravtsov A.A.[1], Prokhorovich E.A.[1], Avxentyeva M.V.[1, 2], Zheleznyakova I.A.[1], Petrovskiy A.V.[2, 3]
[1]The Center for Healthcare Quality Assessment and Control of the Ministry of Health of the Russian Federation, Moscow, Russia
[2]Sechenov First Moscow State Medical University, Moscow, Russia
[3]National Medical Research Center of Oncology named after N.N. Blokhin of the Ministry of Health of Russia, Moscow, Russia

Abstract

The article presents a methodology and results of developing diagnosis related groups (DRGs) for the cases of healthcare provided with the use of radiotherapy and chemoradiotherapy for malignant neoplasms in Russian Federation. A key element of the methodology is the standardized module of healthcare (SM) which allows calculating the tariffs for medical care in accordance with clinical guidelines. As a result of the application of the new methodology, in 2019, changes were made to the DRG model in terms of payment for radiotherapy and chemoradiotherapy. The changes included developing 10 DRGs for in-patient radiotherapy and 10 DRGs in day hospital; 7 DRGs for in-patient chemoradiotherapy and 5 DRGs in day hospital. New classification criteria have been introduced into the DRG model for attributing the case to a certain DRG, in addition to the medical service used before. The number of fractions became a new criterion for radiotherapy, the number of fractions and the international non-proprietary name of the drug were proposed for chemoradiotherapy. A wider range of DRG's weight coefficients was calculated, which allows more differentiated reimbursement of the costs of medical care provided by medical organizations depending on the method and the regimen used.

Keywords: radiotherapy, chemoradiotherapy, diagnosis related group, standardized module of healthcare, clinical guidelines, standard of medical care.

For citations: Ledovskikh Yu.A., Semakova E.V., Omelyanovskiy V.V., Kravtsov A.A., Prokhorovich E.A., Avxentyeva M.V., Zheleznyakova I.A., Petrovskiy A.V. New approaches to formation of diagnosis-related groups for payment for radiotherapy and chemotherapy based on clinical guidelines with the use of standardized modules of healthcare, *Biomedical Photonics*, 2019, vol. 8, no. 4, pp. 36–46. (in Russian) doi: 10.24931/2413–9432–2019–8–4–36–46

Contacts: Ledovskikh Yu.A., e-mail: jledovskih@gmail.com

НОВЫЕ ПОДХОДЫ К ФОРМИРОВАНИЮ КЛИНИКО-СТАТИСТИЧЕСКИХ ГРУПП ДЛЯ ОПЛАТЫ ЛУЧЕВОЙ И ХИМИОЛУЧЕВОЙ ТЕРАПИИ НА ОСНОВЕ КЛИНИЧЕСКИХ РЕКОМЕНДАЦИЙ С ИСПОЛЬЗОВАНИЕМ СТАНДАРТИЗИРОВАННЫХ МОДУЛЕЙ МЕДИЦИНСКОЙ ПОМОЩИ

Ю.А. Ледовских[1], Е.В. Семакова[1], В.В. Омельяновский[1], А.А. Кравцов[1], Е.А. Прохорович[1], М.В. Авксентьева[1, 2], И.А. Железнякова[1], А.В. Петровский[2,3]
[1]Центр экспертизы и контроля качества медицинской помощи Минздрава России, Москва, Россия
[2]Первый Московский государственный медицинский университет им. И.М. Сеченова, Москва, Россия
[3]Национальный медицинский исследовательский центр онкологии имени Н.Н. Блохина Минздрава России, Москва, Россия

Резюме

В статье представлены методика и результаты формирования клинико-статистических групп (КСГ) для оплаты случаев госпитализации при проведении лучевой и химиолучевой терапии больным со злокачественными новообразованиями. КСГ сформированы в результате расчета затрат на оказание медицинской помощи на основе стандартизированных модулей медицинской помощи, которые, в свою очередь, сформированы исходя из клинических рекомендаций. В результате применения новой методики внесены изменения в модель КСГ 2019 г. в части оплаты лучевой и химиолучевой терапии: вместо трех КСГ, существовавших ранее, сформировано по 10 КСГ для лучевой терапии в условиях круглосуточного и дневного стационара; 7 КСГ для химиолучевой терапии в условиях круглосуточного стационара и 5 КСГ для химиолучевой терапии в условиях дневного стационара. В модель КСГ введены новые, дополнительные к медицинской услуге, использованной ранее, классификационные критерии, позволяющие отнести случай госпитализации к КСГ: для лучевой терапии – количество фракций, для химиолучевой – количество фракций и международное непатентованное наименование лекарственного препарата. Увеличен диапазон коэффициентов затратоемкости КСГ, что позволяет более дифференцированно возмещать медицинским организациям затраты за оказанную медицинскую помощь в зависимости от проводимого метода и режима лучевой или химиолучевой терапии.

Ключевые слова: лучевая терапия, химиолучевая терапия, клинико-статистические группы, стандартизированный модуль, клинические рекомендации, стандарты медицинской помощи.

Для цитирования: Ледовских Ю.А., Семакова Е.В., Омельяновский В.В., Кравцов А.А., Прохорович Е.А., Авксентьева М.В., Железнякова И.А.,Петровский А.В. Новые подходы к формированию клинико-статистических групп для оплаты лучевой и химиолучевой терапии на основе клинических рекомендаций с использованием стандартизированных модулей медицинской помощи // Biomedical Photonics. – 2019. – Т. 8, № 4. – С. 36–46. doi: 10.24931/2413–9432–2019–8–4–36–46

Контакты: Ледовских Ю.А., e-mail: jledovskih@gmail.com

Introduction

According to the legislation in the field of healthcare in the Russian Federation (RF), medical care must be provided on the basis of clinical recommendations [1]. Currently, payment for specialized medical care provided in a round-the-clock and day hospital at the expense of compulsory medical insurance (CHI) is effected for a case of hospitalization pertaining to a group of diseases, including the diagnosis-related group (DRG). The DRG-based payment method is used in most of the Russian regions.

In 2018, the DRG intended for payment for antitumor drug therapy of solid tumors in adults was significantly changed; a method was used that allows for bringing the rates for paying for medical care in accordance with clinical recommendations through standardized modules (SM) of medical care [2]. However, the DRG for payments for medical care connected with radiation therapy has not changed since the development of the group: for both round-the-clock (since 2013) and day hospitals (since 2016), there were only three DRGs, and assignment to them was based on the type of service provided, encoded in accordance with the nomenclature of medical services. A small variation in the relative cost-intensity coefficients (CIC) of DRG did not allow for adequate payment for resource-intensive radiation therapy. In this regard, it was necessary to review the DRG in order to align the rates with clinical recommendations, which should contribute to a more equitable reimbursement of expenses of medical organizations that provide care for cancer. The purpose of this work was to form DRGs for payment for radiation and chemoradiation therapy, based on clinical recommendations.

Materials and methods

Coordination of DRG with clinical recommendations was carried out by creating SMs for cases of hospitalization for the purpose of radiation and chemoradiation therapy and calculating the cost of medical care based on them, followed by attributing cases with a similar cost to a single DRG.

The method of forming DRGs on the basis of clinical recommendations with the use of SMs developed by the FSBI "Center for Expertise and Quality Control of Medical Care" of the Ministry of Health of Russia [3], includes 4 stages:

1. The development of SMs containing complexes of medical interventions used to provide medical care with a certain method and mode of radiation or chemoradiation therapy in the case of hospitalization in a round-the-clock or day hospital.
2. The estimation of the expected number of hospitalizations to the round-the-clock and day hospitals for radiotherapy and chemoradiotherapy on a national scale.
3. SM-based calculation of hospitalization costs with the use of each method and radiation or chemoradiation therapy.
4. DRG formation.

SMs at the first stage are formed in the case of hospitalization of a patient with a specific malignant neoplasm for radiation or chemoradiotherapy by a certain method and in a certain mode. The structure of SMs corresponds to the standard structure of medical care approved by order of Ministry of Health of Russia: SMs included lists of the medical services used, medicines and medical supplies, with indication of frequency and number of admin-

istrations within the same hospitalization [4].

SM development was based on the following:

- 35 clinical recommendations for solid tumors in adults approved by the Association of Oncologists of Russia (AOR) at the time of the work (from June to September 2018), which described the methods and modes of radiation or chemoradiation therapy (Table 1);
- the procedure for providing medical care in the "Oncology" profile [5],
- medical services nomenclature [6],
- the state register of selling price limits [7],
- statistical data on the incidence of malignant tumors in 2017 [8].

The SM was formed with due consideration of the method of radiation therapy described in the clinical recommendations: remote (conventional or conformal), contact (intrastitial or intracavity) or radionuclide therapy, as well as of the equipment necessary for radiotherapy (X-ray devices, gamma-ray devices, linear electron accelerators).

The number of hospitalizations for radiotherapy and chemoradiotherapy is predicted at the second stage by constructing and processing decision trees that schematically represent the management options for patients with a certain malignant neoplasm. The tree nodes contain signs that influence the choice of patient management tactics; they were determined for each malignant neoplasm type based on clinical recommendations. The frequency of each treatment option was determined by expert oncologists and radiotherapists. The number of patients to be treated was calculated based on statistical data on the incidence of malignant tumors [8].

The cost of hospitalization for radiation or chemoradiotherapy by a specific method and in a specific mode is calculated at the third stage based on the developed SMs. The cost of the case is formed from the sum of the costs of medical services, medicines and therapeutic food indicated in the SM, and included the salary expenses (doctors, nurses and other medical personnel and specialists with higher and secondary medical education involved in the provision of medical care, and administrative and general support personnel of the institution) and other direct and indirect costs of the medical organization. Based on the actual data on the current practice in the Russian regions, the estimated expected number of hospitalizations was distributed according to the conditions for the provision of actual medical care: 65% of cases were attributed to the conditions of a 24-hour hospital and 35% to a day hospital.

The formation of the DRG at the fourth stage was performed by dividing the SM covering a certain group of radiotherapy and chemoradiotherapy methods into subgroups and then combining subgroups with a similar cost in the DRG, based on the calculated cost of the corresponding SM and the number of hospitalizations received for it. The clinical parameters that characterize the methods and modes of radiation or chemoradiation therapy were determined, allowing for attributing the case of hospitalization to the selected subgroup. These clinical parameters are proposed as classification criteria for assigning a case of hospitalization to a DRG.

Based on the estimated number of hospitalizations included in the DRG and their cost, the weighted average cost of each DRG in rubles was calculated and converted to the cost-intensity coefficient (CIC) by dividing by the base rate equal to 20,911.95 rubles for a 24-hour hospital and 11,629.43 rubles for a day hospital.

Results

Based on 35 clinical recommendations, 245 SMs for radiotherapy and 275 SMs for chemoradiotherapy were created. All but three of the SMs described hospitalization in both round-the-clock and day-care settings. The remaining 3 SMs, for radioiodotherapy, radioiodine ablation and intracranial radiotherapy, have been developed only for round-the-clock hospitalization, as these methods may not be used in a day hospital.

To determine the expected number of hospital admissions, 35 decision trees were constructed, one for each clinical recommendation. For example, figure 1 shows a fragment of the decision tree related to stomach cancer.

Based on the methods used, which are characterized by different resource consumption, the developed SMs for radiation therapy are divided into 4 groups of methods: remote, conformal, contact and radionuclide therapy. SMs for chemoradiotherapy are divided similarly, but according to three groups of methods (Table 2).

Within the groups of radiotherapy and chemoradiotherapy methods, subgroups are identified that are characterized by economic homogeneity, with due account for the distribution of the number of hospitalization cases.

SMs related to the conditions of a 24-hour hospital, developed for conformal teletherapy, were classified into 5 subgroups (Fig. 2), and for conventional therapy, radionuclide therapy, and contact radiotherapy, into 3, 2, and 1 subgroup, respectively.

For teletherapy methods, the number of fractions became the clinical parameter that allows for attributing the case of hospitalization to the selected subgroup; for radionuclide therapy, this factor is the INN of a radiopharmaceutical drug; for chemoradiotherapy methods, two parameters are used: the number of fractions and the INN of the antineoplastic drugs, or a combination of INNs of the antineoplastic drugs. The list of INNs of antitumor drugs or their combinations was formed on the basis of information about antitumor drugs included in the SM of chemoradiotherapy (Table 3).

Таблица 1
Перечень клинических рекомендаций, включенных в работу по формированию СМ для методов и режимов лучевой и химиолучевой терапии
Table 1
List of the clinical guidelines used for the developing SM for methods and regimens of radiotherapy and chemoradiotherapy

№	Наименование клинической рекомендации Clinical guidelines
1	Рак пищевода Esophageal cancer
2	Рак желудка Gastric cancer
3	Рак поджелудочной железы Pancreatic cancer
4	Рак прямой кишки Rectal cancer
5	Рак щитовидной железы Thyroid cancer
6	Рак гортани Cancer of the larynx
7	Рак шейки матки Cervical cancer
8	Рак тела матки Uterine corpus cancer
9	Рак предстательной железы Prostate cancer
10	Рак мочевого пузыря Bladder cancer
11	Меланома кожи Skin melanoma
12	Рак кожи базальноклеточный и плоскоклеточный Basal cell and squamous cell skin carcinoma
13	Рак молочной железы Breast cancer
14	Рак легкого Lung cancer
15	Рак печени Liver cancer
16	Рак желчевыводящих путей Hepatobiliary cancer
17	Мезотелиома плевры Pleural mesothelioma
18	Опухоли средостения и сердца Mediastinal mass and cardiac tumor
19	Рак трахеи Tracheal cancer
20	Опухоли слюнных желез Salivary gland tumors
21	Рак гортаноглотки Cancer of the hypopharynx
22	Рак губы Cancer of the lip
23	Рак носоглотки Cancer of the nasopharynx
24	Рак полости носа и придаточных пазух Cancer of nasal cavity and paranasal sinuses
25	Рак ротоглотки Cancer of the oropharynx
26	Плоскоклеточный рак вульвы Squamous cell vulvar cancer
27	Плоскоклеточный рак влагалища Squamous cell vagina cancer
28	Рак полового члена Penile cancer
29	Герминогенные опухоли у мужчин Germ cell tumors in men
30	Плоскоклеточный рак анального канала, анального края, перианальной кожи Squamous cell cancer of anal canal, anal margin, perianal skin
31	Карцинома Меркеля Merkel cell carcinoma
32	Злокачественные опухоли костей Malignant bone tumors
33	Саркомы мягких тканей Soft tissue sarcoma
34	Первичные опухоли центральной нервной системы Central nervous system primary cancer
35	Метастатическое поражение головного мозга Central nervous system metastatic tumor

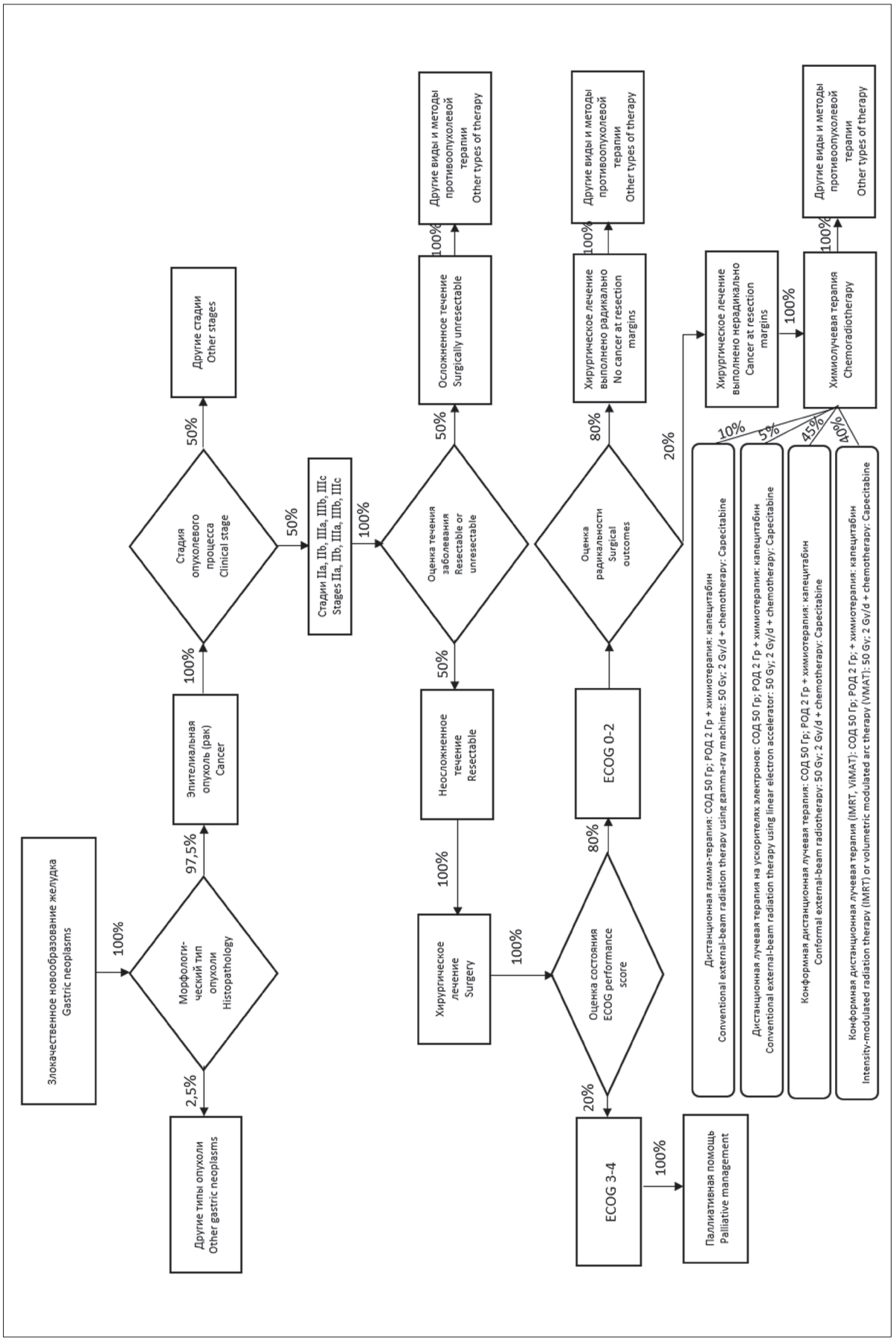

Рис. 1. Фрагмент дерева решений, использованного для расчета количества госпитализаций: ведение больного с раком желудка с использованием разных методов и режимов химиолучевой терапии
Fig. 1. A part of the decision tree for gastric cancer indicating chemoradiotherapy methods and regimens

Таблица 2
Перечень групп методов лучевой и химиолучевой терапии
Table 2
List of groups of radiotherapy and chemoradiotherapy methods

Вид противоопухолевой терапии Type of antineoplastic therapy	Группы методов лучевой и химиолучевой терапии Groups of methods of radiotherapy and chemoradiotherapy
Лучевая терапия Radiotherapy	Дистанционная лучевая терапия конвенциональная (включает терапию на рентгенотерапевтических аппаратах, гамма-аппараты, линейные ускорители электронов) Conventional external-beam radiotherapy (including therapy using X-ray machines, gamma-ray machines, linear electron accelerators)
	Конформная дистанционная терапия (включает технологии IMRT, IGRT, VMAT) Conformal external-beam radiotherapy (including IMRT, IGRT, VMAT technologies)
	Контактная лучевая терапия (включает внутритканевую и внутриполостную терапию) Brachytherapy (including interstitial and intracavitary therapy)
	Радионуклидная терапия Radionuclide therapy
Химиолучевая терапия Chemoradiotherapy	Дистанционная лучевая терапия конвенциональная в сочетании с противоопухолевой лекарственной терапией (включает терапию на гамма-аппараты, линейные ускорители электронов) Conventional external-beam radiotherapy in combination with chemotherapy (including therapy using gamma-ray machines, linear electron accelerators)
	Конформная дистанционная терапия в сочетании с противоопухолевой лекарственной терапией (включает технологии IMRT, IGRT, VMAT) Conformal external-beam radiotherapy in combination with chemotherapy (including IMRT, IGRT, VMAT technologies)
	Контактная лучевая терапия в сочетании с противоопухолевой лекарственной терапией (включает внутриполостную терапию) Brachytherapy in combination with chemotherapy (including interstitial and intracavitary therapy)

IMRT – лучевая терапия с модулированной интенсивностью / intensity-modulated radiation therapy
IGRT – лучевая терапия с визуальным контролем / image-guided radiation therapy
VMAT – ротационное объемно-модулированное облучение / volumetric modulated art therapy

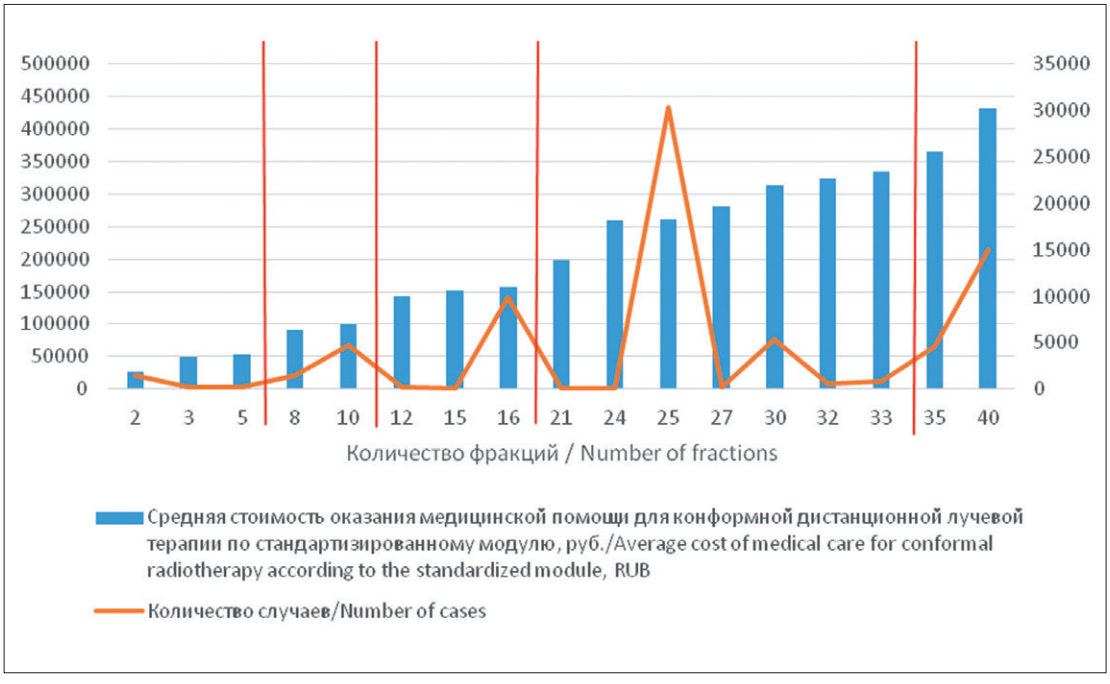

Рис. 2. Определение подгрупп методов лучевой и химиолучевой терапии на примере конформной дистанционной лучевой терапии, проводимой в условиях круглосуточного стационара
Fig. 2. Determination of the subgroups of radiotherapy and chemoradiotherapy methods by the example of conformal external-beam radiotherapy conducted in a full-time hospital

Таблица 3
Перечень международных непатентованных названий лекарственных препаратов и их сочетаний, используемых при формировании клинико-статистических групп
Table 3
List of drugs and their combinations used for developing diagnosis related groups (according to their international non-proprietary name)

№	МНН лекарственных препаратов и их сочетаний Drugs and their combinations
1	Доксорубицин Doxorubicin
2	Капецитабин Capecitabine
3	Карбоплатин Carboplatin
4	Митомицин + капецитабин Mitimycin + Capecitabin
5	Митомицин + фторурацил Mitomycin + Fluorouracil
6	Паклитаксел + карбоплатин Paclitaxel + Carboplatin
7	Темозоломид Temozolomide
8	Трастузумаб Trastuzumab
9	Трастузумаб + пертузумаб Trastuzumab + Pertuzumab
10	Фторурацил Fluorouracil
11	Цетуксимаб Cetuximab
12	Циклофосфамид + доксорубицин + цисплатин Cyclophosphamide + Doxorubicin + Cisplatin
13	Цисплатин Cisplatin
14	Цисплатин + доцетаксел Cisplatin + Docetaxel
15	Цисплатин + капецитабин Cisplatin + Capecitabine
16	Цисплатин + фторурацил Cisplatin + Fluorouracil
17	Этопозид + цисплатин Etoposide + Cisplatin

МНН – международное непатентованное название

In the next stage, some subgroups from different groups of methods were combined into one DRG based on the similar cost.

For methods of remote conventional radiotherapy, including therapy on X-ray devices, gamma-ray devices, linear electron accelerators, 3 DRGs were formed for radiotherapy in round-the-clock and day hospitals with a range of fractions up to 5 (inclusive), from 6 to 20 and more than 21 (inclusive).

For conformal remote radiotherapy, including IMRT, IGRT, and VMAT technologies, 5 DRGs were formed for round-the-clock and day hospitals with a range of fractions up to 7 (inclusive), 8 to 10, 11 to 20, 21 to 32, and more than 33 (inclusive).

Contact radiotherapy, which includes intra-cavity and intra-tissue therapy, is combined with radionuclide therapy, which places radioiodotherapy and radioiodine ablation and strontium chloride therapy [^{89}Sr], into the same DRG for both round-the-clock and day-care hospitals. Interstitial radiation therapy, radioiodine therapy and radioiodine ablation were included only in the DRG for 24-hour hospital.

The two remaining radionuclide therapies (samarium oxabifor [^{153}Sm] and radium chloride [^{223}Ra]) are combined into one DRG due to the higher cost.

For methods of chemoradiotherapy with a combination of remote conventional radiation therapy with antineoplastic drugs (with the exception of Temozolomide, Cetuximab and a combination of Trastuzumab and Pertuzumab), 2 DRGs were formed for a 24-hour hospital with a range of fractions of up to 29 (inclusive) and more than 30 (inclusive) and one DRG for a day hospital (without a division by the number of fractions).

In respect of the combination of conformal remote radiotherapy with antitumor drugs (with the exception of Temozolomide, Cetuximab, a combination of Trastuzumab and Pertuzumab), 2 DRGs were formed for a 24-hour hospital with a range of fractions up to 29 (inclusive) and more than 30 (inclusive), and one DRG for a day hospital (without division by the number of fractions).

Methods of remote radiotherapy in combination with Trastuzumab and Pertuzumab are combined into a single DRG for both round-the-clock and day-care hospitals, regardless of the method of radiation therapy and the number of fractions, since the calculated cost of hospitalization for the SM was largely determined by the cost of antineoplastic medications.

Similarly, methods of remote radiotherapy in combination with temozolomide or cetuximab were also combined into a single DRG for both round-the-clock and day-care hospitals, regardless of the method of radiotherapy and the number of fractions.

Based on the results of the work performed, the DRGs were established, and the corresponding CICs were calculated:

- for payments for radiation therapy, 10 DRGs of a round-the-clock hospital and 10 KSG of a day hospital (Table 4);
- for payments for chemoradiotherapy (radiation therapy in combination with drug therapy), 7 DRGs of a round-the-clock hospital and 5 DRGs of a day hospital (Table 5).

Clinical parameters that characterize methods and modes of radiation or chemoradiation therapy were introduced as additional classification criteria for previously used medical services encoded in accordance with the nomenclature, which made it possible to refer the case

Таблица 4
Клинико-статистические группы для лучевой терапии по условиям оказания медицинской помощи с указанием коэффициентов затратоемкости
Table 4
Diagnosis related groups and their weight coefficients for radiotherapy conducted in full-time and day hospitals

Описание в расшифровщике Name of a DGR	Метод и режим лучевой терапии Method and regimen of radiotherapy	КЗ Coeff.
	Круглосуточный стационар Full-time hospital	
Лучевая терапия (уровень 1) Radiotherapy (level 1)	Конвенциальная дистанционная лучевая терапия (1–5 фракций) Conventional external-beam radiotherapy (1–5 fractions)	1,04
Лучевая терапия (уровень 2) Radiotherapy (level 2)	Конформная дистанционная лучевая терапия (1–7 фракций) Conformal external-beam radiotherapy (1–7 fractions)	1,49
Лучевая терапия (уровень 3) Radiotherapy (level 3)	Контактная и радионуклидная лучевая терапия (радиойодтерапия, радиойодабляция, терапия стронция хлоридом [^{89}Sr]) Brachytherapy and radionuclide therapy (radioiodine therapy, radioiodine ablation therapy, strontium chloride [^{89}Sr] therapy)	4,15
Лучевая терапия (уровень 4) Radiotherapy (level 4)	Конвенциальная дистанционная лучевая терапия (6–20 фракций) Conventional external-beam radiotherapy (6–20 fractions)	5,32
Лучевая терапия (уровень 5) Radiotherapy (level 5)	Конформная дистанционная лучевая терапия (8–10 фракций) Conformal external-beam radiotherapy (8–10 fractions)	4,68
Лучевая терапия (уровень 6) Radiotherapy (level 6)	Конформная дистанционная лучевая терапия (11–20 фракций) Conformal external-beam radiotherapy (11–20 fractions)	7,47
Лучевая терапия (уровень 7) Radiotherapy (level 7)	Радионуклидная лучевая терапия (терапия самария оксабифором [^{153}Sm] и радия хлоридом [^{223}Ra]) Radionuclide therapy (samarium oxabifor [^{153}Sm] therapy and radium chloride [^{223}Ra] therapy)	8,71
Лучевая терапия (уровень 8) Radiotherapy (level 8)	Конвенциальная дистанционная лучевая терапия (более 21 фракций) Conventional external-beam radiotherapy (more than 21 fractions)	9,42
Лучевая терапия (уровень 9) Radiotherapy (level 9)	Конформная дистанционная лучевая терапия (21–32 фракций) Conformal external-beam radiotherapy (21–32 fractions)	12,87
Лучевая терапия (уровень 10) Radiotherapy (level 10)	Конформная дистанционная лучевая терапия (более 33 фракций) Conformal external-beam radiotherapy (more than 33 fractions)	19,73
	Дневной стационар Day hospital	
Лучевая терапия (уровень 1) Radiotherapy (level 1)	Конвенциальная дистанционная лучевая терапия (1–5 фракций) Conventional external-beam radiotherapy (1–5 fractions)	1,06
Лучевая терапия (уровень 2) Radiotherapy (level 2)	Конформная дистанционная лучевая терапия (1–7 фракций) Conformal external-beam radiotherapy (1–7 fractions)	1,83
Лучевая терапия (уровень 3) Radiotherapy (level 3)	Конвенциальная дистанционная лучевая терапия (6–20 фракций) Conventional external-beam radiotherapy (6–20 fractions)	2,31
Лучевая терапия (уровень 4) Radiotherapy (level 4)	Контактная и радионуклидная лучевая терапия (терапия стронция хлоридом [^{89}Sr]) Internal radiotherapy and radionuclide therapy (radioiodine therapy, radioiodine ablation therapy, strontium chloride [^{89}Sr] therapy)	2,84
Лучевая терапия (уровень 5) Radiotherapy (level 5)	Конформная дистанционная лучевая терапия (8–10 фракций) Conformal external-beam radiotherapy (8–10 fractions)	4,16
Лучевая терапия (уровень 6) Radiotherapy (level 6)	Конвенциальная дистанционная лучевая терапия (более 21 фракций) Conventional external-beam radiotherapy (more than 21 fractions)	4,5
Лучевая терапия (уровень 7) Radiotherapy (level 7)	Конформная дистанционная лучевая терапия (11–20 фракций) Conformal external-beam radiotherapy (11–20 fractions)	6,31
Лучевая терапия (уровень 8) Radiotherapy (level 8)	Конформная дистанционная лучевая терапия (21–32 фракций) Conformal external-beam radiotherapy (21–32 fractions)	11,19
Лучевая терапия (уровень 9) Radiotherapy (level 9)	Радионуклидная лучевая терапия (терапия самария оксабифором [^{153}Sm] и радия хлоридом [^{223}Ra]) Radionuclide therapy (samarium oxabifor [^{153}Sm] therapy and radium chloride [^{223}Ra] therapy)	15,29
Лучевая терапия (уровень 10) Radiotherapy (level 10)	Конформная дистанционная лучевая терапия (более 33 фракций) Conformal external-beam radiotherapy (more than 33 fractions)	17,42

КЗ – коэффициент затратности
DRP – diagnosis related group

Таблица 5
Клинико-статистические группы для химиолучевой терапии (лучевая терапия в сочетании с лекарственной терапией) по условиям оказания медицинской помощи с указанием коэффициентов затратоемкости
Table 5
Diagnosis related groups and their weight coefficients for chemoradiotherapy (radiotherapy in combination with chemotherapy) conducted in full-time and day hospitals

Описание в расшифровщике Name of a DGR	Метод и режим лучевой терапии Method and regimen of radiotherapy	КЗ Coeff.
	Круглосуточный стационар Full-time hospital	
Лучевая терапия в сочетании с лекарственной терапией (уровень 1) Chemoradiotherapy (level 1)	Контактная лучевая терапия в сочетании с лекарственной терапией Brachytherapy in combination with chemotherapy	3,85
Лучевая терапия в сочетании с лекарственной терапией (уровень 2) Chemoradiotherapy (level 2)	Конвенциальная дистанционная лучевая терапия (1–29 фракций) в сочетании с лекарственной терапией (за исключением лекарственной терапии темозоломидом, цетуксимабом или трастузумабом+пертузумабом) Conventional external-beam radiotherapy (1–29 fractions) in combination with chemotherapy (excluding Temozolomide, Cetuximab, Trastuzumab + Pertuzumab)	9,47
Лучевая терапия в сочетании с лекарственной терапией (уровень 3) Chemoradiotherapy (level 3)	Конвенциальная дистанционная лучевая терапия (более 30 фракций включительно) в сочетании с лекарственной терапией (за исключением лекарственной терапии темозоломидом, цетуксимабом или трастузумабом+пертузумабом) Conventional external-beam radiotherapy (more than 30 fractions) in combination with chemotherapy (excluding Temozolomide, Cetuximab, Trastuzumab + Pertuzumab)	10,95
Лучевая терапия в сочетании с лекарственной терапией (уровень 4) Chemoradiotherapy (level 4)	Конформная дистанционная лучевая терапия лучевая терапия (1–29 фракций) в сочетании с лекарственной терапией (за исключением лекарственной терапии темозоломидом, цетуксимабом или трастузумабом+пертузумабом) Conformal external-beam radiotherapy (1–29 fractions) in combination with chemotherapy (excluding Temozolomide, Cetuximab, Trastuzumab + Pertuzumab)	13,16
Лучевая терапия в сочетании с лекарственной терапией (уровень 5) Chemoradiotherapy (level 5)	Конформная дистанционная лучевая терапия лучевая терапия (более 30 фракций включительно) в сочетании с лекарственной терапией (за исключением лекарственной терапии темозоломидом, цетуксимабом или трастузумабом+пертузумабом) Conformal external-beam radiotherapy (more than 30 fractions) in combination with chemotherapy (excluding Temozolomide, Cetuximab, Trastuzumab + Pertuzumab)	14,63
Лучевая терапия в сочетании с лекарственной терапией (уровень 6) Chemoradiotherapy (level 6)	Конвенциальная и конформная дистанционная лучевая терапия, в сочетании с лекарственной терапией трастузумабом+пертузумабом Conventional and conformal external-beam radiotherapy in combination with chemotherapy using Trastuzumab + Pertuzumab	19,17
Лучевая терапия в сочетании с лекарственной терапией (уровень 7) Chemoradiotherapy (level 7)	Конвенциальная и конформная дистанционная лучевая терапия, в сочетании с лекарственной терапией темозоломидом или цетуксимабом Conventional and conformal external-beam radiotherapy in combination with chemotherapy using Temozolomide or Cetuximab	31,29
	Дневной стационар Day hospital	
Лучевая терапия в сочетании с лекарственной терапией (уровень 1) Chemoradiotherapy (level 1)	Контактная лучевая терапия в сочетании с лекарственной терапией Brachytherapy in combination with chemotherapy	3,92
Лучевая терапия в сочетании с лекарственной терапией (уровень 2) Chemoradiotherapy (level 2)	Конвенциальная дистанционная лучевая терапия в сочетании с лекарственной терапией (за исключением лекарственной терапии темозоломидом, цетуксимабом или трастузумабом+пертузумабом) Conventional external-beam radiotherapy in combination with chemotherapy (excluding Temozolomide, Cetuximab, Trastuzumab + Pertuzumab)	7,49

Лучевая терапия в сочетании с лекарственной терапией (уровень 3) Chemoradiotherapy (level 3)	Конформная дистанционная лучевая терапия лучевая терапия в сочетании с лекарственной терапией (за исключением лекарственной терапии темозоломидом, цетуксимабом или трастузумабом+пертузумабом) Conformal external-beam radiotherapy in combination with chemotherapy (excluding Temozolomide, Cetuximab, Trastuzumab + Pertuzumab)	13,98
Лучевая терапия в сочетании с лекарственной терапией (уровень 4) Chemoradiotherapy (level 4)	Конвенциальная и конформная дистанционная лучевая терапия в сочетании с лекарственной терапией трастузумабом+пертузумабом Conventional and conformal external-beam radiotherapy in combination with chemotherapy using Trastuzumab + Pertuzumab	25,11
Лучевая терапия в сочетании с лекарственной терапией (уровень 5) Chemoradiotherapy (level 5)	Конвенциальная и конформная дистанционная лучевая терапия дистанционная лучевая терапия в сочетании с лекарственной терапией темозоломидом или цетуксимабом Conventional and conformal external-beam radiotherapy in combination with chemotherapy using Temozolomide or Cetuximab	44,65

КЗ – коэффициент затратности
DRP – diagnosis related group

of hospitalization to the proposed DRG for radiation and chemoradiation therapy. For radiation therapy, an additional classification criterion was the number of fractions, for chemoradiation, the number of fractions and the INN of the drug, in accordance with the list shown in Table 3.

Discussion

The calculation of the cost of medical care to patients with malignant neoplasms with radiotherapy and chemoradiotherapy methods in 2019 allowed us to review the approaches to the formation of DRG used for billing hospital admissions in the CHI system. The costs are calculated by processing the SMs created on the basis of clinical recommendations, thus creating conditions for solving the task facing the Russian healthcare system, i. e., the implementation of clinical recommendations in practice.

As a result of this work, the number of DRGs for radiation therapy in the DRG model 2019 has been increased compared to the previous year: from 3 to 10, for round-the-clock and day hospital conditions. CICs underwent a major revision: if the previous models featured the spread of 2.0–3.53 for a 24-hour hospital and 3.64–6.42 for a day hospital, in the 2019 model they went up to 1.04-19.73 and 1.06-17.42 for a 24-hour hospital and day hospital, respectively. DRGs for chemoradiotherapy were developed, which were absent from the previous versions of the model. New classification criteria have been introduced for classifying a case of hospitalization as DRG in addition to the medical service previously used: the number of fractions for radiation therapy; the number of fractions and INN of antineoplastic drugs for chemoradiotherapy [9].

The changes made to the DRG model should contribute to differentiated and more equitable reimbursement of costs for medical care provided to medical organizations, depending on the treatment performed. The use of additional classification criteria will make it possible to accumulate information about the methods and modes of radiation and chemoradiotherapy used in actual practice, and thus improve the approaches to planning the volume of medical care at the level of the subject of the Russian Federation. In the future, it will be possible to compare the actual data on the methods and modes of radiation and chemotherapy used with expert assessments and use the results of such analysis for the development of the DRG model. This information will also made it possible to evaluate the compliance of the method and the mode of radiation or chemoradiation therapy used in the provision of medical care to a specific patient with clinical recommendations.

The classification of hospital admissions for radiotherapy as DRG based on the number of fractions is used in similar DRG classification systems in European countries, such as Denmark [10] and Germany [5, 6]. However, DRG models are usually based on the data on the actual costs incurred by medical organizations [13]. However, in the Russian Federation, the information about the actual costs of radiation and chemoradiotherapy is very scarce. In addition, there is a widespread belief among specialists that the current CHI rates are insufficient to meet the effective clinical recommendations. The proposed approach is aimed at aligning tariffs with clinical recommendations.

It is obvious that as the clinical recommendations are updated, a revision of the DRG in terms of payment for radiation and chemoradiation therapy will be required, which will continue to maintain the rates for medical care at a level sufficient to comply with the clinical recommendations.

Conclusion

The 2019 DRG model for paying for radiation and chemoradiation therapy was formed on the basis of a

methodology that allows for the alignment of the rates for payments for medical care with clinical recommendations. The proposed DRG model differs from the previous ones by the fact that it features a larger number of groups, includes allocated groups for payment for chemoradiotherapy, uses new classification criteria (the number of fractions and the INN of antineoplastic drugs) and a range of cost-intensity coefficients, which will allow for adequate reimbursement of costs for medical care depending on the method used and the mode of radiation or chemoradiotherapy.

REFERENCES

1. RF Federal Law "On the Basics of Protecting Citizens' Health in the Russian Federation" dated 21.11.2011 No. 323-FZ. (in Russian)
2. Avxentyeva M.V., Omelyanovskiy V.V., Petrovskiy A.V., Davydov M.I., Zheleznyakova I.A. et al. New Approaches to the Development of Diagnostic Related Groups for Cancer Pharmacotherapy in Russian Federation, *Medical Technologies. Assessment and Choice*, 2018, vol. 32, no. 2, pp. 8–23 (in Russian).
3. Ledovskikh Y.A., Semakova E.V., Omelyanovskiy V.V. Methodology for the development of diagnosis related groups based on clinical guidelines using standardized modules of healthcare, *Medical Technologies. Assessment and Choice*, 2019, vol. 37, no. 3, pp. 8–15 (in Russian).
4. Order of the Ministry of Health of Russia "On approval of the procedure for developing standards of medical care" dated 02.02.2018 No. 53n. (in Russian)
5. Order of the Ministry of Health of Russia "On approval of the procedure for the provision of medical care to the patients with oncological deseases" dated 15.11.2012 No. 915n. (in Russian)
6. Order of the Ministry of Health of the Russian Federation "On approval of the nomenclature of medical services" dated 13.10.2017 No. 804n. (in Russian)
7. *State register of maximum selling prices*. Available at: https://grls.rosminzdrav.ru/pricelims.aspx (accessed 05.05.2019). (in Russian)
8. *Malignant neoplasms in Russia in 2017 (morbidity and mortality)*, by Kaprin A.D., Starinsky V.V., Petrova G.V. as eds. Moscow, MNIOI after P.A. Herzen – a branch of the Federal State Budgetary Institution «NMIRTS» of the Ministry of Health of the Russian Federation Publ., 2018. 250 p. (in Russian)
9. Letter dated 11.21.2018 of the Ministry of Health of the Russian Federation No. 11–7/10/2–7543 and of the Federal Compulsory Medical Insurance Fund No. 14525/26–1/i "On methodological recommendations on methods of paying for medical care financed by compalsory medical insurance". (in Russian)
10. Afregning og finansiering (DRG). Available at: https://sundhedsdatastyrelsen.dk/da/afregning-og-finansiering (accessed 12.05.2019).
11. Glocker S., Loskamp N., Bamberg M., Roder N. Evaluation von Fallpauschalen in der Radioonkologie, *Strahlentherapie und Onkol*, 2006, vol. 182, no. 6, pp. 305–311. (in Deutsch)
12. Schmidberger H. Reimbursement of radiotherapy in Germany, *Cancer/Radiothérapie*, 2017, vol. 21, no. 6–7, pp. 544–546.
13. Tan S.S., Geissler A., Serdén L., Heurgren M., van Ineveld B.M., Redekop W.K., Hakkaart-van Roijen L., *Eur. J. Public Health*, 2014, vol. 24, no. 6, pp. 1023–1028.

ЛИТЕРАТУРА

1. Федеральный закон от 21.11.2011 № 323-ФЗ «Об основах охраны здоровья граждан в Российской Федерации».
2. Авксентьева М.В., Омельяновский В.В., Петровский А.В. и соавт. Новые подходы к формированию клинико-статистических групп, объединяющих случаи госпитализации для лекарственного лечения злокачественных новообразований // Медицинские технологии. Оценка и выбор. – 2018. – Т. 32, № 2. – С. 8–23.
3. Ледовских Ю.А., Семакова Е.В., Омельяновский В.В. Методика формирования клинико-статистических групп заболеваний на основе клинических рекомендаций с использованием стандартизированных модулей медицинской помощи // Медицинские технологии. Оценка и выбор. – 2019. – Т. 37, № 3. – С. 8–15.
4. Приказ Минздрава России от 08.02.2018 № 53н «Об утверждении порядка разработки стандартов медицинской помощи».
5. Приказ Минздрава России от 15.11.2012 № 915н «Об утверждении Порядка оказания медицинской помощи населению по профилю «онкология».
6. Приказ Министерства здравоохранения Российской Федерации от 13.10.2017 г. № 804н «Об утверждении номенклатуры медицинских услуг».
7. Государственный реестр предельных отпускных цен. Available at: https://grls.rosminzdrav.ru/pricelims.aspx (accessed 05.05.2019).
8. Злокачественные новообразования в России в 2017 году (заболеваемость и смертность) // Под ред. А.Д. Каприна, В.В. Старинского, Г.В. Петровой – М.: МНИОИ им. П.А. Герцена – филиал ФГБУ «НМИЦ радиологии» Минздрава России, 2018. – 250 с.
9. Письмо от 21.11.2018 Министерства здравоохранения Российской Федерации № 11–7/10/2–7543, Федерального фонда обязательного медицинского страхования № 14525/26–1/и «О методических рекомендациях по способам оплаты медицинской помощи за счет средств обязательного медицинского страхования».
10. Afregning og finansiering (DRG) . Available at: https://sundhedsdatastyrelsen.dk/da/afregning-og-finansiering (accessed 12.05.2019).
11. Glocker S., Loskamp N., Bamberg M., Roder N.Evaluation von Fallpauschalen in der Radioonkologie // Strahlentherapie und Onkol. – 2006. – Vol. 182, No. 6. – P. 305–311.
12. Schmidberger H. Reimbursement of radiotherapy in Germany // Cancer/Radiothérapie. – 2017. – Vol. 21, No. 6–7. – P. 544–546.
13. Tan S.S., Geissler A., Serdén L., et al. DRG systems in Europe: variations in cost accounting systems among 12 countries // Eur. J. Public Health. – 2014. – Vol. 24, No. 6. – P. 1023–1028.

MULTI-COURSE PHOTODYNAMIC THERAPY OF BASAL CELL SKIN CANCER OF THE CENTRAL FACE AREA (CLINICAL STUDY)

Filonenko E.V., Urlova A.N., Vakhabova Yu.V., Medvedev S.V., Matorin O.V., Grigorievykh N.I., Kaprin A.D.
P.A. Herzen Moscow Oncology Research Center – branch of FSBI NMRRC of the Ministry of Health of the Russian Federation, Moscow, Russia

Abstract

The results of an 11-year clinical observation and treatment of a patient with stage II basal cell carcinoma of the face (T2N0M0) are presented. History of the illness is associated with a long (from 2001 to 2008) inadequate treatment, due to the incorrect diagnosis. After the proper diagnosis was established, from 2008 to 2019 at the Center for Laser and Photodynamic Diagnostics and Tumor Therapy of P.A. Herzen Moscow Oncology Research Center, the patient underwent organ-preserving treatment using the multi-course photodynamic therapy (PDT) and drug targeted therapy. In total, 23 courses of PDT were conducted with photosensitizers of the chlorin series and 5-aminolevulinic acid during this period. Since 2018, the patient is in the process of targeted drug treatment with Vismodegib. In the course of targeted drug treatment, a follow-up examination in 2019 revealed continued growth of the residual tumor, and another course of PDT was carried out. Throughout the observation period, the patient tolerated the treatment well, without complications, with a good quality of life and satisfactory cosmetic effect.

Keywords: basal cell skin cancer, photodynamic therapy, photosensitizer, targeted therapy, vismodegib.

For citations: Filonenko E.V., Urlova A.N., Vakhabova Yu.V., Medvedev S.V., Matorin O.V., Grigorievykh N.I., Kaprin A.D. Multi-course photodynamic therapy of basal cell skin cancer of the central face area (clinical study), *Biomedical Photonics*, 2019, vol. 8, no. 4, pp. 47–52. (in Russian) doi: 10.24931/2413–9432–2019–8–4–47–52

Contacts: Grigorievykh N.I., e-mail: n41493@icloud.com

МНОГОКУРСОВАЯ ФОТОДИНАМИЧЕСКАЯ ТЕРАПИЯ ПРИ БАЗАЛЬНО-КЛЕТОЧНОМ РАКЕ КОЖИ ЦЕНТРАЛЬНОЙ ЗОНЫ ЛИЦА (КЛИНИЧЕСКОЕ НАБЛЮДЕНИЕ)

Е.В. Филоненко, А.Н. Урлова, Ю.В. Вахабова, С.В. Медведев, О.В. Маторин, Н.И. Григорьевых, А.Д. Каприн
МНИОИ им. П.А. Герцена – филиал ФГБУ «НМИЦ радиологии» Минздрава России, Москва, Россия

Резюме

Приведены результаты 11-летнего клинического наблюдения и лечения пациентки с базальноклеточным раком кожи лица II стадии (T2N0M0). Анамнез течения заболевания связан с длительным (с 2001 по 2008 гг.) неадекватным лечением, вследствие отсутствия правильного диагноза. После установки диагноза, с 2008 по 2019 гг. в МНИОИ им. П.А. Герцена в Центре лазерной и фотодинамической диагностики и терапии опухолей пациентке проведено органосохраняющее лечение методом многокурсовой фотодинамической терапии (ФДТ) и лекарственной таргетной терапии. Проведено 23 курса ФДТ с фотосенсибилизаторами хлоринового ряда и 5-аминолевулиновой кислоты. С 2018 г. пациентка находится в процессе лекарственного лечения таргетной терапией висмодегибом. На фоне таргетного лекарственного лечения при контрольном осмотре в 2019 г. выявлен продолженный рост остаточной опухоли, проведен очередной курс ФДТ. Весь срок наблюдения пациентка переносила лечение хорошо, без осложнений с хорошим качеством жизни и удовлетворительным косметическим эффектом.

Ключевые слова: базальноклеточный рак кожи, фотодинамическая терапия, фотосенсибилизатор, таргетная терапия, висмодегиб.

Для цитирования: Филоненко Е.В., Урлова А.Н., Вахабова Ю.В., Медведев С.В., Маторин О.В., Григорьевых Н.И., Каприн А.Д. Многокурсовая фотодинамическая терапия при базально-клеточном раке кожи центральной зоны лица (клиническое наблюдение) // Biomedical Photonics. – 2019. – Т. 8, № 4. – С. 47–52. doi: 10.24931/2413–9432–2019–8–4–47–52

Контакты: Григорьевых Н.И., e-mail: n41493@icloud.com

Basal cell carcinoma (BCC) is the most common skin cancer and the most common human malignancy [1]. The incidence of 2.75 million of cases diagnosed worldwide indicates its importance for public health care. Worldwide, upwards of 3.5 million of cases of non-melanoma skin cancer are diagnosed every year. BCC accounts for approximately 75% of these cases, that is not less than 2 million of new cases annually [2,3]. BCC occurs predominately in white people with 30% risk of development during lifetime [4]. The main principles of management of BCC include not only cure but also sparing of function with minimal cosmetic defect especially for tumors on face.

A photodynamic therapy (PDT) is reasonable for BCC with high risk of cosmetic defect following a surgical treatment or radiotherapy. PDT is a method of selective tumor destruction having the advantages of targeting destructive effect on tumor tissue comparing with other types of cancer treatment. Herewith, normal surrounding tissues are not affected offering multiple use of this method without compromising normal tissues and development of treatment resistance of the tumor, PDT has been widely used in the clinical practice for BCC since 1978 worldwide and since 1992 in Russia [5].

Another type of selective anticancer intervention for BCC is a targeted therapy. Vismodegib is an oral first-in-class inhibitor of Hedgehog pathway signaling. This is a small molecule which selectively inhibits a Smoothened (SMO) protein blocking a signal transfer into cell and prohibiting uncontrolled cell division [6]. The efficacy of Hedgehog pathway signaling inhibiting in the treatment of locally advanced and metastatic BCC of the skin was supported by phase II ERIVANCE international multicenter clinical trial. According to results of the trial, Vismodegib was approved by the US Food and Drug Administration (FDA) in 2012 and the European Medicines Agency (EMA) in 2013. In Russia vismodegib was registered in 26.09.2013 (LP-002252) and since that moment has been included into clinical practice of Russian oncologists for treatment of adults with metastatic and locally advanced BCC that has recurred after surgery or who are not candidates for surgery or radiation.

We present the case of long-term management in patient with extended BCC of the central area of the face.

Patient K, 11 y.o., noticed a wound-like skin lesion on the back of her nose in 2001. No self-treatment was performed. In 2002 because of non-healing wound she referred to a local dermatologist. Ointment applications were administered with no effect. In 2004 a laser ablation of the lesion was performed, but no healing or improvement was observed. For 5 years the patient referred to dermatologists in state and private clinics. Non-surgical treatment using various ointments with slight effect was performed. No morphological study was performed, the lesion continued to grow. In October, 2007 the patient was referred to the clinic of skin diseases in the medical university with continued growth of the lesion and new foci on the skin of the nose and adjacent parts of her cheeks. Neurotic excoriation and granuloma annulare were diagnosed; local therapy with Curiosin gel, NO-therapy, Longidaza 3000 ME, Actovegin gel, methyluracil ointment, 5% Xeroform ointment, Uriage gel was performed. There was a 50%–55% regression of lesions. In December, 2007 due to continued growth of the lesion and new focus on the right cheek the patient referred to a for-profit medical center, where a malignant tumor was suspected for the first time and she was referred to P.A. Herzen Moscow Oncology Research Center (MORC). In January, 2008 she presented in P.A. Herzen MORC where exfoliative cytology revealed BCC. The tumor affected all external nasal surfaces extending to cheeks. According to check-up data there were no regional and distant metastases. A clinical case was discussed on the extended consilium, photodynamic therapy (PDT) was recommended.

Taking into account the age of the patient, tumor localization, superficial tumor growth a topical 5-aminolevulinic acid-mediated PDT (ALA-PDT) was considered.

In April and December, 2008 two courses of PDT with ointment based on 5-ALA powder prepared *ex tempore* were performed (Fig. 1).

In February, March and November, 2009 five (two, one and two, respectively) courses of PDT with 5-ALA ointment prepared *ex tempore* were performed.

In December, 2009 for the cytologically confirmed tumor growth along the scar margin PDT with intravenous photosensitizer was considered.

In December, 2009 one course with photohem was conducted.

In April and November, 2010 two courses of PDT (one with Photogem and one with Photoditazine) was performed due to a continued tumor growth in the center and along the margin of the scar (April) and 0.5x0.3 cm tumor along the scar margin on the right side of the nose (November) (Fig. 2).

In December, 2011 one course of PDT with Radachlorin was performed due to the recurrence along the scar margin up to 0.3 cm in diameter. A contrast-enhanced magnetic resonance imaging (MRI) revealed no additional lesions in soft tissues of the right ala against the scar deformation; there was a skin and subcutaneous edema 1 cm above the nasal tip and along the left ala on the area up to 17x12 mm.

In August, 2012 one course of PDT with Radachlorin was performed due to the recurrence on the nasal tip, dorsum, and right and left lateral walls.

In September, 2013 there was no complete tumor regression following multiple courses of PDT and the patient was consulted by prof. Milanov N.O., academician of

Рис. 1. Клиническая картина через 2 мес после первого курса ФДТ (июнь 2008 г.)
Fig. 1. Clinical picture after the first course of PDT (June 2008)

RAS, the head of the Plastic and Maxillofacial Surgery department in I.M. Sechenov First Moscow State Medicine University for chance for extended surgical intervention including reconstruction. Taking into account the presence of intact bone and chondral structures and benefit from previous PDT courses the subsequent multiple PDT courses were considered to be the method of choice.

In September, 2013 one course of PDT with photolon was applied on six foci of recurrent BCC located along the previous PDT area: the right lateral nasal wall near the ala (a dark-pink tumor of 1 cm in diameter), similar foci on the nasal tip (0.8x0.3 cm), the nasal dorsum (0.4 cm), and the nasal root (0.4x0.4 cm). A contrast-enhanced MRI revealed no significant changes in soft tissues of the face comparing with MRI data in 2011.

In March and December, 2014 two courses of PDT with Radachlorin were performed for the continued tumor growth on the lateral nasal wall (1.0 cm) and the nasal dorsum (1.0x1.5 cm), respectively.

In August, 2015 one course of PDT with Radachlorin was performed on five foci of BCC on the right cheek, the nasal tip, left ala, left lateral wall, and dorsum.

A contrast-enhanced MRI of facial skull in November, 2016 revealed no additional lesions in soft tissues of the nose against the scar deformation; there was a slight skin and subcutaneous edema on the right side. No fair MRI evidence for tumor lesion was obtained.

In May and December, 2016 two courses of PDT (Radachlorin and Levulon) were performed for recurrence on the left cheek, nasal dorsum, left lateral wall, and left cheek.

In March, May and December, 2017 three courses of PDT (Photolon, Radachlorin, Levulon) were performed for new tumor near the right internal canthus up to 1 cm in diameter and the continued tumor growth along the scar margin on the left cheek, left nasal lateral wall and nasal vestibule, the right cheek along the lower and upper scar margins. A contrast-enhanced MRI of facial skull in October, 2017: on native and post-contrast scans there are a scar area up to 28 mm in length on the level of zygomatic arch and a 9x13x8 mm tuberous soft-tissue component with well-defined contrast accumulation. No destruction or edema of bone structures and no subcutaneous fluid accumulations were revealed (Fig. 3).

In March and July, 2018 two courses of PDT with Radachlorin were performed for BCC on the nasal root, right

a

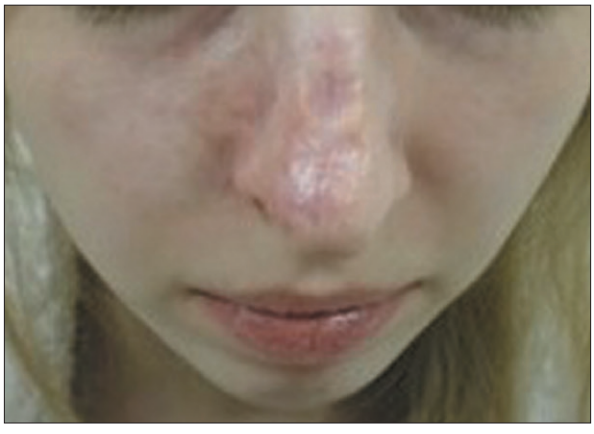

b

Рис. 2. Клиническая картина:
a – до проведения ФДТ (апрель 2010 г.);
b – после проведения ФДТ (июль 2010 г.)
Fig. 2. Clinical picture
a – before PDT (April 2010);
b – after PDT (July 2010)

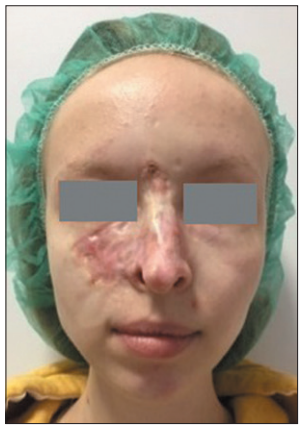

a

b

Рис. 3. Клиническая картина:
a – до проведения ФДТ (март 2017 г.);
b – после проведения ФДТ (июль 2017 г.)
Fig. 3. Clinical picture
a – before PDT (March 2017);
b – after PDT (July 2017)

zygomatic region, right infraorbital region, right buccal region, left lateral nasal wall, right nasal ala, nasal dorsum. A contrast-enhanced MRI of facial skull in January, 2018: a 28x6 mm scar in soft tissue of the right zygomatic region was seen; near the nasal ala within the subcutaneous tissue there was a 9x11x8 mm oval soft-tissue component with cord-like borders and homogenous well-defined contrast accumulation on delayed series. Accordingly, there was a 9x2 mm local thickening of the skin in the nasal root region on the right with contrast accumulation on delayed series (no dynamics since 2017). There were also local areas of hypervascularization in the forehead skin above the nasal root up to 5x3 mm in size (8x3 mm in October, 2017). A 4x5 mm local contrast accumulation within subcutaneous tissue of the half of the right nasal ala, which were not seen on scans performed on 23.10.2017; No destruction or edema of bone structures and no subcutaneous fluid accumulations were revealed.

In July, 2018 a targeted therapy with Vismodegib (a daily dose of 150 mg) was considered. Since September, 2018 up to now a drug therapy has been conducted (Fig. 4).

In August, 2019 during follow-up examination on the background of the targeted therapy with Vismodegib a cytologically confirmed continued tumor growth on the right nasal ala was diagnosed.

An MRI in August, 2019: when comparing with the previous MRI (January, 2018), a positive dynamics was observed (previously detected areas on the lateral nasal wall, right nasal ala and forehead region without pathological contrast accumulation). There was a persisting lesion near the right nasal ala with no changes in size. Morphological confirmation of the continued tumor growth was performed by cytological analysis.

Taking into account a residual tumor, a course of PDT against the targeted therapy was considered on the extended consilium.

In November, 2019 one course of PDT with Photodita-

a

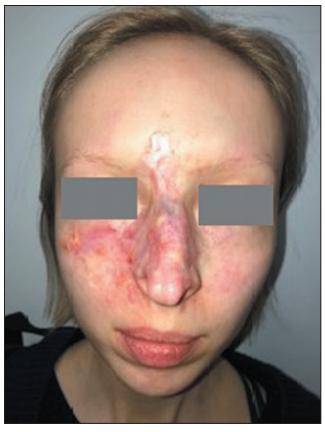

b

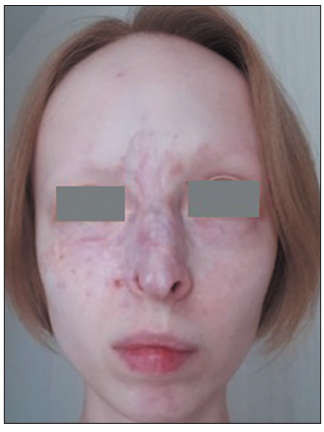

c

Рис. 4. Клиническая картина:
a– до проведения назначения висмодегиба (июль 2018 г.);
b – через 4 мес после начала лечения висмодегибом;
c – через 9 мес после начала лечения висмодегибом
Fig. 4. Clinical picture
a – before treatment with Vismodegib (June 2018);
b – after 4 months of treatment with Vismodegib;
c – after 9 months of treatment with Vismodegib

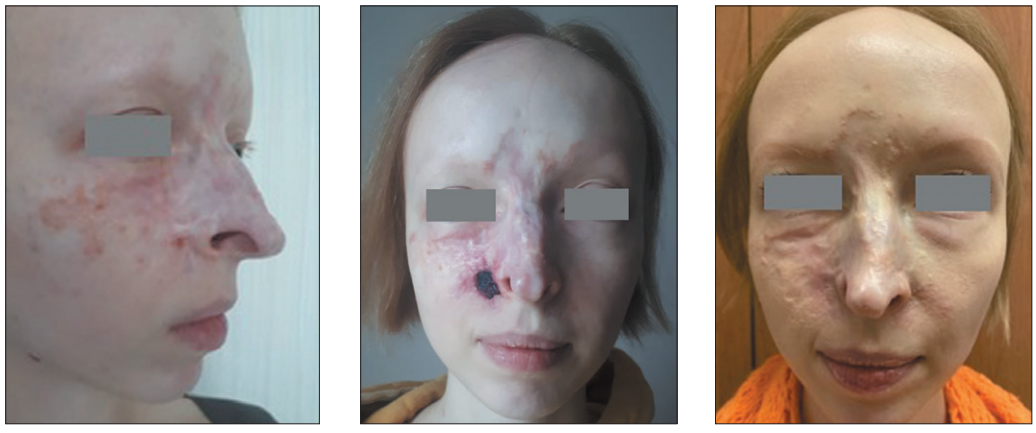

Рис. 5. Клиническая картина (2019 г.):
a – продолженный рост опухоли крыла носа справа до ФДТ;
b – некроз опухоли, 1 неделя после ФДТ;
c – полная регрессия опухоли, 3 мес после ФДТ
Fig. 5. Clinical picture (2019)
a – continued tumor growth on the right wing of the nose before PDT;
b – tumor necrosis, 1 week after PDT;
c – complete tumor regression, 3 months after PDT

zine for the residual tumor was performed. Three months later a complete regression of the tumor was registered (Fig. 5).

Discussion

This clinical case demonstrate a correct management of BCC of the central facial zone with PDT in the young patient, who had a tumor disease complicated by long-lasting incorrect treatment due to misdiagnosis, an absence of cancer alertness in her physicians and delayed morphological study for diagnosis confirmation. PDT was the very optimal strategy which allowed a preservation of the patient's face and stabilizing of initially locally advanced tumor of the central facial zone before market appearance of new generation drugs – targeted therapy for BCC.

The experience of long-term treatment (11 years) of the patient with PDT shows the efficacy of this organ-preserving method in multicourse mode for frequent recurrences of BCC. All courses of PDT were well-tolerated without complications and with good cosmetic and apparent antitumor effect.

5-ALA ointment prepared ex tempore is inefficient because a combination of additive agents responsible for 5-ALA delivery to pathologic tissue plays an important role for topical PDT. Only standardized formulations showed its efficacy in trials of all clinical phases should be used for topical PDT. There are publications showing a high efficiency of topical PDT with ALA-based agents (levulon, ameluz, metvix) for such types of BCC [7,8]. Probably, an inappropriate combination of additive agents did not allowed getting a significant benefit from first six courses of PDT in this patient.

Conclusion

This clinical case demonstrates the efficacy and utility of PDT combined with the targeted therapy with vismodegib in patients with BCC for continued tumor growth during the drug therapy or for repeated recurrences of tumor during multi-course PDT.

REFERENCES

1. *Malignant neoplasms in Russia in 2012 (incidence and mortality)*, by Kaprin A.D., Starinsky V.V., Petrova G.V. as eds. Moscow, MNIOI im. P.A. Gertsena – filial FGBU «NMITs radiologii» Minzdrava Rossii, 2019. 250 p.
2. Rubin A.I., Chen E.H., Ratner D. Basal-cell carcinoma, *N Engl J Med*, 2005, vol. 353(21), pp. 2262–2269.

ЛИТЕРАТУРА

1. Злокачественные новообразования в России в 2018 году (заболеваемость и смертность) / под ред. Каприна А.Д., Старинского В.В., Петровой Г.В. – М.: МНИОИ им. П.А. Герцена – филиал ФГБУ «НМИЦ радиологии» Минздрава России, 2019. – 250 с.
2. Rubin A.I., Chen E.H., Ratner D. Basal-cell carcinoma // N Engl J Med. – 2005. – Vol. 353(21). – P. 2262–2269.

3. Diepgen T.L., Mahler V. The epidemiology of skin cancer, *Br J Dermatol*, 2002, vol. 146(suppl), pp. 1–6.
4. Wong C.S.M., Strange R.C., Lear J.T. Basal cell carcinoma, *Br Med J*, 2003, vol. 327, pp. 794–8.
5. Filonenko E.V. Fluorescence diagnostics and photodynamic therapy – rationale for the use and possibility in oncology, *Fotodinamicheskaya terapiya I Fotodiagnostika*, 2014, vol. 3, no. 1, pp. 3–7. (in Russian)
6. Sekulic A., Migden M.R., Basset-Seguin N., Garbe C., Gesierich A., Lao C.D., Miller C., Mortier L., Murrell D.F., Hamid O. et al. Long-term safety and efficacy of vismodegib in patients with advanced basal cell carcinoma: final update of the pivotal ERIVANCE BCC study, *BMC cancer*, 2017, vol. 17(1), pp. 332.
7. Filonenko E.V., Kaprin A.D., Urlova A.N., Grigorievykh N.I. Photodynamic therapy of basal cell carcinoma with Levulon local application, *Proceedings Volume 11070, 17th International Photodynamic Association World Congress*, 2019, 1107081. https://doi.org/10.1117/12.2525825
8. Morton C.A., Dominicus R., Radny P. et al. A randomized, multinational, non-inferiority, phase III trial to evaluate the safety and efficacy of BF-200 ALA gel versus mal cream in the treatment of non-aggressive basal cell carcinoma with photodynamic therapy (PDT), *Br. J. Dermatol*, 2018, vol. 179, pp. 309–319.

3. Diepgen T.L., Mahler V. The epidemiology of skin cancer // Br J Dermatol. – 2002. – Vol. 146(suppl). – P. 1–6.
4. Wong C.S.M., Strange R.C., Lear J.T. Basal cell carcinoma // Br Med J. – 2003. – Vol. 327. – P. 794–8.
5. Филоненко Е.В. Флюоресцентная диагностика и фотодинамическая терапия – обоснование применения и возможности в онкологии // Фотодинамическая терапия и Фотодиагностика. – 2014. – Т. 3, № 1. – С. 3–7.
6. Sekulic A., Migden M.R., Basset-Seguin N., Garbe C., Gesierich A., Lao C.D., Miller C., Mortier L., Murrell D.F., Hamid O. et al. Long-term safety and efficacy of vismodegib in patients with advanced basal cell carcinoma: final update of the pivotal ERIVANCE BCC study // BMC cancer. – 2017. – Vol. 17(1). – P. 332.
7. Filonenko E.V., Kaprin A.D., Urlova A.N., Grigorievykh N.I. Photodynamic therapy of basal cell carcinoma with Levulon local application // Proceedings Volume 11070, 17th International Photodynamic Association World Congress. – 2019. – 1107081. https://doi.org/10.1117/12.2525825
8. Morton C.A., Dominicus R., Radny P. et al. A randomized, multinational, non-inferiority, phase III trial to evaluate the safety and efficacy of BF-200 ALA gel versus mal cream in the treatment of non-aggressive basal cell carcinoma with photodynamic therapy (PDT) // Br. J. Dermatol. – 2018. – Vol. 179. – P. 309–319.